POLITECNICO DI MILANO
DIPARTIMENTO DI BIOINGEGNERIA
DOTTORATO DI RICERCA IN BIOINGEGNERIA

Granger Causality Analysis in Depressed Baroreflex Regulation Conditions

Doctoral dissertation of:
Tito BASSANI

m. 738558

Advisors:
Prof. Alberto PORTA
Valentina MAGAGNIN, PhD

Tutor:
Prof. Giuseppe BASELLI

Supervisor of the PhD Program:
Prof. Maria Gabriella SIGNORINI

XXIV edition
2009 - 2011

PUBLICATION DATA:
Granger Causality Analysis in Depressed Baroreflex Regulation Conditions

Tito Bassani
Politecnico di Milano
Dipartimento di Bioingegneria
P.za Leonardo da Vinci 32
20133 – Milan, Italy.
e-mail: tito.bassani@mail.polimi.it

POLITECNICO DI MILANO
DIPARTIMENTO DI BIOINGEGNERIA
DOTTORATO DI RICERCA IN BIOINGEGNERIA

Analisi di Causalità secondo Granger in Condizioni di Regolazione Baroriflessa Depressa

Tesi di dottorato di:
Tito BASSANI

m. 738558

Relatori:
Prof. Alberto PORTA
Valentina MAGAGNIN, PhD

Tutor:
Prof. Giuseppe BASELLI

Coordinatore di dottorato:
Prof. Maria Gabriella SIGNORINI

Ciclo XXIV
2009 - 2011

…to Mountains ascended

Acknowledgements

I wish to first and foremost thank my tutor, Prof. Giuseppe Baselli for his helpful suggestions, his interest and kindness.

Sincere and special gratitude goes to my advisors: Prof. Alberto Porta, who suggested this project, for his continuous and stimulating presence, whose guidance was indispensable throughout the whole of PhD and Eng. Valentina Magagnin for her friendship, support and help.

I'm specially thankful to all people that allowed me to acquire the experimental protocol dataset analyzed in this study: Eng. Alessandro Beda and Dr. Marcelo Gama de Abreu in reference to the comparison of mechanical ventilation techniques during deep anaesthesia on animals and for allowing me to have been visiting student at Department of Anaesthesia and Intensive Care, University Hospital of Dresden; Dr. Giuseppe Citerio, Dr. Stefano Guzzetti and the whole of Neuromorfeo team in reference to the comparison of anaesthesiology administration strategies during deep anaesthesia on humans; Eng. Gian Domenico Pinna and Eng. Roberto Maestri in reference to paced breathing and head-up manoeuvre in heart failure patients; Dr. Nicola Montano, Dr. Aparecida Maria Catai and Dr. Anielle Takahashi in reference to the head-up manoeuvres in healthy subjects.

I also sincerely thank Dr. Giuseppe Banfi who supported part of my PhD at Galeazzi Orthopaedic Institute.

I'm profoundly in debt to all my office mates and colleagues, that accompanied me in the last tree years, for being very supportive and friendly throughout the whole of PhD.

Last but not least my heartfelt thanks go to my mother, my father and my friends, for their irreplaceable presence and for their patient, caring support and encouragement. Thanks Manuela for helping me at the crucial stage.

ABSTRACT

The baroreflex sensitivity represents a fundamental clinical parameter helpful to better predict the risk of death in subjects after myocardial infarction. Baroreflex sensitivity is non invasively assessed from spontaneous heart period (RR) and systolic arterial pressure (SAP) variabilities and its estimate is reliable only under the hypothesis of a causal relation from SAP to RR. Currently this hypothesis is unreliably tested. This Doctoral dissertation proposes the use of a Granger causality approach in the time domain to test the hypothesis of the involvement of baroreflex in governing RR-SAP interactions and to deal with the confounding factor of respiratory influences. Numerous simulations were performed to evaluate the reliability of Granger causality tests according to different scheme of interactions among series. The approach was applied to four experimental protocols known to depress baroreflex functions and increase the effect of respiration on both RR and SAP, thus making challenging the assessment of the role of baroreflex in regulating RR and SAP. Simulations results pointed out the importance of accounting for exogenous sources contaminating closed loop interactions in causality studies. Experimental results revealed that the role of baroreflex cannot be correctly judged without accounting for respiration both in physiological conditions and during deep anaesthesia. Causality analysis contributes to the differentiation between diverse strategies of mechanical ventilation and administration of anaesthetic during deep anaesthesia. Unfortunately, when the concept of causality was exploited to improve baroreflex sensitivity estimates, no difference was found compared to a more traditional approach based on squared RR-SAP coherence. This disappointing result prompts for the search for further (i.e. in addition to respiration) unaccounted influences that might bias causality analysis and baroreflex sensitivity estimates.

SUMMARY

Introduction

The cardiovascular system is regulated by numerous control mechanisms acting to guarantee that the necessities of each physiological district are satisfied and that cardiovascular variables do not assume values incompatible with life.

Arterial baroreflex is one of the most important short-term cardiovascular regulatory reflex [Cohen and Taylor, 2002]. The baroreflex regulation is the mechanism that modulates heart rate in response to arterial pressure modifications. The baroreflex sensitivity represents a fundamental clinical parameter that was found valuable e.g. to better predict the risk of death in subjects after myocardial infarction [La Rovere et al., 1998].

The characterization of baroreflex is based on the assessment of the baroreflex sensitivity derived as the variation of heart period, approximated as the time interval between two consecutive R peaks on the ECG (RR), per unit change of systolic arterial pressure (SAP) [Smyth et al., 1969]. Usually the estimation of baroreflex sensitivity is based on the administration of a vasoactive drug inducing an important SAP change capable to drive a measurable RR variation.

Recently, several noninvasive techniques based on the analysis of the spontaneous beat-to-beat RR and SAP variabilities [Laude et al., 2004] have been proposed for the estimation of the baroreflex sensitivity in more physiological conditions, without the need of perturbing cardiovascular regulation with a pharmacological stimulus.

Techniques exploiting spontaneous RR and SAP variabilities are helpful in assessing baroreflex sensitivity only when causality is along baroreflex (i.e. SAP changes contribute to RR variations) [Porta et al., 2000]. Unfortunately, this prerequisite is not properly tested. Usually, assessing the significance of squared coherence function between RR and SAP series is considered to be sufficient [De Boer et al., 1985].

Unluckily, coherence can be high even when RR variations contribute to SAP changes along the reverse causal direction [Porta et al., 2002] imposed by the mechanical feedforward pathway. Without testing causality from SAP to RR, any estimate of the baroreflex sensitivity derived from spontaneous variabilities could be conversely related to the gain of the feedforward mechanical pathway [Porta et al., 2002].

Unfortunately, the estimate of causality between two signals might be biased by the presence of a third one affecting both. When considering RR and SAP, respiration (Resp) can act on both, thus imposing to account for Resp when assessing causality between RR and SAP. Indeed, mechanisms responsible for RR changes at the respiratory rate include the coupling between respiratory and autonomic centres modulating vagal and sympathetic efferent activities, cardiopulmonary reflexes mediated by the activation of atrial and pulmonary receptors, and mechanical stimulation of the sinus node [Saul et al., 1991; Ecberg, 2003; Gilbey et al., 1984; Bainbridge, 1915; Desai et al., 1997; Bernardi et al., 1989].

These mechanisms adjust RR independently of baroreflex. SAP fluctuations synchronous with Resp are the result of respiratory-related fluctuations of stroke volume induced by changes of intrathoracic pressure and venous return [De Boer et al., 1987; Innes et al., 1993; Toska and Eriksen, 1993]. These SAP variations are independent of those mediated by RR changes. As a consequence disregarding Resp might determine an erroneous interpretation of RR-SAP causality and prompt for the inclusion of Resp into the minimal set of signals necessary to assess RR-SAP causality.

The purpose of this Doctoral dissertation is to assess the degree of

correlation between RR and SAP along baroreflex (i.e. the strength of the causal relation from SAP to RR) during experimental protocols known to be able to depress the baroreflex function: i) mechanical controlled versus supported ventilation techniques in juvenile pigs during deep intravenous anaesthesia; ii) volatile versus intravenous anaesthesiology strategies in humans during deep anaesthesia in controlled ventilation; iii) paced breathing and head-up tilt in heart failure subjects; iv) head-up tilt at different inclinations of the tilt table in healthy subjects. Furthermore the aim of this dissertation is to assess the effect of an exogenous source such as respiration on the causal relation from SAP to RR.

Experimental conditions were chosen for the reason that the causal relation from SAP to RR might be insignificant because SAP changes might be insufficient to explore baroreflex and the smallness of baroreflex gain might produce insignificant RR changes (i.e. they are challenging for the assessment of the involvement of baroreflex in regulating cardiovascular function). In addition, especially during deep anaesthesia, respiration is a powerful perturbing source.

The presence of a significant causal relationship from SAP to RR was assessed using Granger causality approach [Granger, 1969] according to two traditional tests in the time domain (i.e. F-test and Wald test).

Spontaneous baroreflex sensitivity was assessed by evaluating the square root of the ratio of the power of RR to that of SAP calculated in low and high frequency bands (i.e. LF and HF, ranging from 0.03 to 0.15 Hz and from 0.15 to 0.5 Hz respectively) [Pagani et al., 1988] for all subjects with coherence function (K^2) in the respective band greater than 0.5 [De Boer et al., 1985].

Baroreflex sensitivity assessed over RR and SAP series with a significant degree of casual relation from SAP to RR was compared with that derived from subjects with a significant RR-SAP correlation to check whether causality analysis provides information helpful to refine the estimate of baroreflex sensitivity.

Methods

Causality is usually tested in time [Riedl et al., 2010; Bernasconi and König, 1999; Marinazzo et al., 2006; Hesse et al., 2003; Sitnikova et al., 2008; Roebroeck et al., 2004; Londei et al., 2006], frequency [Sameshima and Baccalà, 1999; Kaminski et al., 2001; Porta et al., 2002; Schelter et al., 2009; Dhamala et al., 2008; Wang et al., 2007; Astolfi et al., 2006] and information domains [Palus et al., 2001; Hlavackova-Schindler et al., 2007; Faes et al., 2011; Verdes, 2005; Chàvez et al., 2003].

In this Doctoral dissertation, methods assessing causality in time domain were chosen because they do not need to assume that the cardiovascular control mechanisms occur along specific temporal scales and the distribution of the statistic assessing causality under the null hypothesis of absence of a causal relationship between the two series is well-known, thus allowing to easily keep under control the percentage of false causality detections.

According to the Granger definition of causality [Granger, 1969], given two signals, y_i and y_k, y_i is said to Granger-cause y_k if past values of y_i contain information on y_k above and beyond the information contained in past values of y_k.

Given the set of M signals $\Omega_y=\{y_1,y_2,\ldots,y_M\}$ the causal interactions among the M series are described according to a linear time invariant multivariate autoregressive (MAR) model [Lutkepohl, 2005].

The presence of a significant causal relationship between y_i and y_k is assessed according to two traditional tests in the time domain (i.e. F-test and Wald test) [Wald, 1943].

According to the Granger causality approach y_i Granger-causes y_k over Ω_y if the exclusion of y_i from the prediction model of y_k significantly worsens the prediction of y_k.

The F-test checks whether the goodness of fit of the MAR model accounting for y_i is significantly larger than that of the MAR model excluding y_i. The null hypothesis of y_i does not Granger-cause y_k is evaluated comparing the difference between the two goodnesses of fit

with the critical value of the F distribution derived from a given type-I error probability p.

At difference with the F-test the Wald test is carried out directly on the parameters that weight the contribution of y_i towards y_k in the predicted MAR model within the set of signals Ω_y. In the case of Wald test the null hypothesis of y_i does not Granger-cause y_k implies to check whether all the predicted parameters representing the coefficients of the linear regression of y_k on y_i are not significantly different from zero. The Wald test compares the sum of the squared ratios of the values of the parameters to their standard deviation with the critical value of the χ^2 distribution derived for a given type-I error probability p [Wald, 1943].

Simulations

A large number of simulations were performed in order to evaluate the ability of the causality tests to identify uncoupled signals and to study the dependence of causality detection on the dynamical features of the series (e.g. degree of complexity and presence of dominant oscillations), variances of the residuals, gain of the pathways, resonance of the auto-loop and presence of exogenous sources.

Processes characterized by a full or partial unpredictability were generated. White Gaussian noises (WGN) realizations were generated to simulate fully unpredictable processes. Second order autoregressive processes AR(2) were generated to simulate partially predictable processes. More specifically, the phase and the modulus of a pair of complex and conjugated poles were assigned to generate a second order AR(2) process with a dominant rhythm and a given sharpness of the spectral peak.

Pairs formed by two uncoupled WGNs or two uncoupled AR(2) processes were considered to study whether causality tests can detect full uncoupling between signals with similar degree of complexity. In the case of AR(2) processes the rate of false positive was assessed

while varying frequency and sharpness of the spectral peaks. Pairs formed by a WGN and an AR(2) process were also created to examine the effects of different complexity levels of the two signals on the rate of false positives.

The ability of the causality tests to assess causality between coupled signals interacting in closed loop was checked by generating pairs of coupled signals, y_1 and y_2, according to a bivariate AR process. Causality in bivariate AR model was studied over the set $\Omega_y=\{y_1,y_2\}$. Simulations were carried out to clarify whether causality depends on the magnitude of the variances of the residuals, on the gains of the two pathways forming the close loop, and on the gain of the auto-loops.

The effect of an exogenous source on the detection of causality was evaluated by imposing the exogenous influence of a third signal, y_3, on the bivariate AR process. The signal y_3 was shaped to be a second order AR(2) process defined by a pair of complex and conjugated poles whose phase was chosen to be consistent with the physiological respiration rate.

Causality in this model was studied according to two different universes of knowledge about the system: the first universe accounted for all the signals (i.e. $\Omega_y=\{y_1,y_2,y_3\}$), while the second one excluded y_3 from the set of considered signals (i.e. $\Omega_y-\{y_3\}=\{y_1,y_2\}$).

The comparison between the results derived from the two different universes allowed the evaluation of the bias on causality between y_1 and y_2 determined by neglecting y_3. Simulations were carried out to assess the bias on causality induced by the common action of y_3 on the closed loop interactions between y_1 and y_2 and produced by the sole action of y_3 over y_1 in presence of closed loop interactions between y_1 and y_2.

Experimental protocols

Four experimental protocols were considered. Baroreflex sensitivity indexes were assessed with a traditional method based on

the calculation of the power spectrum of RR interval and SAP variability series [Pagani et al., 1988]. In order to guarantee the reliability of baroreflex sensitivity indexes, theirs calculation were performed uniquely for all those subjects exhibiting a significant correlation between RR and SAP assessed via squared coherence function [De Boer et al., 1985].

All the protocols were characterized by a depressed baroreflex regulation, thus allowing to test causality from SAP to RR in critical conditions in which this causal relation might be absent or weak, while the reverse mechanical feedforward pathway is definitely active.

- **Deep anaesthesia on animals**

Eight (8) female juvenile pigs were anesthetized intravenously with propofol as anaesthetic agent and administered at constant infusion rate. Four mechanical ventilated modes were considered: pressure controlled ventilation, pressure supported ventilation, and the random variable implementation of the previous two strategies in which the driving pressure was changed breath-by-breath according to a random Gaussian distribution. During pressure supported ventilation techniques each respiratory cycle was triggered when the initial spontaneous inspiratory airflow of the animal exceeded a predefined threshold, while during pressure controlled ventilation techniques was initiated artificially by the ventilator at a fixed rate.

ECG and invasive arterial pressure were acquired synchronously during each mechanical ventilation mode. Airflow was acquired continuously from the ventilator.

- **Deep anaesthesia on humans**

Thirty-seven (37) subjects were scheduled for craniotomy for supratentorial lesion. After the induction of propofol as intravenous anaesthetic, patients were mechanically ventilated according to a controlled ventilation approach. Anaesthesia was maintained according to two different anaesthesiological strategies involving the volatile administration of sevoflurane (18 subjects) and the

intravenous administration of propofol (19 subjects).

ECG and invasive arterial pressure were continuously monitored and recorded one hour after the craniotomy. Respiratory signal was estimated from respiratory–related ECG amplitude changes.

- **Head-up tilt and paced breathing in heart failure population**

Twenty-two (22) patients in sinus rhythm with dilated cardiomyopathy were enrolled for the study. Patients were recorded during three consecutive sessions: i) for 8 min at rest during spontaneous breathing in supine position; ii) for 8 min in supine position while breathing at a selected paced breathing frequency; iii) for 8 min tilted at 70° during spontaneous breathing.

During these three sessions ECG, lung volume and non-invasive arterial pressure were continuously recorded.

- **Head-up tilt and recovery in healthy humans**

Sixteen (16) healthy subjects were enrolled for the experimental protocol. During the entire protocol the subjects breathed spontaneously. The experimental sessions of the protocol included an initial session of 10 minutes at rest in supine position followed by two head up tilt manoeuvres at 45° and 90°, 10 minutes each, carried out in random order. Each tilt manoeuvre was followed by a recovery session of 40 minutes.

ECG, respiratory signal via thoracic belt and non-invasive arterial blood pressure were continuously recorded.

Results

- **Simulation results**

Both F-test and Wald test performed similarly in terms of detections of the causal relations.

Simulations performed on uncoupled series proved the reliability

of the statistical tests to detect the absence of a causal relation. Performances were independent of the type of dynamics, sharpness of the spectral peak and degree of unpredictability characterizing signals.

Simulations performed on coupled series operating in closed loop pointed out the dependency of the detection of causal relations on the magnitude of the variances of the residuals, namely λ^2_i with i=1,…,M, (e.g. in a bivariate AR process if $\lambda^2_1 << \lambda^2_2$ then $y_2 \rightarrow y_1$) on the gains of the pathways forming the close loop, namely $|A_{ij}|$ with {i,j}=1,…,M and i≠j, (e.g. in a bivariate AR process if $|A_{12}| << |A_{21}|$ then $y_1 \rightarrow y_2$) and on the gains of the auto-loop, namely $|H_{ii}|$ with i=1,…,M, (e.g. in a bivariate AR process if $|H_{22}| >> 1$ then $y_2 \rightarrow y_1$).

The presence of an exogenous source affecting the series operating in closed loop was able to bias the detection of the causal relation. The importance of the bias depended on the gain of the pathways linking the exogenous source to the interacting signals (e.g. in a bivariate AR process driven by an exogenous input, y_3, if $|A_{13}| >> |A_{23}|$ then $y_1 \rightarrow y_2$, where $|A_{13}|$ and $|A_{23}|$ are the gains of the pathways from y_3 to y_1 and to y_2 respectively).

Assessing causality by accounting for the exogenous source allowed the cancellation of this biasing effect.

- **Experimental protocol results**

The presence of a significant causal relation from SAP to RR was detected in a large percentage of humans or animals thus suggesting that baroreflex control actively participated to the RR-SAP regulation in all the experimental situations. Only during deep anaesthesia in humans using a volatile administration strategy the percentage of subjects exhibiting a significant link from SAP to RR was quite low (i.e. 39%).

When accounting for respiration baroreflex control was found less involved in the RR-SAP regulation in animals undergoing mechanical controlled ventilation in comparison to assisted ventilation, in humans undergoing deep anaesthesia during both volatile and intravenous

administration strategies and in healthy subjects during recovery sessions.

Causality analysis suggested differences during deep anaesthesia between different ventilatory strategies in animals (i.e. pressure controlled vs pressure supported ventilation) and between different procedures of administration of aneasthetic agents (i.e. volatile vs intravenous administration).

As expected baroreflex sensitivity was depressed during anaesthesia both in animals and humans, during paced breathing and head-up tilt in heart failure population and during tilt sessions in healthy subjects. In detail, animals undergoing deep anaesthesia showed significantly smaller values of baroreflex sensitivity during mechanical controlled ventilation in comparison to assisted ventilation. In the human subjects during deep anaesthesia in controlled ventilation intravenous anaesthesiological strategy significantly decreased baroreflex sensitivity in the HF band with respect to volatile strategy. Heart failure patients had very low values of baroreflex sensitivity in LF during paced breathing and head-up tilt manoeuvre with respect to rest. In healthy subjects baroreflex sensitivity significantly decreased during head-up tilt compared to baseline and slightly increased during recovery with respect to rest.

In all the considered situations baroreflex sensitivity derived after excluding the subjects without a significant causal relation from SAP to RR along baroreflex was not significantly different from that derived when considering solely those subjects with a significant correlation between RR and SAP series as assessed using squared coherence.

Conclusions

The Doctoral dissertation demonstrated over simulated and real data the importance of accounting for an exogenous source contaminating closed loop interactions in causality studies.

This result has been published in [Porta et al., 2011a]. The procedure to assess the consequence of disregarding an exogenous

source on causality is general with possible applications in different fields of time series analysis ranging from physiology to economy, from neuroscience to finance, from social sciences to climatology. In cardiovascular variability analysis performed during deep anaesthesia in controlled mechanical ventilation and in healthy subjects during a recovery from a sympathetic activation maneouvre such as head-up tilt, disregarding Resp leads to erroneously attribute to baroreflex the direct influences of Resp on RR.

Even though baroreflex sensitivity was depressed during anaesthesia both in animals [Wiklund et al., 2002; Kolh et al., 2004] and humans [Tanaka and Nishikawa, 1999; Sato et al., 2005], in heart failure population at rest [La Rovere et al., 1998; Pinna et al., 2005] and during head-up tilt both in healthy and heart failure population [Baselli et al., 1994; Nollo et al., 2005], analysis of causality from SAP to RR suggested that a relevant percentage of subjects preserved a significant causal relation along baroreflex.

These results, published in [Bassani et al., 2011], demonstrated that baroreflex control is still present and working both during deep anaesthesia and in heart failure population. Notable exception is under deep anaesthesia in humans using a volatile administration strategy, thus providing a tool to assess the different abilities of anaesthesiological treatments in preserving an active cardiovascular control. Causality analysis suggested also differences during deep anaesthesia between different ventilatory strategies in animals, thus making available a tool to assess the performances of different mechanical ventilation strategies.

In all the considered experimental protocols the estimate of baroreflex sensitivity computed after the exclusion of the subjects without a significant causal relation from SAP to RR along baroreflex was similar to that derived from the group of subjects with a significant RR-SAP correlation.

This result suggests that assessing causality did not improve the estimate of baroreflex sensitivity with respect to the assessment of the correlation between RR and SAP series based on squared

coherence. This result was disappointing and largely unexpected since causality from SAP to RR is a prerequisite for a reliable assessment of baroreflex sensitivity. This finding indicates that the estimate of the baroreflex sensitivity from spontaneous RR and SAP variabilities, even when causality from SAP to RR is verified, might be still affected by important biases and unaccounted influences.

It can be hypothesized that using methods for the estimation of spontaneous baroreflex sensitivity more sophisticated than that here adopted (i.e. spectral method) and, thus, less affected by biases might make clearer the advantage of introducing causality analysis in the procedure for the estimate of baroreflex sensitivity.

Contents

Abstract i

Summary iii

1 Cardiovascular Regulation Mechanisms and Granger causality 1

1.1 Cardiovascular regulation mechanism 1

1.2 Modelling the relationship between heart period and arterial pressure 3

1.3 Toward a more general model of the relationship between heart period and arterial pressure. 4

1.4 Characterization of baroreflex control 8

1.5 Granger causality approach. 9

1.5.1 Granger Causality in the time domain 10

1.5.2 Granger Causality in the frequency domain. . . 14

1.5.3 Granger Causality in the information domain . . 17

1.6 Conclusions 23

2 Advanced Methods in Testing Causality between Multiple Time Series 25

2.1 Introduction 25

2.2 Multivariate modeling. 27

2.3 Assessing Granger causality. 29

2.3.1 F-test 29

2.3.2 Wald test. 31

2.4 Conclusions 32

3 Simulations **35**
3.1 Introduction 35
3.2 Type-I simulations: detection of causality between uncoupled series 36
3.2.1 Type-I.a simulation: fully unpredictable processes 36
3.2.2 Type-I.b simulation: partially predictable processes 36
3.2.3 Type-I.c simulation: processes with different levels of predictability. 39
3.3 Type-II simulations: detection of causality between coupled series 39
3.3.1 Type-II.a simulation: effects of the magnitude of residual variances 41
3.3.2 Type-II.b simulation: effects of the closed loop pathway gains 41
3.3.3 Type-II.c simulation: effects of the auto-loop resonance 42
3.4 Type-III simulations: detection of causality between coupled series affected by an exogenous source . . . 43
3.4.1 Type-III.a simulation: effects of y_3 affecting both y_1 and y_2 44
3.4.2 Type-III.b simulation: effects of y_3 affecting uniquely y_1 45
3.5 Conclusions 45

4 Experimental Protocols and Data Analysis **47**
4.1 Introduction 47
4.2 Deep anaesthesia on animals 48
4.3 Deep anaesthesia on human subjects 49
4.4 Paced breathing and head-up tilt manoeuvre in pathological subjects 50
4.5 Head-up tilt manoeuvres in healthy subjects 51
4.6 Extraction of beat-to-beat variability series. 52

4.7 Assessing causality along baroreflex. 54
4.8 Assessing baroreflex sensitivity 55
4.9 Statistical analysis 57
4.10 Conclusions 58

5 Simulation Results **61**
5.1 Introduction 61
5.2 Type-I simulations: results 62
5.3 Type-II simulations: results. 66
5.3.1 Type-II.a simulation: effects of the residuals variance magnitude 66
5.3.2 Type-II.b simulation: effects of the closed loop pathways gains 67
5.3.3 Type-II.c simulation: effects of the auto-loop resonance 68
5.4 Type-III simulations: results 70
5.4.1 Type-III.a simulation: effects of y_3 affecting y_1 and y_2 70
5.4.2 Type-III.b simulation: effects of y_3 affecting uniquely y_1 72
5.5 Conclusions 74

6 Experimental Results **75**
6.1 Introduction 75
6.2 Deep anaesthesia on animals 76
6.2.1 Causality along baroreflex in animals 76
6.2.2 Baroreflex sensitivity in animals. 78
6.3 Deep anaesthesia on human subjects 80
6.3.1 Causality along baroreflex in humans 80
6.3.2 Baroreflex sensitivity in humans 81
6.4 Paced breathing and head-up tilt manoeuvre in heart failure subjects. 83
6.4.1 Causality along baroreflex in heart failure subjects 83

6.4.2 Baroreflex sensitivity in heart failure subjects . 84
6.5 Head-up tilt maneuvers in healthy subjects 86
6.5.1 Causality along baroreflex in healthy subjects . 86
6.5.2 Baroreflex sensitivity in healthy subjects . . . 88
6.6 Conclusions 90

7 Discussion and Conclusion 91
7.1 Assessing causality along baroreflex in situations depressing baroreflex regulation 91
7.2 Assessing Granger causality in time domain using F- test and Wald test 93
7.2.1 Reliability of F-test and Wald test in assessing Granger causality. 94
7.2.2 Assessing reliability of time-domain Granger causality tests over uncoupled signals 95
7.2.3 Assessing reliability of time-domain Granger causality tests over coupled signals interacting in closed loop. 95
7.2.4 Assessing reliability of time-domain Granger causality tests over coupled signals interacting in closed loop under the action of an exogenous input 97
7.3 Assessing causality along baroreflex in experimental protocols. 98
7.3.1 Assessing causality along baroreflex under deep anaesthesia in animals. 99
7.3.2 Assessing causality along baroreflex under deep anaesthesia in humans. 100
7.3.3 Assessing causality along baroreflex in heart failure subjects 102
7.3.4 Assessing causality along baroreflex in healthy subjects 103
7.4 Conclusions 104
7.5 Limitations and future developments 105

Appendix A. **107**

Bibliography **117**

List of Tables

3.1 Type-I.b.1 simulation: AR(2) processes with assigned phases and random modulus. 38
3.2 Type-I.b.2 simulation: AR(2) processes with assigned modulus and random phases. 38
3.3 Summary of performed simulations. 46
5.1 Type-I simulation results. 62
6.1 Percentages of significant coherence function and detected causality relation in animals during deep anaesthesia 77
6.2 Significance of differences between significant coherence function at LF in animals during deep anaesthesia 78
6.3 Percentages of significant coherence function and detected causality relation in humans during deep anaesthesia 80
6.4 Significance of differences between causality relations detected accounting for and excluding Resp in humans during deep anaesthesia 81
6.5 Percentages of significant coherence function and detected causality relation in heart failure subjects . . . 83
6.6 Percentages of significant coherence function and detected causality relation in healthy subjects. 86
6.7 Significance of differences between significant coherence function at LF in healthy subjects. 87
6.8 Significance of difference between accounting for and excluding Resp in healthy subjects 88

A.1.I RR indexes in animals during deep anaesthesia . . . 108
A.1.II SAP indexes in animals during deep anaesthesia . . . 109
A.1.III Squared coherence in animals during deep anaesthesia 109
A.2.I RR indexes in humans during deep anaesthesia . . . 110
A.2.II SAP indexes in humans during deep anaesthesia . . . 111
A.2.III Squared coherence in humans during deep anaesthesia 111
A.3.I RR indexes in heart failure subjects 112
A.3.II SAP indexes in heart failure subjects 113
A.3.III Squared coherence in heart failure subjects 113
A.4.I RR indexes in healthy subjects 114
A.4.II SAP indexes in healthy subjects 115
A.4.III Squared coherence in healthy subjects 115

List of Figures

1.1 Block diagram scheme interpreting cardiovascular regulation control mechanisms 2
1.2 Block diagram scheme interpreting blood pressure feedback regulating mechanism 4
1.3 Closed loop model of the arterial pressure regulation . . 5
1.4 Block diagram describing the closed loop interactions between heart period and systolic arterial pressure accounting for the effects of respiration. 7
1.5 Example of schemes of causal interactions 11
1.6 Example of diagram depicting the coupling strength of the interactions among cardiovascular variables in pre-eclampisia. 12
1.7 Example of linear causality index among subcortical local field potentials before and after the visual event in a cat 14
1.8 Example of causal coherence causality index in heart transplant subjects 16
1.9 Example of partial directed coherence assessing causality between cortex and thalamus in rats 17
1.10 Example of cross-conditional entropy approach applied during head-up tilt with different inclinations 19
1.11 Example of conditional mutual information method applied to EEG recordings in an epileptic patient. 21
1.12 Examples of real and surrogate data obtained when assessing causality through conditional entropy estimation in EEG signals. 22
3.1 Bivariate AR model generating type-II closed loop

interacting series. 40
3.2 Bivariate AR model plus the contribution of exogenous source generating type-III closed loop interacting series 43
4.1 Example of beat values location over ECG, arterial pressure and respiration signals 53
4.2 Example of beat-to-beat RR, SAP and Resp series extraction. 54
5.1 Example of relation between modulus of AR(2) processes in type-I.b simulation detected causality 64
5.2 Example of relation between phases of AR(2) processes in type-I.b simulation detected causality 65
5.3 Type-II.a simulation results 67
5.4 Type-II.b simulation results 68
5.5 Type-II.c simulation results 69
5.6 Type-III.a simulation results 71
5.7 Type-III.b simulation results 73
6.1 Baroreflex sensitivity indexes results in animals during deep anaesthesia 79
6.2 Baroreflex sensitivity indexes results in humans during deep anaesthesia 82
6.3 Baroreflex sensitivity indexes results in heart failure subjects. 85
6.4 Baroreflex sensitivity indexes results in healthy subjects . 89

Chapter 1

Cardiovascular Regulation Mechanisms and Granger Causality

1.1 Cardiovascular regulation mechanisms

The observation that cardiovascular variables such as heart period and systolic arterial pressure exhibit, when considered on a beat-to-beat basis, small, non random, changes around their mean values with a frequency well below the heart rate (below 0.5 Hz in humans) has intrigued physicians, physiologists and biophysicists (see Cohen and Taylor [2002] for a review of these pioneering studies) and prompted them to interpret these variations as an evidence of the cardiovascular regulation.

The maintenance of the homeostasis of the entire organism, the fulfilment of the needs of all its sub-districts and the accomplishment of all tasks typical of a lively human being are the major determinants of the complexity of the cardiovascular regulation. The complexity of cardiovascular control mechanisms has been clearly outlined by Koepchen et al. [1984].

As illustrated in Fig. 1.1 the regulation of cardiovascular variables is assumed to be the result of the action of multiple feed-back systems and autonomous self-sustained oscillators.

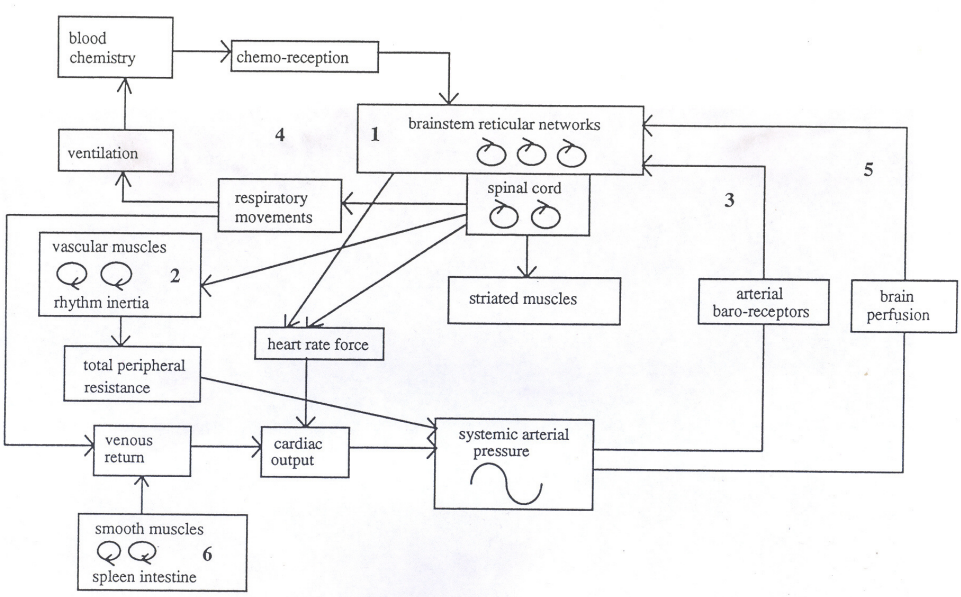

Fig. 1.1: Block diagram scheme proposed by Koepchen et al. [1984] to interpret cardiovascular regulation control mechanisms. Heart rate is regulated by self-sustained autonomous oscillators (1), arterial pressure through baroreceptive mechanism (3), respiration through chemoreceptive mechanism (4) and cerebral pressure via brain perfusion feedback (5). Arterial pressure is affected by cardiac output, cardiac contractility, heart rate, respiration, vasomotion (6) and peripheral resistance (2).

Heart rate force is affected by the triggering action of self-sustained autonomous oscillators situated at brain stem and spinal cord level modulating vagal and sympathetic outflows, by brain perfusion feedback, by systemic arterial pressure control governed by baroreceptor inputs, and by respiration through chemoreceptive mechanisms. Systemic arterial pressure is affected by cardiac contractility, heart rate, cardiac output, respiration, smooth muscles activity (i.e. vasomotion) and peripheral resistance.

1.2 Modelling the relationship between heart period and arterial pressure

Although heart rate and blood pressure are influenced by several control mechanisms, the complexity of the interactions between these two variables is usually simplified by considering their closed loop relation and disregarding all the other above-mentioned mechanisms [Laude et al., 2004; Taylor and Eckberg, 1996]. This approach, although very trivial, makes sense when considering the quickness of the baroreflex control with respect to other regulatory mechanisms (e.g. chemoreflex) and its incessant action even during baseline conditions compared to other mechanisms taking priority in threatening situations (e.g. brain perfusion regulation).

Baroreflex feedback is one of the most important short-term neural control system aiming at guarantee the homeostasis of the organism [Cohen and Taylor, 2002]. Arterial pressure perturbations, sensed by the baroreceptors, induces, through the involvement of the regulatory centres of the autonomic nervous system, the activation of the efferent vagal and sympathetic fibers directed to the heart and, thus, the modification of heart period.

Figure 1.2 shows baroreflex feedback regulation scheme proposed by Pedotti [1989]. The autonomic nervous system, in response to the activation of baroreceptors, modulates heart rate through parasympathetic and sympathetic fibres. Changes of heart rate

produce modifications of cardiac output and, in turn, variations of blood pressure. Baroreflex reacts to an increase of blood pressure by diminishing heart rate, while a decrease of blood pressure leads to an increase of heart rate, thus limiting arterial pressure variations.

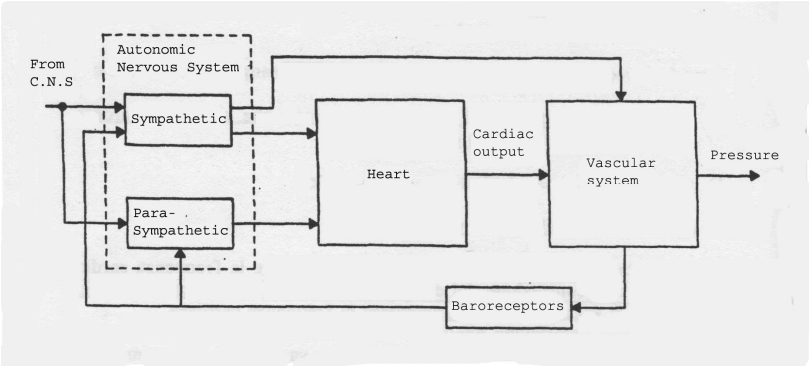

Fig. 1.2: Block diagram scheme interpreting blood pressure feedback regulating mechanism mediated by the autonomic nervous system The reflex is triggered by the activity of baroreceptors. Parasympathetic fibres, innerving heart, act in diminishing heart rate while parasympathetic fibres, innerving both heart and vascular system, act in augmenting heart rate and vascular resistance. From Pedotti [1989].

1.3 Toward a more general model of the relationship between heart period and arterial pressure

Kitney et al. [1982] proposed a non-linear model interpreting the respiratory sinus arrhythmia (i.e. the spontaneous variability of heart rate at the respiratory frequency) as the effect of the interaction of respiration and baroreceptor loop. As shown in Fig. 1.3, the baroreceptor loop, which controls arterial blood pressure, is directly affected by respiration. This model takes into account the direct effect of respiration on autonomic centres located at the brain stem and

spinal cord levels but it disregards the direct influences of respiration on heart rate and blood pressure.

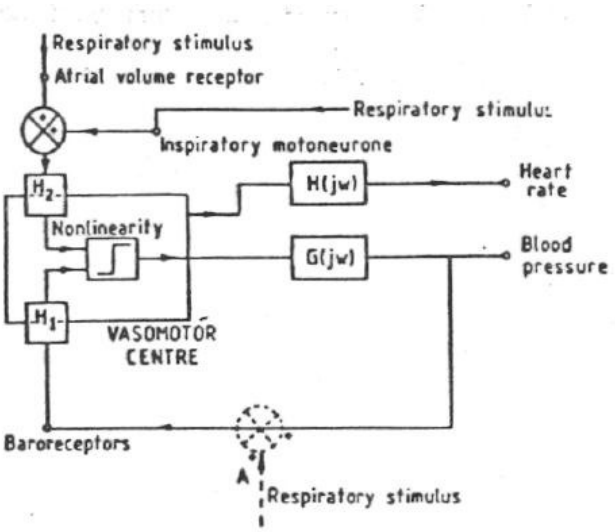

Fig. 1.3: Closed loop model of the arterial pressure regulation proposed by Kitney et al. [1982]. G(jω) is the frequency response of the block converting neural cardiac inputs into arterial pressure changes; H_1 and H_2 are gain factors; and H(jω) is the frequency response of the block linking neural cardiac inputs to heart rate. Respiration affects directly vasomotor centres but only indirectly heart rate and blood pressure.

Baselli et al. [1988] make the Kitney's model more complete by modelling, in addition to the closed loop interactions between heart period (RR) and systolic arterial pressure (SAP), the direct influences of respiration (Resp) on both SAP and RR. As shown in Fig. 1.4, Baselli et al. [1988] modelled the SAP changes as caused by RR variations according to diastolic runoff and Starling's law (i.e. the mechanical feedforward pathway) and the RR changes as caused by SAP

variations through the activation of baroreceptors (i.e. the baroreflex feedback).

Respiration directly affects SAP and, indirectly, RR through baroreflex. The direct effect of Resp on SAP described the effects of intra-thoracic pressure and venous return changes leading to modification of left and right ventricular preloads, stroke volume and level of arterial pressure [De Boer et al., 1987; Innes et al., 1993; Toska and Eriksen, 1993].

Respiration directly affects RR and, indirectly, SAP via the mechanical feedforward. The direct effects of Resp on RR account for cardiopulmonary reflexes from lung receptors (sensing the variations of tidal volume) and from atrial receptors (sensing the variations in the cardiac filling) [Bainbridge, 1915; Desai et al., 1997], for the coupling between respiratory and autonomic centres modulating vagal and sympathetic efferent activities directed to the heart [Eckberg, 2003; Gilbey et al., 1984], and for direct mechanical influences of changes of the thoracic pressure on the sinus node activity [Bernardi et al., 1989].

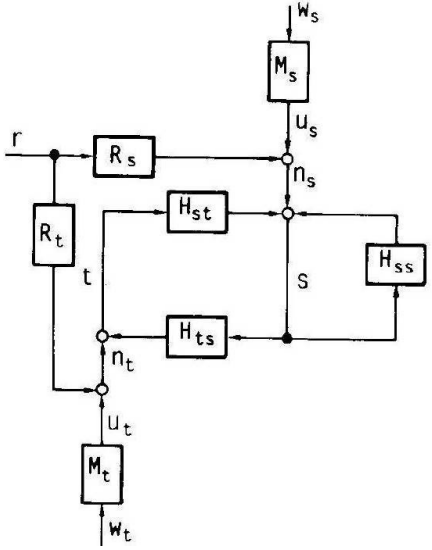

Legend

w_s, w_t = white noises

u_s, u_t = inputs of external or central origin to the s-t-s regulating loop

M_s, M_t = spectral factors of u_s and u_t

R_s = direct effect of r on s (changes in chest pressure, in venous return, etc..)

R_t = direct effect of r on t (changes induced by lung receptors, atrial pressure receptors, central effects, etc..)

H_{st} = non-neural effects of t on s

H_{ts} = baroreceptor and neural mechanisms

H_{ss} = vascular control, peripheral resistances and arterial compliances, myocardial contractility, venous return, etc..

n_s = disturbance on s independent from t and ffom the past of s

n_t = disturbance on t independent from s

Fig. 1.4: Block diagram describing the closed loop interactions between heart period (t) and systolic arterial pressure (s) and the effects of respiration (r) on both [Baselli et al., 1988]. The physiological mechanisms, which are taken into account in the suggested model, are listed in the legend.

1.4 Characterization of baroreflex control

The characterization of baroreflex regulation is mainly carried out through the assessment of baroreflex sensitivity [La Rovere et al., 1998]. In clinics the baroreflex sensitivity is traditionally assessed as the variation of RR per unit change of SAP induced by the administration of a vasoactive drug [Smyth et al., 1969].

More sophisticated techniques exploited random respiration approach or made use of surgical procedures opening closed loop baroreflex regulation to reliably infer baroreflex sensitivity [Kashihara et al., 2008; Saul et al., 1991].

Recently, several non-invasive techniques based on the analysis of the spontaneous beat-to-beat RR and SAP variabilities [Laude et al., 2004] have been proposed for the estimation of the baroreflex sensitivity in more physiological conditions, without the need of perturbing cardiovascular regulation with an artificial stimulus such as a pharmacological intervention, experimental manoeuvre or surgical procedure [Kashihara et al., 2008; Saul et al., 1991; Smyth et al., 1969].

Non-invasive techniques exploiting spontaneous RR and SAP variabilities are helpful in assessing baroreflex sensitivity only when causality is along baroreflex (i.e. SAP changes contribute to RR variations) [Porta et al., 2000]. Unfortunately, this prerequisite is not properly tested.

Usually, assessing the significance of squared coherence function between RR and SAP series is considered to be sufficient [De Boer et al., 1985], but unfortunately it can be high even when RR variations contribute to SAP changes along the reverse causal direction [Porta et al., 2002]. Indeed, RR can cause SAP variations via the Starling law (a longer RR induces a larger left ventricular filling and, in turn, a larger SAP at the next cardiac beat) and the diastolic runoff (a longer RR induces a smaller diastolic pressure and, thus a smaller SAP at a given pulse pressure).

Without testing causality from SAP to RR any estimate of the baroreflex sensitivity derived from spontaneous variabilities could be conversely related to the gain of the feed-forward mechanical pathway linking RR to SAP [Porta et al., 2002], thus prompting for the inclusion of the concept of causality when assessing baroreflex sensitivity.

Taking into account causality could lead to a more reliable estimate of baroreflex sensitivity derived from spontaneous cardiovascular variabilities.

1.5 Granger causality approach

A practical approach to the assessment of causality in time series analysis has been proposed by Clive Granger, the Nobel prize in economy winner in 2003.

Granger causality assessment is based on the concept of predictability improvement. According to the definition of Granger causality, if a signal y_1 "Granger-causes" a signal y_2, then past values of y_1 contain information that helps to predict y_2 above and beyond the information contained in past values of y_2 alone.

Its mathematical formulation is based on a linear regression modelling of stochastic processes [Granger, 1969; 1980]. Granger causality was developed in 1960s and has been widely used in economics since the 1960s. However, it is only within the last few decades that it has become more and more frequently applied to evaluate cardiovascular and cardiorespiratory interactions [Riedl et al., 2010; Faes et al., 2008; Porta et al., 2002; Marinazzo et al., 2006, Nollo et al., 2009; Verdes, 2005], to detect directionality in neural signals [Palus et al., 2001; Faes et al., 2011; Hesse et al., 2003; Schelter et al., 2009; Kaminski et al., 2001; Dhamala et al., 2008, Wang et al., 2007], and to asses brain connectivity [Bernasconi and König, 1999; Sameshima and Baccalà, 1999; Sitnikova et al.,

2008; Roebroeck et al., 2004; Londei et al., 2006; Chàvez et al., 2003; Astolfi et al., 2006].

Several approaches have been developed since the general formulation given by Granger. These approaches can be roughly categorized according to the domains exploited to interpret causal interactions (i.e. time, frequency and information domains).

1.5.1 Granger causality in the time domain

The assessment of Granger causality approach in time domain is based on a statistical test for determining whether one signal is useful in forecasting another. The interaction between the supposed "cause" and "effect" is commonly described by means of multivariate linear parametric models. The causality test is based on the assessment of whether the introduction of the supposed "cause" in the model describing the dynamics of the supposed "effect" is able to improve prediction of the "effect" signal [Lutkepohl, 2005].

The original approach proposed by Granger exploited the linear modeling framework. However this approach has been extended to non parametric and non linear kernels [Bell at al., 1996; Freiwald et al., 1999]. Nonlinear extended Granger causality was applied by Chen et al. [2010] to multiple nonlinear interacting signals. Chen et al. [2010] proposed a conditional extended Granger causality measure to determine whether the causal relation between two signals was direct or mediated by another process.

In Fig. 1.5 the graph describes two typical situations explored by Chen et al [2010]: in both Figs. 1.5a and 1.5b the causal interaction between B and C are perturbed by a third signal A. The only limitation related to this method is represented by the need of large amount of data required for a reliable analysis. This limitation prevents its exploitation over short data sequences usually utilized in short-term cardiovascular variability studies (i.e. about 300 samples).

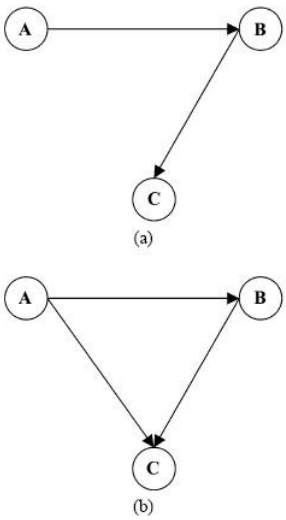

Fig. 1.5: Two schemes of causal interactions studied in Chen et al. [2010]. (a) A drives B and B drives C. (b) A drives both B and C in presence of a direct pathway from B to C.

Granger causality in time domain approach has been applied both in cardiovascular and neuroscience fields.

Causality approach was exploited to assess coupling among cardiovascular variables in pre-eclampsia [Reidl et al., 2010], a serious pregnancy-specific disorder causing significant neonatal and maternal morbidity and mortality. Riedl et al [2010] investigated the nonlinear coupling between Resp, SAP and diastolic arterial pressure (DAP), and heart rate.

It was found a significant increased respiratory influence on DAP and heart rate in patients affected by pre-eclampsia (Fig. 1.6). Interestingly the influence of SAP on the heart rate was weak (Fig. 1.6), thus indicating that baroreflex was not actively involved in the regulation of cardiovascular system in pre-eclampsia and raising the

issue of the reliability of baroreflex sensitivity estimates in this pathological condition. It is worth noting that the influence of Resp was stronger on heart rate than on SAP (Fig. 1.6).

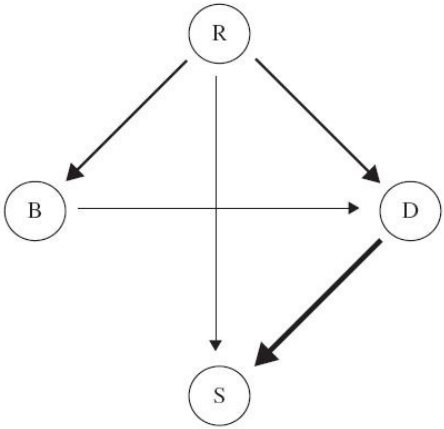

Fig. 1.6: Diagram depicting the coupling strength of the interactions among heart rate (B), Resp (R), DAP (D) and SAP (S) in patients suffering from pre-eclampsia [Riedl et al., 2010]. The thickness of the arrows encodes the magnitude of the link between the interacting signals.

In the field of neuroscience Bernasconi and König [1999] applied Granger causality approach to investigate the directionality of neural interactions. Bernasconi and König [1999] assessed the linear relationship among the subcortical local field potentials from the cat visual system. They applied causality analysis to pairs of signals corresponding to recordings from the supragranular layers and from granular and infragranular layers.

As shown in Fig. 1.7, they was able to assess causality from the supragranular layers to granular and infragranular layers before and

after the visual event in cats. They noted that after visual event the coupling in the direction from supragranular to infragranular layers was significantly stronger than in the reverse direction.

Finally they pointed out that the adopted approach can offered valuable insights into brain functioning that would had be very difficult to obtain using other methods. Bernasconi and König [1999] also underlined how the test implemented to determinate Granger causality (i.e. Wald statistic, [Wald, 1943]) seemed to have the most favourable properties over short data sequences in comparison to more sophisticated approaches involving likelihood ratio statistics [Geweke et al., 1983].

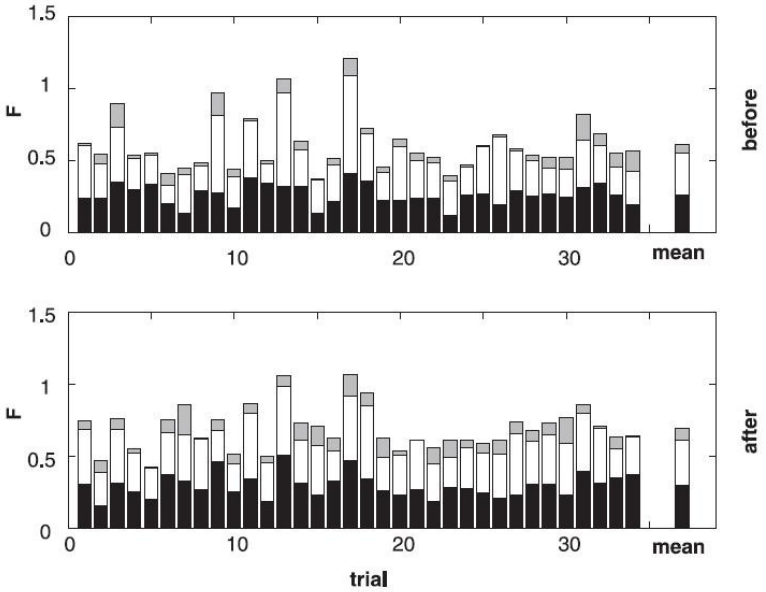

Fig. 1.7: Example of linear causality index (F) before (upper row) and after (lower row) the visual event in a cat (34 trials). The signal pairs for coupling analysis correspond to recordings from the supragranular layers and from granular and infragranular layers. Black bars quantify causality from the second group to the first; white bars refer to the opposite direction and grey bars indicate the amount of instantaneous dependence. From Bernasconi and König [1999].

1.5.2 Granger causality in the frequency domain

The assessment of Granger causality approach in frequency domain is usually performed by assessing correlation between signals along a given causal direction of the interactions at a given frequency.

The value of correlation calculated over the original signals is compared with a threshold derived from a surrogate data set.

Surrogate data set are usually constructed according to the null hypothesis of absence of interactions among signals. A typical surrogate data is constructed by preserving power spectral densities and distribution of all the considered signals but randomizing phases according to different random realizations (i.e. phase randomized isospectral isodistribution surrogates) [Schreiber and Schmitz, 2000]. Due to phase randomization with different white noise realizations all the signals are uncoupled.

In the exploration of the interactions among cardiovascular variables, Porta et al. [2002] defined and applied the causal coherence to quantify the degree of correlation along the causal direction from SAP to RR and vice-versa.

Causal coherence function was compared with traditional coherence function [De Boer et al. 1985]. The proposed method allowed Porta et al. [2002] to demonstrate that in subjects underwent heart transplantation, in which SAP variations did not cause RR interval changes as a result of the cardiac denervation, the method correctly detected a significant coupling only along the pathway from RR to SAP.

As shown in Fig. 1.8 the traditional coherence function confirmed that the two series were significantly linked at high frequency (HF) (Fig. 1.8c). However, only the application of the causal coherence showed that this coupling was the result of a causal relationship from RR to SAP, while the link in the reverse baroreflex causal direction was virtually absent.

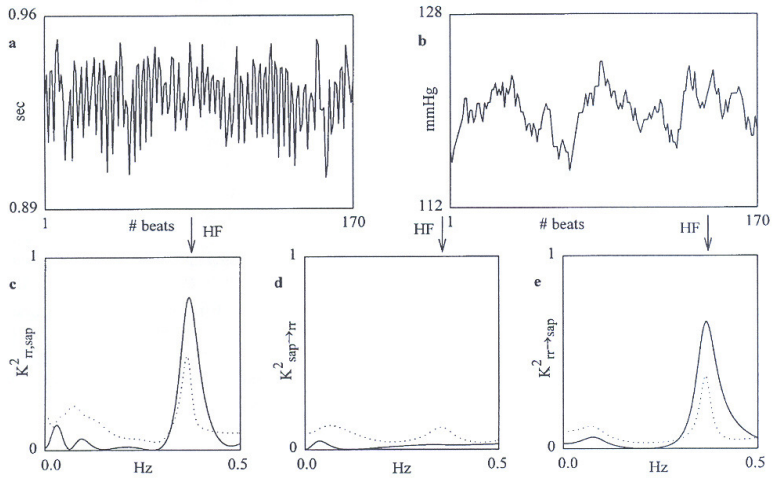

Fig. 1.8: Example of beat-to-beat series of RR and SAP in a subject after recent heart transplantation (a,b). The squared coherence function $K^2_{rr,sap}$ (c, solid line) and its significance threshold (dotted line), assessed according to a surrogate data approach, is compared to the causal coherence from sap to rr $K^2_{sap\to rr}$ (d) and from rr to sap $K^2_{rr\to sap}$ (e). It is worth noting in (d) the absence of the coupling along the baroreflex feedback sap→rr. From [Porta et al., 2002].

Sameshima and Baccalà [1999] applied Granger causality in frequency domain in the field of neuroscience. The authors defined and applied the partial directed coherence function to describe neuronal ensemble interactions. They compared partial directed coherence with traditional squared coherence function.

As shown in Fig. 1.9, the proposed method allowed the authors to demonstrate that partial directed coherence went a step beyond classical coherence because of its ability to suggest the direction of information flow from cortex to thalamus in rats engaged in exploratory activity.

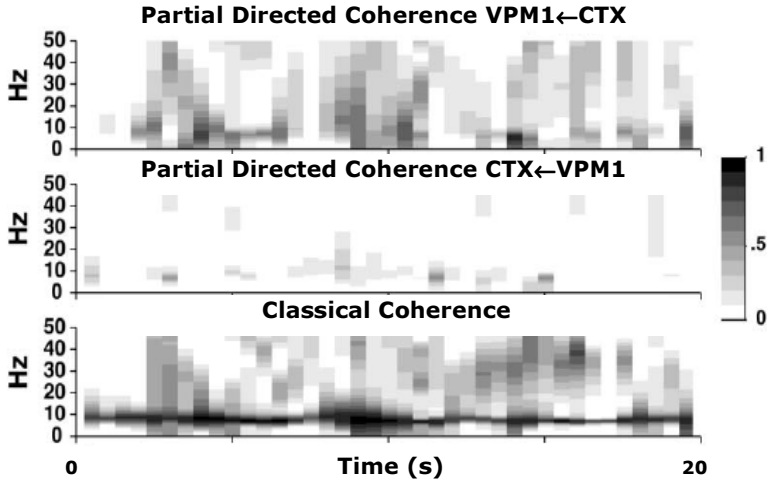

Fig. 1.9: Time-frequency representation of causality revealed consistent and predominant flow of information from cortex (CTX) to thalamus (VPM1) in a rat engaged in exploratory activity (upper panel). Evidence of connection in the reverse direction (feed-back) can be detected in the middle of the record (middle panel). Traditional coherence was unable to derive this information (lower panel). From Sameshima and Baccalà [1999].

1.5.3 Granger causality in the information domain

The assessment of Granger causality approach in the information domain is designed to quantify the exchange of information between two, or more, variables [Hlavackova-Schindler et al., 2007].

An advantage of the information domain approach in causality analysis is that it is sensitive to nonlinear signal properties and do not assume a model of the interactions. In this domain y_2 is said to Granger-causes y_1 whether the inclusion of past values of the signal y_2 decreases the amount of information carried by the signal y_1 (y_2 allows a better prediction of y_1) above and beyond past values of y_1.

The key feature for assessing causality in the information domain is the assessment of the conditional entropy of a signal given another one (or more).

In the exploration of the interactions among cardiovascular variables Porta et al. [2011b] applied cross-conditional entropy [Porta et al., 1999] to assess causality between RR and SAP in heart transplant recipients and during graded head-up tilt manoeuvre on healthy subjects. The authors compared the information domain causal approach with a more traditional method involving the assessment of cross-spectral phases, their transformation into delays or advancements and their comparison with the baroreflex latency.

The cross-conditional entropy method allowed Porta et al. [2011b] to detect a lack of causal relation from SAP to RR in recent heart transplant recipients and the gradual restoration of the causal link from SAP to RR with time after transplantation. It was also found that (Fig. 1.10C) head-up tilt protocol induced the progressive shift from the prevalent causal direction from RR to SAP at rest to the reverse causality from SAP to RR during head-up tilt.

Furthermore, the comparison of the results of causality analysis with those derived from cross-spectral approach (i.e. assessment of phases) suggested that that information-based causality approach is more efficient because it does not require the knowledge of baroreflex latency conversely necessary in the cross-spectral approach.

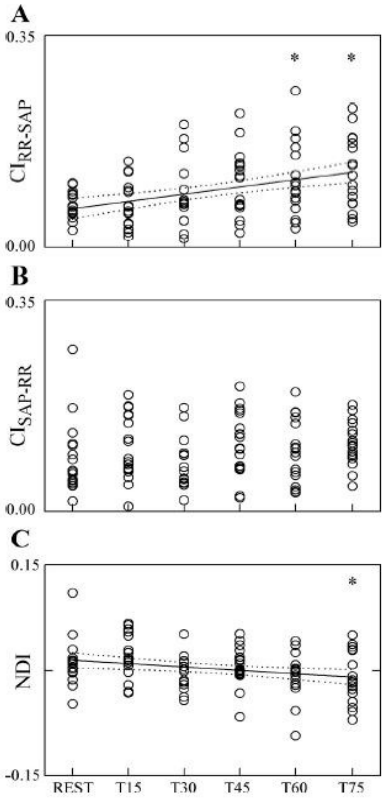

Fig. 1.10: Each circle represents an individual value of the coupling index from SAP to RR (CI_{RR-SAP}; A), coupling index from RR to SAP (CI_{SAP-RR}; B), and normalized directionality index NDI (C) defined as $NDI=(CI_{SAP-RR}-CI_{RR-SAP})/(CI_{SAP-RR}+ CI_{RR-SAP})$ during the graded head-up tilt protocol. CI was assessed using a cross-conditional entropy approach at rest (REST) and during head-up tilt with different inclinations of the tilt table angle (TXX where XX indicates the degrees of the angle). The linear regressions (solid line) calculated overall the values and their 95% confidence intervals (dotted lines) are plotted as well when the slope of the regression line was found significantly different from 0. From Porta et al. [2011b].

An information domain approach was proposed by Palus et al. [2001] in the field of neurosciences for studying synchronization phenomena in experimental bivariate time series. The authors introduced a conditional mutual information measure between signals. This measure allows to quantify the amount of information exchanged between two systems and to establish the direction of information flow between coupled systems, thus discerning the driving system from the driven one. The method introduced was then applied to EEG recordings derived from an epileptic patient.

As shown in Fig. 1.11, in correspondence of the epileptic seizure the amount of information carried by the two signals increased (Fig. 1.11c). The mutual information increases as well, thus suggesting that the two channels, uncoupled before the seizure, start sharing a large amount of information (Fig. 1.11c). Since the amount of information of X given Y is smaller than that of Y given X (Fig. 1.11d) it can be hypothesized that the direction of the information flow is from Y to X, thus allowing the localization of the primary epilectogenic areas.

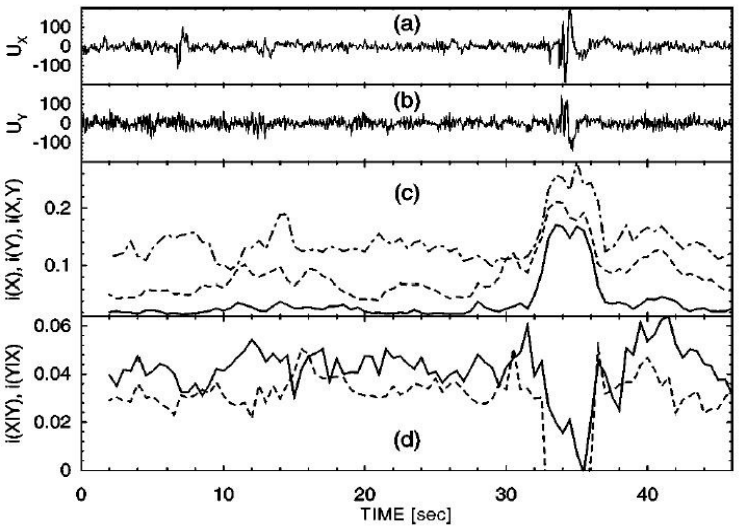

Fig. 1.11: An EEG segment with a short seizure, recorded from two different leads U_x (a) U_y (b). (c) The information carried by X, i(X) (dashed line), the information carried by Y, i(Y) (dash-and-dotted line) and the mutual information carried by X and Y. i(X,Y) (full line). (d) The conditional mutual information of X given Y, i(X|Y) (dashed line) and of Y given X, i(Y|X) (full line). From Palus et al. [2001].

Testing causality of the interactions with an information domain approach requires a comparison between the index derived from the original signals with the distribution of such an index under the null hypothesis of absence of coupling over the assigned causal direction.

As the analytic distribution of the proposed causality measure under the null hypothesis of absence of casual interactions is not available, the use of surrogates data to empirically build the distribution is, thus, necessary. Figure 1.12 [Faes et al., 2011] shows the results obtained from real and surrogate data obtained when assessing causality through conditional entropy estimation among

multiple time series extracted from EEG signals acquired in different cortical areas. As shown in Fig. 1.12a Faes et al. [2011] found statistically significant causal relations from posterior cortical area to central and frontal areas in condition of closed eyes, thus indicating that the EEG activity in this situation propagates mainly along a back-to-front direction, while front-to-back propagation is absent.

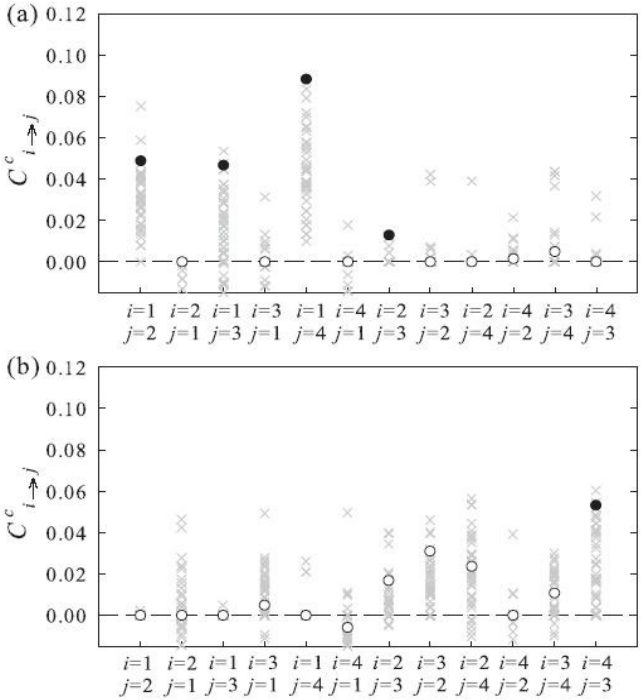

Fig. 1.12: Application of the procedure for non uniform multivariate embedding to EEG signals measured with eyes closed (a) and with eyes open (b). Each plot depicts the estimated causal coupling from X_i to X_j ($C^c_{i\to j}$) evaluated for the original series (circles) and for the set of surrogate series (gray crosses). Filled circles represent statistically significant causal coupling. X_1=posterior cortical area; X_2=left central; X_3=right central; X_4=frontal. From Faes et al. [2011].

1.6 Conclusions

The present chapter describes the complexity of cardiovascular regulation through some examples of modelling approaches proposed in the scientific literature to describe and interpret the physiological mechanisms.

The attention has been focused in particular on the relation between heart period and arterial blood pressure, and on the direct effects that respiration plays on both. Heart period and arterial blood pressure interactions play an important role in cardiovascular control since they involve both neural reflexes (e.g. baroreflex) and mechanical pathways (e.g. cardiac contractility).

The estimate of baroreflex sensitivity (i.e. the most utilized parameter to describe baroreflex) with non-invasive techniques is reliable only when causality is along baroreflex. Unfortunately, this prerequisite is not properly tested.

According to the necessity of a reliable assessment of baroreflex sensitivity, this PhD dissertation explores Granger causality approach.

This chapter reviews applications of Granger causality approaches in time, frequency and information domains, to both cardiovascular and neuroscience research fields. Several examples were listed to stress the broad-band applications of this approach in several fields of science.

Chapter 2

Advanced Methods in Testing Causality between Multiple Time Series

2.1 Introduction

The parametric modelling approach is widely used to describe the interaction between time series [Xiao et al., 2005; Batzel et al., 2009; Porta et al, 2009].

While monovariate signal analysis techniques (e.g., power spectral analysis) may be applied to quantify the magnitude of the fluctuations in specific frequency bands, multivariate system identification approaches permit the dynamic characterization of the causal interactions among cardiovascular regulatory mechanisms responsible for coupling the variability between signals (e.g. heart rate, arterial pressure and respiratory signal) [Xiao et al., 2005; Batzel et al., 2009; Porta et al., 2009]. Multivariate characterization is not solely helpful both to derive information about the gain and phase of the relationship linking any signal pair but also to estimate causality (i.e. who drives whom) in multivariate recordings.

Causality is usually tested in time [Riedl et al., 2010; Bernasconi and König, 1999; Marinazzo et al., 2006; Hesse et al., 2003; Sitnikova et al., 2008; Roebroeck et al., 2004; Londei et al., 2006], frequency [Sameshima and Baccalà, 1999; Kaminski et al., 2001;

Porta et al., 2002; Schelter et al., 2009; Dhamala et al., 2008; Wang et al., 2007; Astolfi et al., 2006] and information domains [Palus et al., 2001; Hlavackova-Schindler et al., 2007; Faes et al., 2011; Verdes, 2005; Chàvez et al., 2003].

Methods assessing causality in time domain has three advantages rendering them more appealing than those in frequency and information domain ones: i) they do not need to assume that the cardiovascular control mechanisms occur along specific temporal scales as in the case of techniques in the frequency domain; ii) the percentage of false causality detections can be rigorously kept under control by assigning the type I error probability accepted by the tests; iii) the distribution of the statistic assessing causality under the null hypothesis of absence of a causal relationship between the two series follows classical statistical distributions, thus allowing the analytical calculation of the critical value above which the null hypothesis is rejected (conversely techniques in frequency and information domain require time consuming Montecarlo techniques based on surrogate data generation) [Faes et al., 2010].

In the following chapter a linear time invariant multivariate parametric modelling approach chosen to characterize the interactions among a set of signals is presented. This modelling approach is exploited to infer causality in the time domain according to the Granger causality paradigm.

Two statistical tests (i.e. F-test and Wald test) assessing the Granger causality in the time domain and implemented according to the modelling strategy are described.

2.2 Multivariate modelling

Given the series $Y_1=\{Y_1(n),\ n=1,\ldots,N\}$, $Y_2=\{Y_2(n),\ n=1,\ldots,N\}$, … , $Y_M=\{Y_M(n),\ n=1,\ldots,N\}$ where n is the progressive counter and N is the series length, they are first demeaned and, then, divided by the standard deviation, thus obtaining y_1, y_2, …, y_M series with zero mean and unit variance. The set of M signals, $\Omega_y=\{y_1,y_2,\ldots,y_M\}$, represents the universe of our knowledge about the system under examination where all possible signals are included and none of them can be completely derived from the others.

The causal interactions among the M series can be described according to a multivariate AR (MAR) process [Soderstrom and Stoica, 1988]

$$y(n)=A(z)\times y(n)+w(n) \tag{2.1}$$

where $y=||y_1\ \ y_2\ \ldots\ y_M||^T$ is the column vector of the signals (the symbol ^{T} denotes the transpose operator), $w=||w_1\ w_2\ \ldots\ w_M||^T$ is the column vector of the zero mean white Gaussian noises uncorrelated each other even at zero lag with variances λ^2_1, λ^2_2, ..., λ^2_M respectively, and A(z) is the MxM matrix of causal finite impulse response filters of order p describing the interactions among signals.

The elements of A(z) along the main diagonal

$$A_{kk}(z)=\sum_{j=1}^{p} a_{kk}(j)\cdot z^{-j} \tag{2.2}$$

describe the dependence of y_k on its own past values ($1\le k\le M$), while the elements outside the main diagonal

$$A_{kl}(z)=\sum_{j=\tau_{kl}}^{p} a_{kl}(j)\cdot z^{-j} \tag{2.3}$$

describe the dependence of y_k on past values of y_l ($l\ne k$ and

$1 \le k,l \le M$), where z^{-1} is the one delay operator in the z-domain (i.e. $z^{-1} \cdot y_k(n)=y_k(n-1)$). While (2.2) suggests that immediate effects of y_k on itself are not allowed (i.e. $a_{kk}(0)=0$), (2.3) suggests that immediate effects of y_l on y_k might be allowed by setting $\tau_{kl}=0$ according to the structure chosen for $A(z)|_{z=\infty}$. The condition $a_{kk}(0)=0$ avoids the impractical immediate action of $y_k(n)$ over itself, while the specific structure chosen for $A(z)|_{z=\infty}$ prevents the formation of loops involving several different variables with circular effects without delays.

When expressed in terms of prediction the MAR process [Lutkepohl, 2005] is given by

$$\hat{y}(n)=\hat{A}(z)\times y(n) \tag{2.4}$$

where $\hat{y}(n)$ represents the best prediction of $y(n)$ given present and past values of y (i.e. $y(k)$ with $k \le n$) and $\hat{A}(z)$ is the matrix $A(z)$ where the coefficients of the polynomials are estimated according to an optimization criterion (here the least squares approach minimizing the determinant of the variance matrix of w) [Soderstrom and Stoica, 1988]. More specifically, the prediction of y_k,

$$\hat{y}_{k,ARX_{M-|\{k\}|}}(n)=\hat{A}_{kk}(z)\times y_k(n)+\sum_{j=1,\ldots,M}^{j\neq k}\hat{A}_{kj}(z)\times y_j(n) \tag{2.5}$$

assumes the form of a linear regression over past values of y_k (i.e. the AR part) and over current and past values of M-|{k}| X inputs (i.e. all the series with the exclusion of y_k), where |{k}| denotes the cardinality of {k} (i.e. |{k}|=1).

2.3 Assessing Granger causality

By definition, a time series y_i is said to Granger-cause y_k if it can be shown that the past values of y_i provide statistically significant information about future values of y_k. In other words, we say that y_i is causing y_k if we are better able to predict y_k using all available information rather than if the information apart from y_i had been used [Granger, 1969].

2.3.1 F-test

According to the Granger causality approach y_i Granger-causes y_k over Ω_y, in the following indicated as $y_i \rightarrow y_k|_{\Omega_y}$, if the exclusion of y_i from the prediction model of y_k

$$\hat{y}_{k,ARX_{M-|\{k,i\}|}}(n)=\hat{A}_{kk}(z)\times y_k(n)+\sum_{j=1,..,M}^{j\neq k,j\neq i}\hat{A}_{kj}(z)\times y_j(n) \tag{2.6}$$

significantly worsens the prediction of y_k [Granger, 1969]. The mean squared prediction error is utilized to quantify the ability to predict y_k as

$$\hat{\lambda}^2_{k,ARX_{M-|\{k\}|}}=\frac{1}{N}\sum_{n=1}^{N}(y_k(n)-\hat{y}_{k,ARX_{M-|\{k\}|}}(n))^2 \tag{2.7}$$

in the case of (2.5), and

$$\hat{\lambda}^2_{k,ARX_{M-|\{k,i\}|}}=\frac{1}{N}\sum_{n=1}^{N}(y_k(n)-\hat{y}_{k,ARX_{M-|\{k,i\}|}}(n))^2 \tag{2.8}$$

in the case of (2.6). Due to normalization of the series both (2.7) and (2.8) range from 0, indicating perfect prediction, to 1, suggesting

null fitting. Therefore, if $\hat{\lambda}^2_{k,ARX_{M-|\{k,i\}|}}$ is significantly larger than $\hat{\lambda}^2_{k,ARX_{M-|\{k\}|}}$, then $y_i \rightarrow y_k|_{\Omega_y}$.

The comparison between $\hat{\lambda}^2_{k,ARX_{M-|\{k,i\}|}}$ and $\hat{\lambda}^2_{k,ARX_{M-|\{k\}|}}$ is carried out according to the F-test [Soderstrom et al., 1988]. If

$$F_{y_i \rightarrow y_k|_{\Omega_y}} = \frac{(\hat{\lambda}^2_{k,ARX_{M-|\{k,i\}|}} - \hat{\lambda}^2_{k,ARX_{M-|\{k\}|}})}{\hat{\lambda}^2_{k,ARX_{M-|\{k\}|}}} \cdot \cdot \frac{[N-p-(M-|\{k\}|)\cdot(p+1)+\sum_{j=1,\ldots,M}^{j\neq k}\tau_{kj}]}{(p+1-\tau_{ki})} \qquad (2.9)$$

is larger than the critical value of the F distribution derived from a given type-I error probability, p, (the degrees of freedom of the numerator and denominator are equal to $p+1-\tau_{ki}$ and $N-p-(M-|\{k\}|)\cdot(p+1)+\sum_{j=1,\ldots,M}^{j\neq k}\tau_{kj}$ respectively), the null hypothesis that y_i does not Granger-cause y_k is rejected and the alternative hypothesis of $y_i \rightarrow y_k|_{\Omega_y}$ is accepted (unidirectional causality from y_i to y_k). Reversing the role of y_i and y_k allows the assessment of $y_k \rightarrow y_i|_{\Omega_y}$.

If both $y_i \rightarrow y_k|_{\Omega_y}$ and $y_k \rightarrow y_i|_{\Omega_y}$ are contemporaneously found, a closed loop relation (bidirectional causality) can be argued (i.e. $y_i \leftrightarrow y_k|_{\Omega_y}$). If the null hypothesis that y_i does not Granger-cause y_k and vice versa cannot be rejected, y_i and y_k are uncoupled over Ω_y.

2.3.2 Wald test

In the Wald test [Wald, 1943] the series y_k is modeled as in (2.5). At difference with the F-test the Wald test is carried out directly on the coefficients, $a_{ki}(j)$'s, of $A_{ki}(z)$. Instead of the mean squared prediction error: the null hypothesis of y_i does not Granger-cause y_k implies that $a_{ki}(j)=0$ for all $j=\tau_{ki},\dots,p$.

Let us be $\varphi(n)=||y_k(n-1),\dots,y_k(n-p)\ \dots\ y_i(n-\tau_{ki}),\dots,y_i(n-p)\ \dots\ y_{M-1}(n-\tau_{k(M-1)}),\dots,y_{M-1}(n-p)||^T$ the column vector containing the past values of y_k (i.e. the AR part) and the current and past values of M-|{k}| X inputs (i.e. all the series with the exclusion of y_k), and $a_k=||a_{kk}(1),\dots, a_{kk}(p)\ \dots\ a_{ki}(\tau_{ki}),\dots,a_{ki}(p)\ \dots\ a_{k(M-1)}(\tau_{k(M-1)}),\dots,a_{k(M-1)}(p)||^T$, the column vector of model parameters, the solution of the least squares identification problem of the ARX model [Soderstrom and Stoica, 1988] is

$$\hat{a}_k=\frac{R(N)^{-1}}{N}\times\sum_{n=1}^{N}\varphi(n)\times y(n) \tag{2.10}$$

where R(N) is the covariance matrix of the data

$$R(N)=\frac{1}{N}\sum_{n=1}^{N}\varphi(n)\times\varphi^T(n) \tag{2.11}$$

The covariance matrix of $\hat{a}_k$ depends on the covariance matrix of the data, R(N), and on the mean squared prediction error of the ARX model, $\hat{\lambda}^2_{k,ARX_{M-|\{k\}|}}$, as follows [Soderstrom and Stoica, 1988]

$$\mathrm{var}\left[\hat{a}_k\right]=\frac{R(N)^{-1}}{N}\cdot\hat{\lambda}^2_{k,ARX_{M-|\{k\}|}} \tag{2.12}$$

The Wald test compares the value of $\hat{a}_k$ with respect to a proposed value a_0 under the assumption that the difference $(\hat{a}_k - a_0)$ is a random variable with covariance $var[\hat{a}_k]$ whose asymptotic distribution converges to a Gaussian distribution under the weak condition of the central limit theorem.

Comparison is limited only to the part of $\hat{a}_k$ relevant to the coefficients of $\hat{A}_{ki}(z)$ (i.e. $\hat{a}_{ki} = ||\hat{a}_{ki}(\tau_{ki}),\ldots,\hat{a}_{ki}(p)||^T$) and to the part of $var[\hat{a}_k]$ relevant to the covariance of $\hat{a}_{ki}$ (i.e. $var[\hat{a}_{ki}]$). Thus, the Wald test [Wald, 1943] checks whether the value

$$W_{ki}=(\hat{a}_{ki}-a_0)^T \times var[\hat{a}_{ki}]^{-1} \times (\hat{a}_{ki}-a_0) \tag{2.13}$$

is larger enough to reject the null hypothesis of absence of causality from y_i to y_k. Under this null hypothesis a_0 is the null vector (i.e. $a_0(j)=0$ for all $j=\tau_{ki},\ldots,p$).

The calculated W_{ki} value is compared with the critical value of the χ^2 distribution with $p-\tau_{ki}+1$ degrees of freedom derived for a given type-I error probability, p. If W_{ki} is larger than the critical value the null hypothesis that y_i does not Granger-cause y_k is rejected and the alternative hypothesis of a significant causal relationship from y_i to y_k is accepted.

2.4 Conclusions

The present chapter describes in detail F-test and Wald test as advanced methods to assess Granger causality in the time domain. Both statistical tests are successful and widely utilized to characterize the interactions among multiple signals.

While F-test evaluates the hypothesis of lack of causality between the supposed "cause" and "effect" signals by assessing the predictability improvement of accounting for "cause" when predicting

"effect", Wald test is carried out directly on the coefficients that weight the contribution of "cause" in the prediction of "effect".

Chapter 3

Simulations

3.1 Introduction

Simulations represents a fundamental tool when assessing the reliability of an advanced method for the evaluation of causality relation between discrete series [Baselli et al., 1988; Porta et al., 2002].

In the following chapter are presented the numerous simulations performed in order: I) to evaluate the ability of the causality tests to identify uncoupled series in dependence of theirs degree of complexity and presence of dominant oscillations (i.e. type-I simulations); II) to study the dependence of causality detection on the dynamical features (e.g. variances of the residuals, gain of the pathways, resonance of the auto-loop) of coupled series operating in closed loop (i.e. type-II simulations); III) to assess the bias on causality between coupled series operating in closed loop due to the presence of exogenous sources (i.e. type-III simulations).

In all the performed simulations the series were first demeaned and, then, divided by the standard deviation, thus obtaining series with zero mean and unit variance before applying causality analysis. In every type of simulation 1000 realizations were generated. The series length was 300 samples.

3.2 Type-I simulations: detection of causality between uncoupled series

Type-I simulations deal with uncoupled series. Being uncoupled pairs consistent with the null hypothesis of lack of causality between the two series, a detection of causal interactions between the two series was considered a false positive and the percentage of false positives was monitored. Uncoupled processes were generated simply by modifying the seed of white noise utilized to generate the final process.

We generated processes characterized by a full (i.e. white noises) or partial unpredictability (i.e. autoregressive processes).

Uncoupled pairs of white noises were analyzed in type-I.a simulation. Uncoupled pairs of autoregressive processes were considered in type-I.b simulation. Uncoupled pairs formed by a white noise and an autoregressive process were analyzed in type-I.c simulation.

Type-I simulations were generated to better understand whether different predictability levels played a role in producing false detections of causality.

3.2.1 Type-I.a simulation: fully unpredictable processes

Realizations of White Gaussian noises (WGNs) with zero mean and unit variance were generated to simulate fully unpredictable processes. Realizations were generated with different seeds, thus being all uncoupled. Pairs of WGNs underwent causality analysis.

3.2.2 Type-I.b simulation: partially predictable processes

Second order autoregressive processes AR(2) realizations driven by WGNs were generated to simulate partially predictable processes.

More specifically, we assigned the phase, φ, and the modulus, ρ, of the pair of complex and conjugated poles characterizing the transfer function of the AR(2) to generate a process with a dominant rhythm and a given sharpness of the spectral peak. While the frequency of the dominant rhythm of the AR(2) depends on the chosen value of φ, the dominant spectral peak becomes sharper with ρ (i.e. the sharpness decreases with the distance between the poles and the unit circle in the complex plane).

Two different strategies of simulation were followed to generate the series y_1 and y_2: in the type-I.b.1 simulation we assigned the pole phase difference, φ_2-φ_1=$\Delta\varphi$, while the pole modulus, ρ_1 and ρ_2, were randomly selected inside the range 0.1 to 0.9; in the type-I.b.2 simulation we assigned the pole modulus difference, ρ_2-ρ_1=$\Delta\rho$, while the pole phases, φ_1 and φ_2, were randomly selected inside the range from 0.03 to 0.5 cycles/sample. AR(2) realizations were generated with different seeds, thus being all uncoupled. Pairs of AR(2) processes underwent causality analysis.

Table 3.1 illustrates type-I.b.1 simulations. In order to evaluate the effect of separation between spectral peaks of the two signals on the rate of false positives, $\Delta\varphi$ was assigned to: i) 0.01 cycles/sample, with φ_1=0.10 and φ_2=0.11 cycles/sample; ii) 0.01 cycles/sample, with φ_1=0.26 and φ_2=0.25 cycles/sample; iii) 0.05 cycles/sample, with φ_1=0.05 and φ_2=0.1 cycles/sample; iv) 0.15 cycles/sample, with φ_1=0.1 and φ_2=0.25 cycles/sample; v) 0.20 cycles/sample, with φ_1=0.05 and φ_2=0.25 cycles/sample; vi) 0.4 cycles/sample, with φ_1=0.05 and φ_2=0.45 cycles/sample.

TABLE 3.1

Type-I.b.1 SIMULATION SUBTYPES: AR(2) PROCESSES WITH ASSIGNED PHASE φ_2 AND φ_1 ($\Delta\varphi=\varphi_2-\varphi_1$) EXPRESSED IN CYCLE/SAMPLE AND RANDOM MODULUS RANGING FROM 0.1 TO 0.9

Simulation subtype	φ_2	φ_1	$\Delta\varphi$
i	0.11	0.10	0.01
ii	0.26	0.25	0.01
iii	0.10	0.05	0.05
iv	0.25	0.10	0.15
v	0.25	0.05	0.20
vi	0.45	0.05	0.40

As reported in Table 3.2, in the type-I.b.2 simulations, in order to evaluate the effect of the different degree of regularity of the two signals on the rate of false positives, $\Delta\rho$ was assigned to: i) 0.04, with ρ_1=0.90 and ρ_2=0.94; ii) 0.14, with ρ_1=0.80 and ρ_2=0.94; iii) 0.34, with ρ_1=0.60 and ρ_2=0.94.

TABLE 3.2

Type-I.b.2 SIMULATION SUBTYPES: AR(2) PROCESSES WITH ASSIGNED MODULUS ρ_2 AND ρ_1 ($\Delta\rho=\rho_2-\rho_1$) AND RANDOM PHASES RANGING FROM 0.03 TO 0.5 CYCLES/SAMPLE

Simulation subtype	ρ_2	ρ_1	$\Delta\rho$
i	0.94	0.90	0.04
ii	0.94	0.80	0.14
iii	0.94	0.60	0.34

3.2.3 Type-I.c simulation: processes with different levels of predictability

Uncoupled pairs formed by a WGN and an AR(2) process were also created to examine the effects of completely different levels of complexity of the two signals on the rate of false positives. The modulus and phase of the AR(2) process were varied in the range from 0.1 to 0.9 and from 0.03 to 0.5 respectively.

3.3 Type-II simulations: detection of causality between coupled series

The ability of the causality tests to assess causality between coupled signals interacting in closed loop was checked by generating pairs of coupled signals, y_1 and y_2, according to a bivariate AR process as described in the model shown in Fig. 3.1 where w_1 and w_2 are uncorrelated zero mean Gaussian white noises with variances λ^2_1 and λ^2_2 respectively.

The model was designed to simulate the closed loop interactions between y_2 and y_1 via the gains a_{12} and a_{21}, the delays τ_{12} and τ_{21} and the resonance mechanism on y_2 capable to amplify y_2 through the parameters of $a_{22}(1)$ and $a_{22}(2)$ defined in $A_{22}(z)$ as $A_{22}(z) = a_{22}(1) \cdot z^{-1} + a_{22}(2) \cdot z^{-2}$, where z^{-1} is the one delay operator in the z-domain (i.e. $z^{-1} \cdot y_k(n) = y_k(n-1)$).

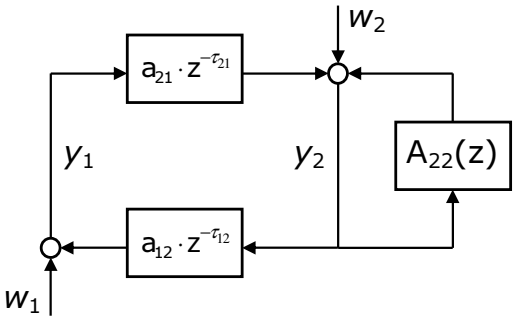

Fig. 3.1: Bivariate AR model driven with uncorrelated WGNs (i.e. w_1 and w_2) and generating closed loop interacting series y_1 and y_2.

According to the model choice the difference equations describing the interaction of the discrete series $y_1(n)$ and $y_2(n)$ (with n=1,…,N) are shown in equations (3.1) and (3.2) respectively:

$$y_1(n)=a_{12} \cdot y_2(n-\tau_{12})+w_1(n) \tag{3.1}$$

$$\begin{aligned} y_2(n) = {} & a_{22}(1) \cdot y_2(n-1) + a_{22}(2) \cdot y_2(n-2) + \\ & + a_{21} \cdot y_1(n-\tau_{21}) + w_2(n) \end{aligned} \tag{3.2}$$

Causality in bivariate AR model was studied over the set $\Omega_y=\{y_1,y_2\}$. Three types of simulations were carried out to clarify whether causality depends on the magnitude of the variances of the residuals (i.e. type-II.a simulation), on the gains of the two pathways forming the closed loop (i.e. type-II.b simulation), and on the resonance of the auto-loop (i.e. type-II.c simulation).

3.3.1 Type-II.a simulation: effects of the magnitude of residual variances

In the type-II.a bivariate simulation a_{21}=-0.7 and a_{12}=0.7 set the closed loop interaction between y_1 and y_2, $a_{22}(1)$=0 and $a_{22}(2)$=0 excluded the effects of the auto-loop on y_2, λ^2_1 was varied in the set {0.001, 0.01, 0.1, 1, 10, 100, 1000} with λ^2_2=1, thus progressively increasing the importance of w_1 over w_2.

The delays in the closed loop were fixed to τ_{21}=2 and τ_{12}=0. The values of the gains and of the delays characterizing the closed loop were chosen in order to guarantee a stable resonance peak at 0.25 cycles/sample. The difference equations (3.1) and (3.2) thus becoming as described by (3.3) and (3.4):

$$y_1(n) = 0.7 \cdot y_2(n) + w_1(n) \tag{3.3}$$

$$y_2(n) = -0.7 \cdot y_1(n-2) + w_2(n) \tag{3.4}$$

3.3.2 Type-II.b simulation: effects of the closed loop pathway gains

In the type-II.b bivariate simulation the importance of the noises, w_1 and w_2, were maintained equal (i.e. $\lambda^2_1=\lambda^2_2$=1), while the gain of the two pathways forming the closed loop, a_{12} and a_{21}, were progressively unbalanced by varying the ratio $|a_{12}/a_{21}|$ in the set {10000, 100, 1, 100, 10000}.

In order to maintain model stability, the product $|a_{12}\cdot a_{21}|$ was less than 1 and kept constant (i.e. $|a_{12}\cdot a_{21}|$=0.49): thus, the selected pairs of parameters were a_{12}=70 and a_{21}=-0.007, a_{12}=7 and a_{21}=-0.07, a_{12}=0.7 and a_{21}=-0.7, a_{12}=0.07 and a_{21}=-7, and a_{12}=0.007 and a_{21}=-70. As in type-II.a bivariate simulation auto-loop on y_2 was prevented ($a_{22}(1)=a_{22}(2)$=0) and the delays in the closed loop were τ_{21}=2 and τ_{12}=0.

The difference equations (3.1) and (3.2) thus becoming as described by (3.5) and (3.6):

$$y_1(n) = a_{12} \cdot y_2(n) + w_1(n) \tag{3.5}$$

$$y_2(n) = a_{21} \cdot y_1(n-2) + w_2(n) \tag{3.6}$$

3.3.3 Type-II.c simulation: effects of the auto-loop resonance

Differently with type-II.a and type-II.b bivariate simulation in type-II.c bivariate simulation the coefficients $a_{22}(1)$ and $a_{22}(2)$ were different from 0 to study the effects of an auto-loop on y_2.

The transfer function of the auto-loop was $H_{22}(z)=1/(1-A_{22}(z))$ with $A_{22}(z)=a_{22}(1)\cdot z^{-1}+a_{22}(2)\cdot z^{-2}$. Parameters $a_{22}(1)$ and $a_{22}(2)$ were chosen such a way that $H_{22}(z)$ exhibited a pair of complex and conjugated poles with phases $\varphi=\pm 0.1$ cycles/sample and modulus $\rho=0.7$, thus producing a resonance peak of 3.34.

As in the type-II.a bivariate simulation $a_{21}=-0.7$ and $a_{12}=0.7$ imposed the closed loop interactions between y_1 and y_2 and λ^2_1 was varied in the set $\{0.001, 0.01, 0.1, 1, 10, 100, 1000\}$ with $\lambda^2_2=1$ to increase the importance of w_1 over w_2.

The delays in the closed loop were fixed to $\tau_{21}=2$ and $\tau_{12}=0$. The difference equations (3.1) and (3.2) thus becoming as described by (3.7) and (3.8):

$$y_1(n) = 0.7 \cdot y_2(n) + w_1(n) \tag{3.7}$$

$$\begin{aligned} y_2(n) = {} & a_{22}(1) \cdot y_2(n-1) + a_{22}(2) \cdot y_2(n-2) + \\ & - 0.7 \cdot y_1(n-2) + w_2(n) \end{aligned} \tag{3.8}$$

3.4 Type-III simulations: detection of causality between coupled series affected by an exogenous source

Causality was evaluated on the trivariate AR process modeled as shown in Fig. 3.2 imposing the exogenous (X) influence of a third signal, y_3, on the bivariate AR process described by (3.1) and (3.2).

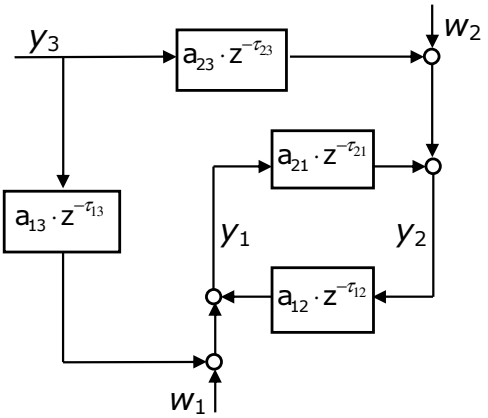

Fig. 3.2: Bivariate AR model driven with uncorrelated WGNs (i.e. w_1 and w_2) plus the contribution of an exogenous source y_3 affecting the closed loop interacting series y_1 and y_2.

According to the model choice, the difference equations describing the interaction of the discrete series y_1 and y_2 are shown in equations (3.9) and (3.10) respectively:

$$y_1(n) = a_{12} \cdot y_2(n - \tau_{12}) + a_{13} \cdot y_3(n - \tau_{13}) + w_1(n) \tag{3.9}$$

$$\begin{aligned} y_2(n) = {} & a_{22}(1) \cdot y_2(n-1) + a_{22}(2) \cdot y_2(n-2) + \\ & + a_{21} \cdot y_1(n - \tau_{21}) + a_{23} \cdot y_3(n - \tau_{23}) + w_2(n) \end{aligned} \tag{3.10}$$

The series y_3 was shaped to be a second order AR(2) process defined by a pair of complex and conjugated poles with phases $\varphi=\pm 0.35$ cycles/sample and modulus $\rho=0.85$. The variance of y_3 was imposed to be equal to 1. The action of y_3 on y_1 was modeled according to the gain a_{13} and the delay τ_{13}, while that on y_2 according to the gain a_{23} and the delay τ_{23}.

Causality in this model was studied according to two different universes of knowledge about the system: the first universe accounted for all the signals (i.e. $\Omega_y=\{y_1,y_2,y_3\}$), while the second one excluded y_3 from the set of considered signals (i.e. $\Omega_y-\{y_3\}=\{y_1,y_2\}$).

The comparison between the results derived from the two different universes allows the evaluation of the bias on causality between y_1 and y_2 determined by neglecting y_3.

The first type of simulation (i.e. type-III.a trivariate simulation) assessed the bias on causality induced by the common action of y_3 on the closed loop interactions between y_1 and y_2, while the second type of simulation (i.e. type-III.b trivariate simulation) evaluated the bias produced by the sole action of y_3 over y_1 in presence of closed loop interactions between y_1 and y_2.

3.4.1 Type-III.a simulation: effects of y_3 affecting both y_1 and y_2

In the type-III.a trivariate simulation the parameters $a_{21}=-0.7$, $a_{12}=0.7$, $a_{22}(1)=a_{22}(2)=0$, $\lambda^2_1=0.001$, $\lambda^2_2=1$, $a^2_{23}=1$ (with $\tau_{21}=2$ and $\tau_{12}=\tau_{13}=\tau_{23}=0$) were kept constant, while a^2_{13} was varied in the set $\{0.001, 0.01, 0.1, 1, 10, 100, 1000\}$. The difference equations (3.9) and (3.10) thus becoming as described by (3.11) and (3.12):

$$y_1(n) = 0.7 \cdot y_2(n) + a_{13} \cdot y_3(n) + w_1(n) \tag{3.11}$$

$$y_2(n) = -0.7 \cdot y_1(n-2) + y_3(n) + w_2(n) \tag{3.12}$$

Since both a^2_{13} and a^2_{23} were different from 0, y_3 contaminated both y_1 and y_2, but the relative magnitude of the influences were modulated according to the changes imposed to a^2_{13}. Indeed, the X influences of y_3 on y_1 were smaller than those on y_2 when a^2_{13}=0.001, 0.01 and 0.1. The opposite situation was observed when a^2_{13}=10, 100 and 1000. The X influences of y_3 on y_1 and y_2 were balanced when a^2_{13}=1.

3.4.2 Type-III.b simulation: effects of y_3 affecting uniquely y_1

In the type-III.b trivariate simulation the parameters were set as in type-III.a trivariate simulation except for a^2_{23}=0. Like in type-III.a trivariate simulation a^2_{13} was varied in the set {0.001, 0.01, 0.1, 1, 10, 100, 1000}. Since $a^2_{13}\neq 0$ while a^2_{23}=0, y_3 contaminated directly y_1 and indirectly y_2 through the link from y_1 to y_2. The magnitude of influences varied according to the changes imposed to a^2_{13}. The difference equations (3.9) and (3.10) thus becoming as described by (3.13) and (3.14):

$$y_1(n) = 0.7 \cdot y_2(n) + a_{13} \cdot y_3(n) + w_1(n) \tag{3.13}$$

$$y_2(n) = -0.7 \cdot y_1(n-2) + w_2(n) \tag{3.14}$$

3.5 Conclusions

The present chapter illustrates the numerous simulations performed in order to assess the reliability of the method (i.e. F-test and Wald test) exploited for the evaluation of causality relations in the time domain. The structures of the simulations are set up to check the ability of the causality tests to: I) identify uncoupled series; II) study the dependence of causality on specific features of the model describing the interactions among series; III) assess the bias on

causality between coupled series operating in closed loop due to the presence of an exogenous source. Table 3.3 summarizes the entire set of simulations.

TABLE 3.3

SUMMARY OF SIMULATIONS SET UP TO ASSESS THE RELIABILITY OF GRANGER CAUSALITY TESTS AND TO LINK RESULTS WITH SPECIFIC FEATURES OF THE MODEL

<table>
<tr><td rowspan="4">type-I
(uncoupled series)</td><td colspan="2">type-I.a
(fully unpredictable processes)</td></tr>
<tr><td rowspan="2">type-I.b
(predictable processes with dominant oscillations)</td><td>type-I.b.1 (vi subtypes)
(effects of the frequency of the dominant rhythm on causality)</td></tr>
<tr><td>type-I.b.2 (iii subtypes)
(effects of the sharpness of the spectral peak on causality)</td></tr>
<tr><td colspan="2">type-I.c
(effects of different degree of complexity on causality)</td></tr>
<tr><td rowspan="3">type-II
(coupled series operating in closed loop)</td><td colspan="2">type-II.a
(effects of magnitude of residual variances on causality)</td></tr>
<tr><td colspan="2">type-II.b
(effects of closed loop pathway gains on causality)</td></tr>
<tr><td colspan="2">type-II.c
(effects of auto-loop resonance on causality)</td></tr>
<tr><td rowspan="2">type-III
(exogenous source affecting coupled series)</td><td colspan="2">type-III.a
(effect of an exogenous source affecting both coupled series on causality)</td></tr>
<tr><td colspan="2">type-III.b
(effects of an exogenous source affecting uniquely one series on causality)</td></tr>
</table>

Chapter 4

Experimental Protocols and Data Analysis

4.1 Introduction

In this chapter four experimental protocols known to be able to depress baroreflex regulation are presented. The protocols have been chosen because they allow to test causality from SAP to RR in critical conditions in which this causal relation might be absent or weak.

The first protocol was designed to assess baroreflex control during controlled or supported mechanical ventilation during deep intravenous anaesthesia on animals.

The second protocol investigated baroreflex control during volatile and intravenous anaesthetic administration strategies during deep anaesthesia on humans in mechanical controlled ventilation.

The third protocol explored the effects of paced breathing and head-up tilt manoeuvre in pathological humans affected by dilated cardiomyopathy.

The last protocol investigated the effects on baroreflex control induced by head-up manoeuvres at different tilt table angles in healthy humans.

In the following the protocols and the data analysis approaches to assess causality along baroreflex and baroreflex sensitivity are reviewed in detail.

4.2 Deep anaesthesia on animals

Data belong to a database acquired thanks to the collaboration with the Department of Anaesthesia and Intensive Care, University Hospital of Dresden, Germany.

After approval by the local Animal Care Committee, eight (8) female juvenile pigs (32–42 kg) were anaesthetized intravenously with propofol as sedative agent and fentanest as analgesic. They were, intubated and instrumented with a catheter in the femoral artery.

Four mechanically ventilated (MV) modes were considered: pressure controlled ventilation (PCV), pressure supported ventilation (PSV), and the random variable implementation of the two (nPCV and nPSV respectively) in which the driving pressure is changed breath-by-breath according to a random Gaussian distribution with desired mean and standard deviation [Gama de Abreu et al., 2008].

During PSV and nPSV each respiratory cycle was triggered when the initial spontaneous inspiratory airflow of the animal exceeded a predefined threshold (5-7L/min), while during PCV and nPCV was initiated artificially by the ventilator at a fixed rate [Tobin, 2001].

Then, in all modes, a positive driving pressure was delivered by the ventilator until a cycling-off condition occurred, namely the airflow went below a given percentage of the peak inspiratory airflow (15-25%) during PSV and nPSV, or after a fixed time during PCV and nPCV. These cycling off conditions were manually adjusted to achieve an inspiration/expiration ratio (IEr) of 0.3.

The inspiratory driving pressure was tuned cycle-by-cycle by an automatic control system [Beda et al., 2010] to achieve a target mean tidal volume (V_T) of 12ml/kg in all modes, a random breath-by-breath V_T variability of 30% for nPCV and nPSV [Spieth et al., 2009], and no variability for PCV and PSV. Finally, the inspiration was followed by passive expiration.

Then, the animals underwent 30 minutes of each MV modes in a randomized order according to a Latin square design. Throughout the

experimental protocol, anaesthetic agents were administered at constant infusion rates, the inspired fraction of O_2 was 0.4 and the positive end-expiratory pressure was 5 cmH_2O.

One non-standard lead of ECG and arterial blood pressure from the femoral artery were acquired synchronously during the last 20 minutes of each MV mode with sampling frequency of 2 kHz. Airflow was acquired continuously from the ventilator and synchronized off-line with the other signals. The respiratory volume signal was obtained integrating in time the airflow ventilator signal.

4.3 Deep anaesthesia on human subjects

This database contains data recorded during the Neuromorfeo trial [Citerio et al., 2009] designed to compare volatile and intravenous anaesthetics for neurosurgical procedures in elective craniotomy.

Thirty seven (37) subjects (age range from 18 to 75 years) were scheduled for craniotomy for supratentorial lesion. All subjects did not exhibit signs of intracranial hypertension, were in good physical state (ASA I-III, Glasgow Coma Scale equal to 15) and were randomly assigned to one of two strategies of anaesthesia.

Anaesthesia was induced with propofol, a sedative-hypnotic agent, as intravenous anaesthetic agent (2-3 $mg \cdot Kg^{-1}$ i.v.) and remifentanil, an antagonist of opioid μ-receptor, as analgesic (0.25 $mg \cdot Kg^{-1} \cdot min^{-1}$ i.v. infused for 3 minutes) for both techniques. After intubation of the trachea, patients were mechanically ventilated with an inspire mixture of air and oxygen (2:1). Ventilation was carried out using a closed breathing system (fresh gas flow of 0.75 $L \cdot min^{-1}$ oxygen and 1.5 $L \cdot min^{-1}$ air during anaesthesia). Ventilatory rate and amplitude was adjusted to achieve an end-tidal carbon dioxide of 30-35 mmHg.

Anaesthesia was maintained according to two different strategies involving the volatile administration of sevoflurane, a halogenated inhalational anesthetic agent, plus remifentanil (VA, 18 subjects) or the intravenous administration (IA, 19 subjects) of propofol plus

remifentanil. The sevoflurane was maintained in a 0.75 to 1.25 MAC range, while propofol was maintained with continuous infusion at 10 $mg \cdot Kg^{-1} \cdot h^{-1}$ for the first 10 minutes, then reduced to 8 $mg \cdot Kg^{-1} \cdot h^{-1}$ for the next 10 minutes and reduced to 6 $mg \cdot Kg^{-1} \cdot h^{-1}$ thereafter. The dosage and the administration of drugs were strictly imposed during the surgeries for both groups.

ECG (lead II) and invasive arterial pressure from the femoral artery were continuously monitored and recorded from the patient-monitor one hour after craniotomy. Signals were sampled at 250 Hz.

4.4 Paced breathing and head-up tilt manoeuvre in pathological subjects

Data belong to a database acquired thanks to the collaboration with the Department of Bioengineering of the IRCCS Institution Fondazione Maugeri, Pavia, Italy.

Twenty two (22) patients (age 57 ± 8, mean ± std) in sinus rhythm with dilated cardiomyopathy were enrolled for the study. All patients were under beta-blocker and showed left ventricular ejection fraction of 29% ± 5% (mean ± std). None of the patients had pulmonary or neurological disease, recent myocardial infarction or cardiac surgery (within the previous 6 months), recent changes in therapy (last 2 weeks), or any other disease limiting survival.

Recordings were carried out between 9:00 a.m. and 11:00 a.m. After instrumentation and calibration, patients underwent a session of familiarization with the paced breathing protocol. They were instructed to follow recorded instructions to breath in and out at a frequency of 0.25 Hz, with the inspiratory duty cycle (inspiratory time/total breath time) set at 0.4.

After an initial trial, they were asked whether they felt comfortable with the paced breathing frequency or would rather prefer to slightly increase or decrease it. Accordingly, an adjustment was made within ±10% of the target value (0.25 Hz). After signal

stabilization, patients were recorded during three consecutive sessions: i) for 8 min at rest during spontaneous breathing in the supine position (R); ii) for 8 min in the supine position while breathing at the selected paced breathing frequency (C); iii) for 8 min tilted at 70° during spontaneous breathing (T).

During these three sessions ECG, lung volume (Respitrace Plus, Non-Invasive Monitoring Systems) and non-invasive finger arterial blood pressure monitoring (Finapres 2300, Ohmeda) with sampling frequency of 250 Hz were recorded. In order to avoid artifacts in the arterial pressure signal, the Finapres self-adjustment was disconnected during the recordings, and temporarily switched on between spontaneous and paced breathing sessions to allow the recalibration of arterial blood pressure through sphygmomanometer device.

4.5 Head-up tilt manoeuvres in healthy subjects

The collaboration with the Department of Clinical Sciences, University of the Study of Milan, Hospital L. Sacco, Milan, Italy, allowed to acquire this database.

Sixteen (16) healthy subjects (age 26 ± 6, mean ± std) were enrolled for the experimental protocol. All the subjects had no history and no clinical evidence of any disease. They did not take any medication and refrained from consuming any caffeine or alcohol containing beverages in the 24 h before the recording. All the experiments were performed in the morning.

The subjects were on the tilt table supported by two belts at the level of thigh and waist, respectively, and with both feet touching the footrest of the tilt table. During the entire protocol the subjects breathed spontaneously, but they were not allowed to talk. An written consent was obtained from all subjects. The protocol adhered to the principles of the Declaration of Helsinki. The human research and ethical review boards of the L. Sacco Hospital, the Department of

Clinical Sciences, and the Department of Technologies for Health approved the protocol.

The experimental sessions of the protocol included an initial 10 minutes session at rest in supine position (R) followed by two head up tilt manoeuvres at 45° and 90°, 10 minutes each, carried out in random order (T45 and T90 respectively). Each tilt manoeuvre was followed by a 40 minutes recovery session (R45 and R90 according to the tilt session).

ECG (lead II), respiratory signal (thoracic belt Marazza, Monza, Italy), non-invasive arterial blood pressure (Finapres 2300, Ohmeda) with sampling frequency of 1 kHz were recorded during sessions. The arterial pressure was measured from the middle finger of the left hand, which was maintained at the level of the heart by fixing the subject's arm to the thorax during the upright position. The arterial pressure signal was cross-calibrated in each session with the use of a measure provided by a sphygmomanometer at the onset of rest. The auto-calibration procedure of the arterial pressure device was switched off after the first automatic calibration at the onset of the session.

4.6 Extraction of beat-to-beat variability series

The QRS apex was located over the ECG signal using parabolic interpolation. Heart period was approximated as the time distance between two consecutive QRS peaks on the ECG (RR).

Systolic arterial pressure (SAP) was assessed as the maximum arterial blood pressure inside RR. When the respiratory signal was recorded respiratory series (Resp) was obtained by taking the values of the respiratory signal at the R apex.

When the respiratory signal was not recorded Resp series was derived from respiratory–related ECG amplitude changes. Figure 4.1 shows the RR(n), SAP(n) and Resp(n) values obtained from ECG, arterial pressure and respiratory signals.

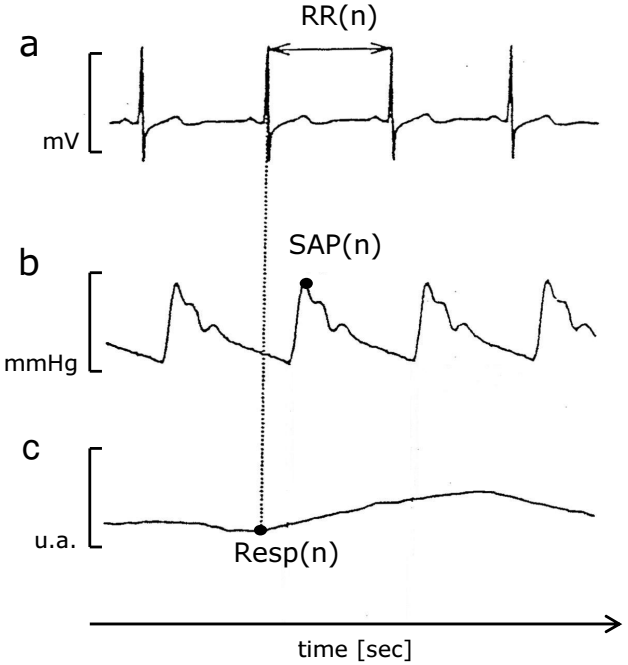

Fig. 4.1: Evolution in time expressed in seconds [sec] of ECG (a), arterial blood pressure (b) and respiratory signal (c) expressed in millivolt [mV], millimeters of mercury [mmHg] and arbitrary units [u.a.]. The SAP(n) is taken inside RR(n) and the Resp(n) value corresponds in time to the first R apex defining RR(n).

Considering N consecutive beats permits to obtain the beat-to-beat series as shown in Fig. 4.2 where RR, SAP and Resp are expressed in seconds [sec], millimeters of mercury [mmHg] and arbitrary units [u.a.].

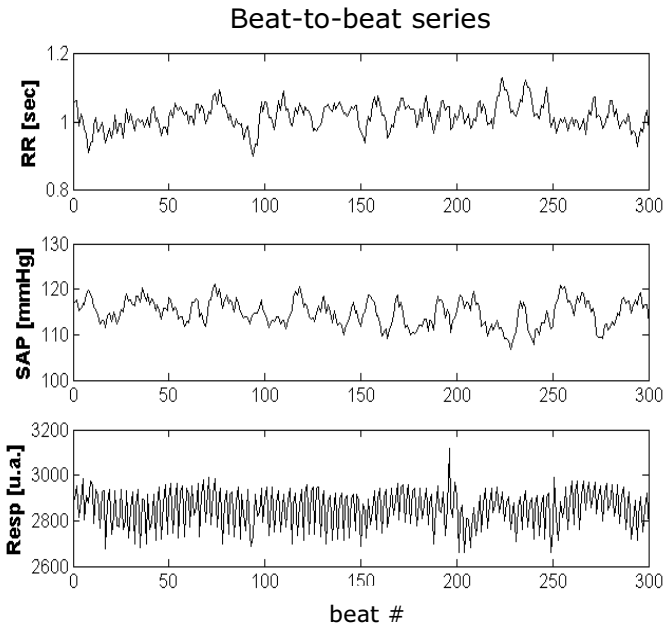

Fig. 4.2: Beat-to-beat RR, SAP and Resp series expressed in seconds [sec], millimeters of mercury [mmHg] and arbitrary units [u.a.].

In all the considered experimental protocols sequences of 250-300 consecutive RR, SAP and Resp values (i.e. recordings of few minutes) were analyzed. All signals were manually edited to avoid artefacts.

4.7 Assessing causality along baroreflex

The activation of baroreflex regulatory mechanism was assessed by testing Granger causality from SAP to RR (i.e. SAP→RR) according to F-test and Wald test (presented in Chapter 2). Immediate effects of SAP on RR in the same beat were allowed. The reverse causality (i.e.

from RR to SAP, RR→SAP) along the mechanical pathway accounting for the Starling law and runoff effect was assessed simply by reversing the role between SAP and RR. Immediate effects of RR on SAP were not allowed simply because RR(n) was not ended when SAP(n) occurred (one-beat delay from RR(n) to SAP(n) was set).

Causality was studied according to two different universes of knowledge about the system: the first universe excluded Resp from the set of considered signals (i.e. Ω-{Resp}={RR,SAP}) while the second one accounted for all the signals (i.e. Ω={RR,SAP,Resp}).

The comparison between the results derived from the two different universes allows the evaluation of the effect on causality between RR and SAP determined by neglecting Resp. Immediate effects of Resp(n) on SAP(n) and RR(n) were allowed in agreement with the rapidity of vagal reflexes on RR and with the prompt action of respiratory-related changes of thoracic pressure and venous return on SAP.

4.8 Assessing baroreflex sensitivity

The observation that oscillations in RR intervals and SAP series are significantly correlated around 0.1 Hz and at the frequency of respiration has prompted many researchers to focus on the relationship between these two signals.

Several techniques have been proposed to evaluate the baroreflex sensitivity based on the spontaneous variability of SAP and RR series.

The traditional method adopted in the present dissertation is based on the calculation of the power spectrum of RR interval and SAP variability series [Pagani et al., 1988]. RR and SAP series were modeled as an autoregressive process RR. The parameters of the AR model were estimated using Levinson-Durbin recursion [Kay and Marple, 1981]. The model order ranged between 14 and 18. The optimal number of the coefficients was chosen according to the Akaike figure of merit [Akaike, 1974]. The residual whiteness was checked.

The power spectrum was calculated directly from the model coefficients [Kay and Marple, 1981]. The AR power spectrum was decomposed into components the sum of which gave the whole power spectrum [Zetterberg, 1969]. The powers of RR and SAP series were computed in the very low frequency (VLF) band (below 0.03 Hz), low frequency (LF) band (from 0.03 to 0.15 Hz), and high frequency (HF) band (from 0.15 to 0.5 Hz). Attention was paid that HF frequency did not drop in the LF band.

The VLF, LF and HF powers were obtained as the sum of the powers of all the components the central frequency of which dropped in the LF and HF bands respectively. The absolute powers of RR and SAP series were computed in the LF and HF bands (i.e. LFa and HFa respectively). The squared root of the ratio of the LFa power of RR on that of SAP

$$\alpha_{LF} = \sqrt{\frac{LFa[RR]}{LFa[SAP]}} \tag{4.1}$$

and the squared root of the ratio of the HFa power of RR on that of SAP

$$\alpha_{HF} = \sqrt{\frac{HFa[RR]}{HFa[SAP]}} \tag{4.2}$$

were utilized as estimates of the baroreflex sensitivity in the LF and HF bands respectively.

It is important to notice that causality was not accounted into the estimation of baroreflex sensitivity according to (4.1) and (4.2). Indeed it is calculated taking uniquely in consideration the power spectral density of each considered series in the corresponding frequency band.

These indexes are reliable if the coherence function (K^2) sampled at LF and HF is greater than 0.5 [De Boer et al., 1985], thus meaning that RR and SAP signals are significantly correlated at the specific

frequency. The assessment of the strength of the SAP-RR relation was estimated via K^2 measuring the degree of linear correlation between SAP and RR series as a function of the frequency (f). The squared coherence function is assessed in (4.3) as

$$K^2_{SAP-RR}(f) = \frac{\left|C_{SAP-RR}(f)\right|^2}{S_{SAP}(f) \cdot S_{RR}(f)} \tag{4.3}$$

where $|C_{SAP-RR}(f)|^2$ is the squared cross-spectrum modulus between SAP and RR series and $S_{SAP}(f)$ and $S_{RR}(f)$ are the power spectra of RR and SAP series. Index $K^2_{SAP-RR}(f)$ ranges from 0 to 1, respectively indicating a perfect uncorrelation and a full correlation. The calculation of $C_{SAP-RR}(f)$ requires a bivariate AR approach instead of the monovariate one required by spectral analysis.

At this regard, parametric approach based on bivariate AR model [Baselli et al., 1986] was chosen to estimate $C_{SAP-RR}(f)$, $S_{SAP}(f)$ and $S_{RR}(f)$. The model order was fixed to 10 and the coefficients of the bivariate AR model were identified via least squares approach [Porta et al., 2006; Baselli et al., 1997]. Index $K^2_{SAP-RR}(f)$ was sampled in correspondence of the weighted average of the central frequencies of the LF and HF components found in the RR series, where the weights were the powers of the components, thus obtaining K^2_{LF} and K^2_{HF} indexes.

4.9 Statistical analysis

When assessing causality along baroreflex χ^2 test, or Fisher exact test whenever possible, was utilized to evaluate the difference between the percentages of subjects with significant SAP→RR elicited by the different experimental steps.

Firstly the difference between the percentages of causal relations from SAP to RR were tested separately in the universes Ω-{Resp} and Ω. Secondarily, if no significant differences were found among the

experimental steps, the percentages of significant SAP→RR along all the steps were pooled together and the difference between the percentages of significant SAP→RR detected in Ω-{Resp} and in Ω was tested with χ^2 test or McNemar's test whenever possible.

Baroreflex sensitivity was assessed according to three different strategies: i) over all subjects with significant K^2; ii) over all the subjects with significant SAP→RR in Ω-{Resp}; iii) over all the subjects with significant SAP→RR in Ω. One way Analysis of Variance test (ANOVA) was carried out to assess the differences in each experimental step among the baroreflex sensitivities calculated according to i), ii) and iii). If no significant differences were found in each experimental step, baroreflex values calculated according to i), ii) and iii) were pooled together and the effects of the experimental protocol among the respective steps were compared via ANOVA or unpaired t-test whenever possible.

When the normality test failed, Kruskal-Wallis Analysis of Variance on ranks was used instead of ANOVA and Mann-Whitney rank sum test was utilized instead of unpaired t-test.

A $p<0.05$ was considered as significant for all the performed statistical analysis.

4.10 Conclusions

The chapter presents four experimental protocols appropriate to test causality in the direction of baroreflex in critical conditions in which this causal relation might be absent or weak. Along with this topic, the collected datasets allow to evaluate the role of respiration as exogenous source on the assessment of causality and on baroreflex sensitivity estimation calculated with non causal indexes.

The protocols have been acquired thanks to the collaboration with different national and international Institutions: 1) Department of Anaesthesia and Intensive Care, University Hospital of Dresden, Germany; 2) Department of Perioperative Medicine and Intensive

Care, San Gerardo Hospital, Monza, Italy; 3) Department of Bioengineering of the IRCCS Institution Fondazione Maugeri, Pavia, Italy; 4) Department of Clinical Sciences, University of the Study of Milan, Hospital L. Sacco, Milan, Italy.

They are relevant to the comparison of mechanical ventilation techniques during deep anaesthesia on animals (protocol 1), to the comparison of anaesthesiology administration strategies during deep anaesthesia on humans (Neuromorfeo trial, protocol 2), to paced breathing and head-up manoeuvre in heart failure patients (protocol 3), to the head-up manoeuvres in healthy subjects (protocol 4).

Chapter 5

Simulation Results

5.1 Introduction

The reliability of F-test and Wald test in detecting Granger causality relation between discrete series was tested on specific simulations (described in Chapter 3), summarized in Table 3.3.

The ability in finding a significant causal relation was tested on different types of uncoupled processes (i.e. I.a, I.b, I.b.1, I.b.2 and I.c simulations), of coupled series interacting in closed loop generated by bivariate AR processes (i.e. II.a, II.b and II.c simulations) and of coupled series interacting in closed loop and affected by an exogenous source (i.e. III.a and III.b simulations).

The results of the simulations are provided in the following. Both F-test and Wald test performed similarly in terms of detections of the causal relations. For this reason the results are reported solely in the case of F-test.

5.2 Type-I simulations: results

Since in type-I simulations the series were uncoupled, any detection of causal interactions between the two series was considered a false positive.

F-test performed similarly in terms of detection of the causal relations in all the type-I simulations (i.e. type-I.a, type-I.b and type-I.c). As shown in Table 5.1 when assessing causality between uncoupled series y_1 and y_2 over $\Omega_y=\{y_1,y_2\}$ at significance level p=0.01, the percentage of false positives was found smaller than 1% when considering bidirectional causality (i.e. $y_1 \leftrightarrow y_2|_{\Omega_y}$) and smaller than 9% when considering unidirectional causality (i.e. $y_1 \rightarrow y_2|_{\Omega_y}$ or $y_2 \rightarrow y_1|_{\Omega_y}$) while the absence of causality (i.e. $y_1 \;\; y_2|_{\Omega_y}$) was found larger than 90%.

TABLE 5.1

Type-I SIMULATION RESULTS: PERCENTAGES OF BIDIRECTIONAL ($\leftrightarrow$), UNIDIRECTIONAL ($\rightarrow$) AND ABSENCE OF CAUSALITY ASSESSED WITH F-TEST OVER $\Omega_y=\{y_1,y_2\}$ AT p=0.01 BETWEEN UNCOUPLED SERIES y_1 AND y_2

	$y_1 \leftrightarrow y_2\|_{\Omega_y}$	$y_1 \rightarrow y_2\|_{\Omega_y}$ U $y_2 \rightarrow y_1\|_{\Omega_y}$	$y_1 \;\; y_2\|_{\Omega_y}$
F-test	<1%	<9%	>90%

When assessing type-I.b simulations the percentage values reported in Table 5.1 were found for every sub-type of simulation belonging to type-I.b.1 (i.e. from i to vi) and to type-I.b.2 (i.e. from i to iii). When assessing causality relations in type-I.b.1 simulations no

correlation was found between the modulus of the uncoupled AR(2) processes y_1 and y_2.

Figure 5.1 shows an example of analysis carried out over the type-I.b.1.v simulation. One-thousand uncoupled pairs of AR(2) processes y_1 and y_2 were generated with fixed phase (i.e. φ_2=0.25 and φ_1=0.05 cycles/sample) and random modulus, ρ_2 and ρ_1, ranging from 0.1 to 0.9. Every open circle represents the generation of an uncoupled y_1 and y_2 pair and it is located in the graph according to the result of causality test (upper left panel: $y_1 \leftrightarrow y_2|_{\Omega_y}$; upper right panel: $y_1 \rightarrow y_2|_{\Omega_y}$; lower left panel: $y_2 \rightarrow y_1|_{\Omega_y}$; lower right panel: $y_1 \;\; y_2|_{\Omega_y}$) at the corresponding modulus pair (i.e. (ρ_2, ρ_1)). Since the scatter plot did not reveal any particular deterministic structure, results do not depend on the particular values of ρ_2 and ρ_1.

When assessing causality relations in type-I.b.2 simulations no correlation was found between the phases of the uncoupled AR(2) processes y_1 and y_2.

Figure 5.2 shows an example of analysis carried out over type-I.b.2.iii simulation. One-thousand uncoupled pairs of AR(2) y_1 and y_2 processes were generated with fixed modulus (i.e. ρ_2=0.94 and ρ_1=0.60) and random phases φ_2 and φ_1, ranging from 0.03 to 0.5 cycles/samples. Every open circle represents the generation of an uncoupled y_1 and y_2 pair and it is located in the graph according to the results of causality test at the corresponding phase pair (i.e. (φ_2,φ_1)). Since the scatter plot did not reveal any particular deterministic structure, results do not depend on the particular values of φ_2 and φ_1.

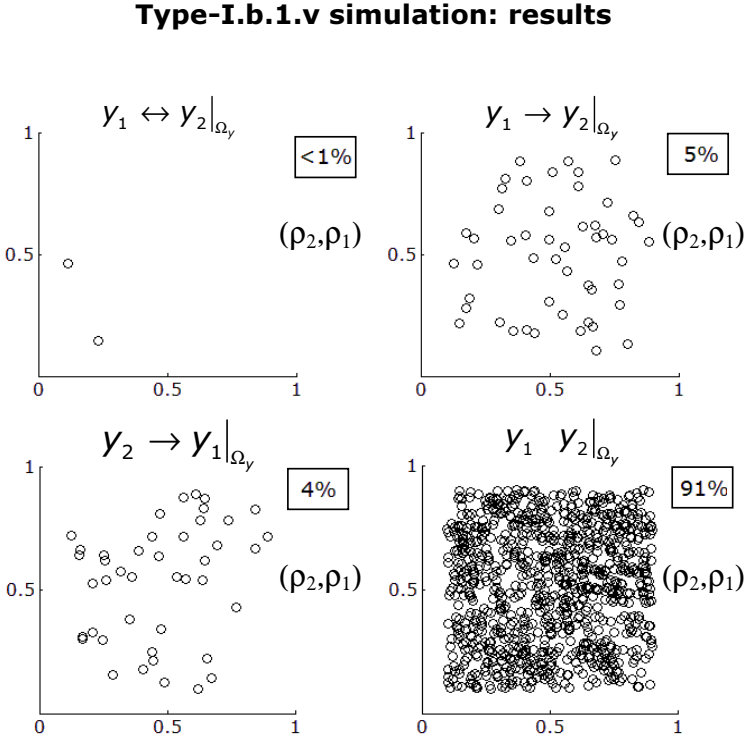

Fig. 5.1: Simulation type-I.b.1.v: 1000 uncoupled pairs of AR(2) processes y_1 and y_2 were generated with fixed phase (i.e. φ_2=0.25 and φ_1=0.05 cycles/sample) and random modulus, ρ_2 and ρ_1, ranging from 0.1 to 0.9. Every open circle represents the result of a simulation and it is located at the pair (ρ_2 ,ρ_1). The percentage values in the squared boxes, at the subplots upper right corners, represent the percentage of bidirectional-causality ($y_1 \leftrightarrow y_2|_{\Omega_y}$), unidirectional causalities ($y_1 \rightarrow y_2|_{\Omega_y}$ and $y_2 \rightarrow y_1|_{\Omega_y}$) and absence of causality ($y_1 \quad y_2|_{\Omega_y}$) assessed with F-test over Ω_y={y_1,y_2} at p=0.01 significance level.

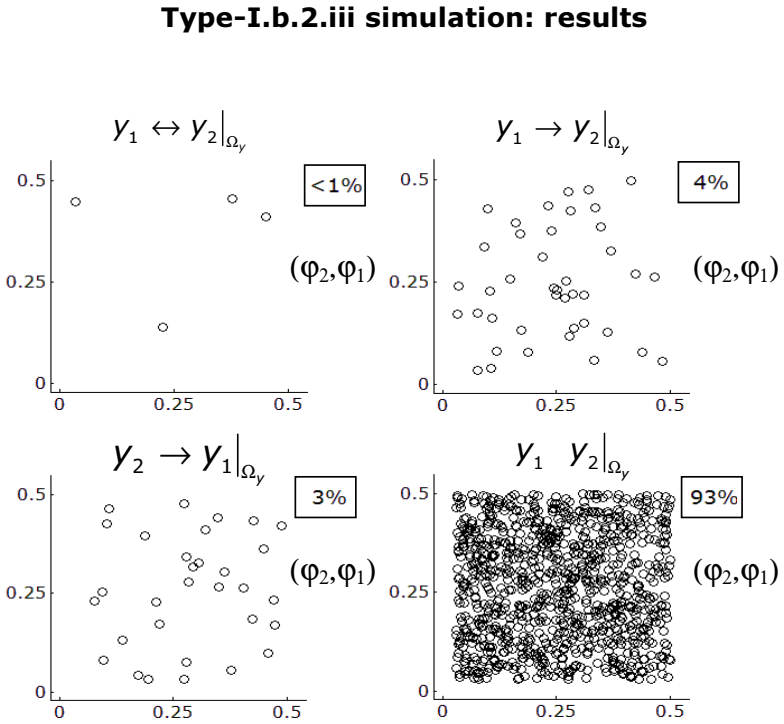

Fig. 5.2: Simulation type-I.b.2.iii: 1000 pairs of AR(2) y_1 and y_2 processes were generated with fixed modulus (i.e. ρ_2=0.94 and ρ_1=0.60) and random phases φ_2 and φ_1, ranging from 0.03 to 0.5 cycles/samples. Every open circle represents the result of a simulation and it is located at the pair (φ_2 ,φ_1). The percentage values in the squared boxes, at the subplots upper right corners, represent the percentage of bidirectional causality ($y_1 \leftrightarrow y_2|_{\Omega_y}$), unidirectional causalities ($y_1 \rightarrow y_2|_{\Omega_y}$ and $y_2 \rightarrow y_1|_{\Omega_y}$) and absence of causality ($y_1 \quad y_2|_{\Omega_y}$) assessed with F-test over Ω_y={y_1,y_2} at p=0.01 significance level.

5.3 Type-II simulations: results

5.3.1 Type-II.a simulation: effects of the residuals variance magnitude

Results of causality analysis in type-II.a bivariate AR simulation are shown in Fig. 5.3. F-test detected $y_2 \rightarrow y_1|_{\Omega_y}$ in a percentage of simulations close to 100% when $\lambda^2{}_1$ was negligible (i.e. 0.001 and 0.01) with respect to $\lambda^2{}_2$. Conversely, $y_1 \rightarrow y_2|_{\Omega_y}$ was found in a percentage of simulations close to 100% when $\lambda^2{}_1$ was large (i.e. 100 and 1000) compared to $\lambda^2{}_2$. When $\lambda^2{}_1$ and $\lambda^2{}_2$ were more balanced (i.e. $\lambda^2{}_1/\lambda^2{}_2$=0.1, 1, and 10) none of the causal relations took priority and F-test detected a predominant presence of closed loop interactions (i.e. $y_1 \leftrightarrow y_2|_{\Omega_y}$).

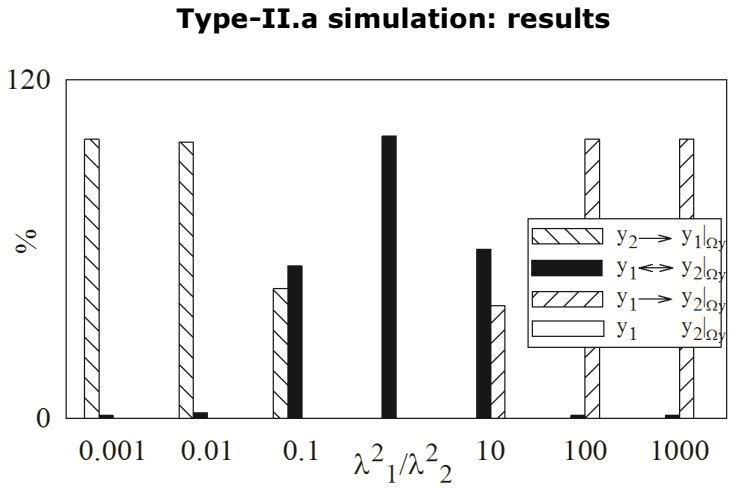

Fig. 5.3: Percentage of causal interactions relevant to type-II.a bivariate AR process shown in Fig. 3.1 with a_{21}=-0.7, a_{12}=0.7, τ_{12}=0, τ_{21}=2, $a_{22}(1)=a_{22}(2)=0$. Bars show the percentage of $y_2 \to y_1|_{\Omega_y}$ (backslash-pattern bar), $y_1 \leftrightarrow y_2|_{\Omega_y}$ (solid bar), $y_1 \to y_2|_{\Omega_y}$ (slash-pattern bar) and uncoupled y_1 and y_2 (open bar) as a function of the ratio of λ^2_1/λ^2_2 with $\lambda^2_2=1$. Causality was assessed over $\Omega_y=\{y_1,y_2\}$.

5.3.2 Type-II.b simulation: effects of the closed loop pathways gains

Results of causality analysis in type-II.b bivariate AR simulation are shown in Fig. 5.4. When the ratio $|a_{12}/a_{21}|$ was high, F-test detected $y_2 \to y_1|_{\Omega_y}$ in 100% and in 97% of simulations with $|a_{12}/a_{21}|$=10000 and 100 respectively. Conversely, when the ratio $|a_{12}/a_{21}|$ was close to 0 (i.e. 0.01 and 0.0001) $y_2 \to y_1|_{\Omega_y}$ was found in 96% and 98% of simulations respectively. When a_{12} and a_{21} were

balanced (e.g. the ratio $|a_{12}/a_{21}|=1$) F-test suggested always the presence of closed loop interactions (i.e. $y_1 \leftrightarrow y_2|_{\Omega_y}$).

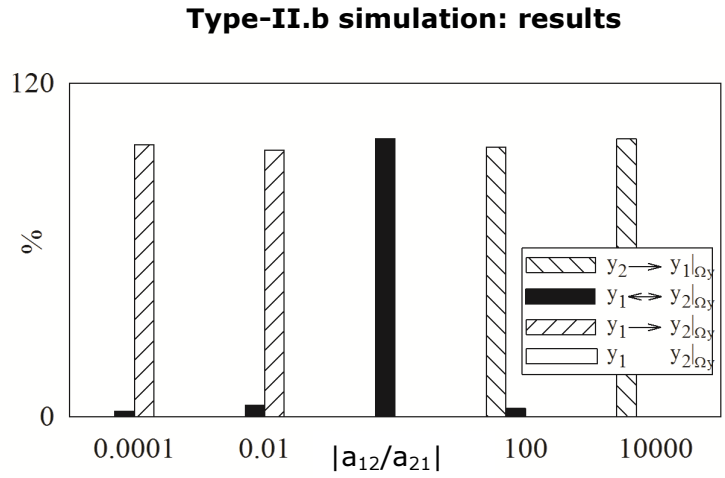

Fig. 5.4: Percentage of causal interactions relevant to type-II.b bivariate AR process shown in Fig. 3.1 with $\lambda^2_1=\lambda^2_2=1$, $\tau_{12}=0$, $\tau_{21}=2$ and $a_{22}(1)=a_{22}(2)=0$. Bars show the percentages of $y_2 \rightarrow y_1|_{\Omega_y}$ (backslash-pattern bar), $y_1 \leftrightarrow y_2|_{\Omega_y}$ (solid bar), $y_1 \rightarrow y_2|_{\Omega_y}$, (slash-pattern bar) and uncoupled y_1 and y_2 (open bar) as a function of the ratio $|a_{12}/a_{21}|$ with $|a_{12}\cdot a_{21}|=0.49$. Causality was assessed over $\Omega_y=\{y_1,y_2\}$.

5.3.3 Type-II.c simulation: effects of the auto-loop resonance

Results of causality analysis in type-II.c bivariate AR simulation are shown in Fig. 5.5. Results of F-test closely resembled those of Fig. 5.3. The exceptions were at $\lambda^2_1/\lambda^2_2=100$ and 1000 where the percentage of $y_1 \rightarrow y_2|_{\Omega_y}$ was smaller than 100% and the presence of

$y_1 \leftrightarrow y_2|_{\Omega_y}$ was significant (i.e. given that the resonance of the auto-loop is larger than 1, the bell shape distribution of the dark bars moves toward right), thus suggesting a more important presence of $y_2 \rightarrow y_1|_{\Omega_y}$ at the highest values of $\lambda^2{}_1/\lambda^2{}_2$. In the case of the resonance of the auto-loop over y_2 was smaller than 1, the bell shape distribution of the dark bars moves toward left.

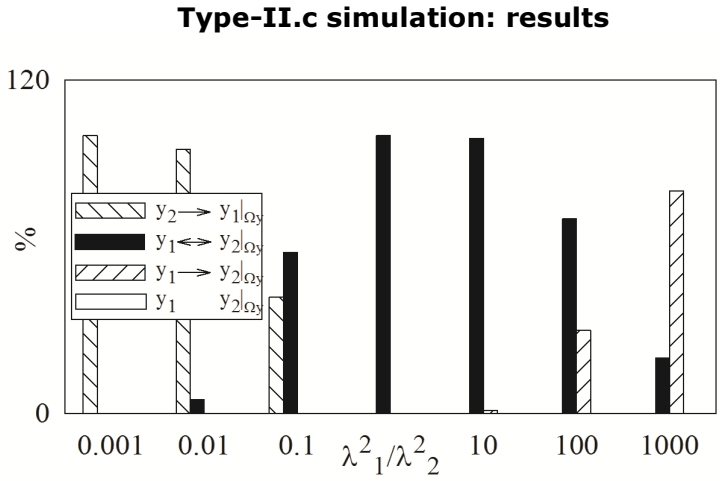

Fig. 5.5: Percentage of causal interactions relevant to type-II.c bivariate AR process shown in Fig. 3.1 with a_{21}=-0.7, a_{12}=0.7, τ_{12}=0 and τ_{21}=2. The parameters of the auto-loop on y_2, $H_{22}(z)=1/(1-A_{22}(z))$ with $A_{22}(z)=a_{22}(1)\cdot z^{-1}+a_{22}(2)\cdot z^{-2}$ were $a_{22}(1)$=1.133 and $a_{22}(2)$=-0.49. The percentage of $y_2 \rightarrow y_1|_{\Omega_y}$ (backslash-pattern bar), $y_1 \leftrightarrow y_2|_{\Omega_y}$ (solid bar), $y_1 \rightarrow y_2|_{\Omega_y}$, (slash-pattern bar) and uncoupled y_1 and y_2 (open bar) as a function of the ratio $\lambda^2{}_1/\lambda^2{}_2$. Causality was assessed over $\Omega_y=\{y_1,y_2\}$.

5.4 Type-III simulations: results

5.4.1 Type-III.a simulation: effects of y_3 affecting y_1 and y_2

Figure 5.6 shows the results of causality analysis in type-III.a bivariate AR simulation with exogenous input.

Figure 5.6-a shows findings obtained when excluding y_3 from the set of signals over which causality was assessed. F-test detected $y_2 \rightarrow y_1|_{\Omega_y - \{y_3\}}$ in 74% of simulations at a^2_{13}=0.001 (Fig. 5.6-a). The percentage of $y_2 \rightarrow y_1|_{\Omega_y - \{y_3\}}$ progressively decreased and reached 0% at a^2_{13}=1. Conversely, the percentage of $y_1 \leftrightarrow y_2|_{\Omega_y - \{y_3\}}$ gradually raised from 26% at a^2_{13}=0.001 to 100% at a^2_{13}=1 and remained stable at 100% for a^2_{13}>1.

Figure 5.6-b shows findings obtained when all the signals were included in the universe over which causality was assessed. Results are completely different from those depicted in Fig. 5.6-a. F-test found $y_2 \rightarrow y_1|_{\Omega_y}$ in a percentage of simulations larger than 97% (the percentage was smaller only at a^2_{13}=1000).

This result is in agreement with the result found in bivariate AR simulations given the variances of the residuals and gains of the closed loop pathways.

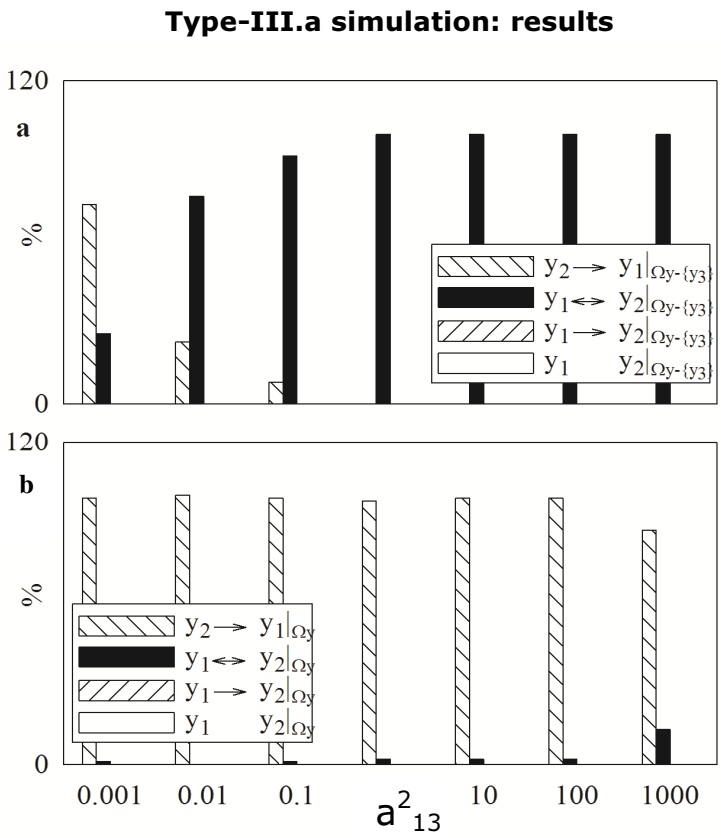

Fig. 5.6: Percentage of causal interactions relevant to type-III.a trivariate AR process shown in Fig. 3.2 with a_{21}=-0.7, a_{12}=0.7, λ^2_1=0.001, λ^2_2=1, τ_{21}=2, τ_{12}= τ_{13}=τ_{23}=0 and $a_{22}(1)$=$a_{22}(2)$=0. the percentage of $y_2 \rightarrow y_1|_{\Omega_y}$ (backslash-pattern bar), $y_1 \leftrightarrow y_2|_{\Omega_y}$ (solid bar), $y_1 \rightarrow y_2|_{\Omega_y}$, (slash-pattern bar) and uncoupled y_1 and y_2 (open bar) as a function of a^2_{13} with a^2_{23}=1. Given the set of signals Ω_y=$\{y_1,y_2,y_3\}$, causality analysis was carried out over the reduced set Ω_y -$\{y_3\}$=$\{y_1,y_2\}$ in (a), while in (b) the entire set Ω_y was considered.

5.4.2 Type-III.b simulation: effects of y_3 affecting uniquely y_1

Figure 5.7 shows the results of causality analysis in type-III.b bivariate AR simulation with exogenous input.

Figure 5.7-a shows findings obtained when excluding y_3 from the set of signals over which causality was assessed. The F-test found primarily $y_2 \rightarrow y_1|_{\Omega_y - \{y_3\}}$ when a^2_{13} was close to 0 (i.e. 0.001 and 0.01), a predominant percentage of $y_1 \leftrightarrow y_2|_{\Omega_y - \{y_3\}}$ when a^2_{13}=0.1, 1 and 10 and primarily $y_2 \rightarrow y_1|_{\Omega_y - \{y_3\}}$ when a^2_{13} was high (i.e.100 and 1000).

Figure 5.7-b shows findings obtained when all the signals were included in the universe over which causality was assessed. Results are completely different from those depicted in Figs.5.7-a. F-test finds $y_2 \rightarrow y_1|_{\Omega_y}$ in a percentage of simulations larger than 96% (the percentage was smaller only at a^2_{13}=1000).

This result is in agreement with the result found in bivariate AR simulations given the variances of the residuals and gains of the closed loop pathways.

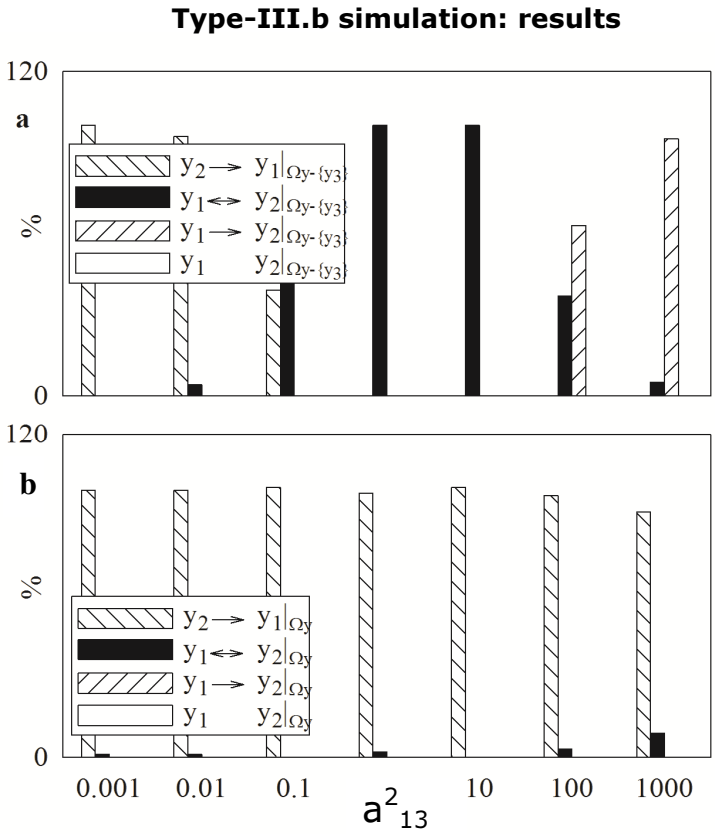

Fig. 5.7: Percentage of causal interactions relevant to type-III.b trivariate AR process shown in Fig. 3.2 with a_{21}=-0.7, a_{12}=0.7, λ^2_1=0.001, λ^2_1=1, τ_{21}=2, τ_{12}= τ_{13}=τ_{23}=0 and $a_{22}(1)$=$a_{22}(2)$=0. the percentage of $y_2 \to y_1|_{\Omega_y}$ (backslash-pattern bar), $y_1 \leftrightarrow y_2|_{\Omega_y}$ (solid bar), $y_1 \to y_2|_{\Omega_y}$, (slash-pattern bar) and uncoupled y_1 and y_2 (open bar) as a function of a^2_{13} with a^2_{23}=0. Given the set of signals Ω_y=$\{y_1,y_2,y_3\}$, causality analysis was carried out over the reduced set Ω_y-$\{y_3\}$=$\{y_1,y_2\}$ in (a), while in (b) the entire set Ω_y was considered.

5.5 Conclusions

The present chapter reports the results of the numerous simulations (summarized in Table 3.3) performed in order to assess the reliability of F-test and Wald test in detecting Granger causality relation between discrete series.

Both F-test and Wald test performed similarly in terms of detections of the causal relations.

Simulations performed on uncoupled series proved the reliability of the statistical tests to detect the absence of a causal relation. Results were independent of the type of dynamics, sharpness of the spectral peak and degree of unpredictability characterizing signals.

Simulations performed on coupled series operating in closed loop pointed out the dependency of the detection of causal relations on the magnitude of the variances of the residuals, on the gains of the pathways forming the close loop, and on the gains of the auto-loop.

The presence of an exogenous source affecting the series operating in closed loop was able to bias the detection of the causal relation. The importance of the bias depended on the gain of the pathways linking the exogenous source to the interacting signals. Assessing causality by accounting for the exogenous source allowed the cancellation of this biasing effect.

Chapter 6

Experimental Results

6.1 Introduction

The assessment of the causal relation between RR and SAP in the direction of baroreflex (i.e. from SAP to RR) and of baroreflex sensitivity based on the power spectra were performed on four experimental protocols described in Sections 4.2, 4.3, 4.4 and 4.5.

The significance of causal relation from SAP to RR (i.e. SAP→RR) was evaluated as explained in Section 4.7 considering two different universes of knowledge: the first universe excluded respiration (i.e. Resp) from the set of considered signals (i.e. $SAP \rightarrow RR|_{\Omega-\{Resp\}}$, Ω-{Resp}={RR,SAP}) while the second one accounted for all the signals (i.e. $SAP \rightarrow RR|_{\Omega}$, Ω={RR,SAP,Resp}).

Baroreflex sensitivity at LF and HF frequency bands (i.e. α_{LF} and α_{HF}) was calculated according to a well-established approach considering all subjects with coherence function (K^2) evaluated in LF and HF (i.e. K^2_{LF} and K^2_{HF}) larger than 0.5 (see Section 4.8) and according to a new approach taking into account only subjects with a significant causal relation from SAP to RR in Ω-{Resp} and Ω respectively.

If no significant difference was found among the considered approaches in each experimental step, baroreflex data were pooled

together independently of the strategy utilized to assess them and differences of α_{LF} and α_{HF} values among experimental steps was then assessed.

In the present chapter percentages of subjects with K^2_{LF} and K^2_{HF} larger than 0.5 and significant $SAP \rightarrow RR|_{\Omega-\{Resp\}}$ and $SAP \rightarrow RR|_{\Omega}$ causal relation are presented in tables while α_{LF} and α_{HF} values are shown in bar histograms figures.

Mean, variance, spectral indexes and squared coherence functions results of RR and SAP analysis are presented in detail in Appendix A.

6.2 Deep anaesthesia on animals

6.2.1 Causality along baroreflex in animals

Table 6.1 shows the results of assessing coherence function and causal relation along baroreflex in pigs undergoing controlled (PCV) versus supported mechanical ventilation (PSV) techniques and the random variable implementation of the two strategies (nPCV and nPSV) during deep intravenous anaesthesia.

Significant K^2_{LF} was found in 50% of pigs during PCV and nPCV and in 100% during PSV and nPSV. High significant K^2_{HF} values (100%) were found during each experimental condition except in nPSV (87%).

When assessing causality excluding respiration ($SAP \rightarrow RR|_{\Omega-\{Resp\}}$) 100% of subjects exhibited significant causal relation from SAP to RR in all the experimental conditions except PCV (87%). When accounting for respiration ($SAP \rightarrow RR|_{\Omega}$) 100% percentages were found during PSV and nPSV while lower percentages were detected during PCV and nPCV (62% and 87% respectively).

Coherence and causality results seem to suggest that baroreflex control is less involved in the RR-SAP regulation in animals

undergoing mechanical controlled ventilation in comparison to assisted ventilation.

TABLE 6.1

PERCENTAGES OF SIGNIFICANT K^2_{LF}, K^2_{HF} AND CAUSALITY FROM SAP TO RR (SAP→RR) DETECTED WHEN CONSIDERING $\Omega-\{Resp\}$ AND Ω IN PIGS DURING CONTROLLED AND SUPPORTED VENTILATION (PCV AND PSV) AND THE RANDOM VARIABLE IMPLEMENTATION OF THE TWO STRATEGIES (nPCV AND nPSV) WITH F-TEST AT $p=0.01$

	PCV	**nPCV**	**PSV**	**nPSV**
$\boldsymbol{K^2_{LF}>0.5}$	50%	50%	100%	100%
$\boldsymbol{K^2_{HF}>0.5}$	100%	100%	100%	87%
$\mathbf{SAP\rightarrow RR|_{\Omega-\{Resp\}}}$	87%	100%	100%	100%
$\mathbf{SAP\rightarrow RR|_{\Omega}}$	62%	87%	100%	100%

As reported in Table 6.2, statistical significant difference was found between the percentage of cases with $K^2_{LF}>0.5$, detected during controlled ventilation techniques (i.e. PCV U nPCV) and that detected during supported ventilation (i.e. PSV U nPSV). No differences were found when assessing the percentage of subjects with $K^2_{HF}>0.5$, with $SAP\rightarrow RR|_{\Omega-\{Resp\}}$ and with $SAP\rightarrow RR|_{\Omega}$.

TABLE 6.2

DIFFERENCE BETWEEN PERCENTAGES OF CASES WITH $K^2_{LF}>0.5$ OBTAINED DURING CONTROLLED VENTILATION (PCV U nPCV) AND SUPPORTED VENTILATION (PSV U nPSV)

	PCV U nPCV vs PSV U nPSV
$K^2_{LF}>0.5$	p=0.01

6.2.2 Baroreflex sensitivity in animals

Baroreflex sensitivity α_{LF} and α_{HF} are reported in Figs. 6.1-a and 6.1-b respectively.

During each experimental step the exclusion of subjects without significant $SAP \rightarrow RR|_{\Omega-\{Resp\}}$ and $SAP \rightarrow RR|_{\Omega}$ led to estimates of baroreflex sensitivity, α_{LF} and α_{HF}, similar to those derived from all subjects with a significant K^2_{LF} and K^2_{HF} respectively.

When baroreflex sensitivity indexes were pooled together independently of the strategy utilized to assess them, α_{LF} and α_{HF} depended on the ventilation technique as shown in Figs. 6.1-a and 6.1-b.

Significantly different smaller values of α_{LF} and α_{HF} were found when comparing pooled values belonging to PCV and nPCV versus pooled values belonging to PSV and nPSV, thus suggesting that supported ventilation is better able to maintain baroreflex sensitivity regulation than controlled ventilation technique.

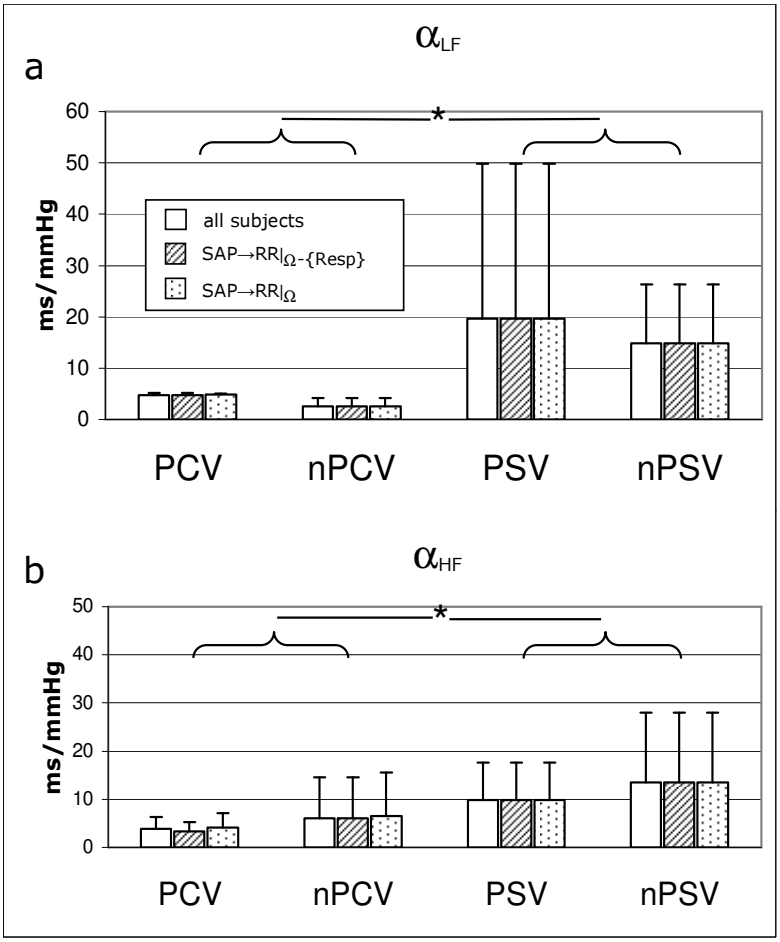

Fig. 6.1: Mean α_{LF} + SD (a) and mean α_{HF} + SD (b) expressed in ms/mmHg calculated considering all subjects with K^2_{LF}>0.5 (a) and K^2_{HF}>0.5 (b) (open bar), then excluding subjects without SAP→RR|$_{\Omega\text{-}\{Resp\}}$ (slash-pattern bar) and subjects without SAP→RR|$_{\Omega}$ (dotted-pattern bar) in pigs during controlled and supported ventilation (PCV and PSV) and the random variable implementation of the two strategies (nPCV and nPSV). *, indicates p<0.001 statistical significance.

6.3 Deep anaesthesia on human subjects

6.3.1 Causality along baroreflex in humans

Table 6.3 shows the results of assessing coherence function and causality relation along baroreflex in humans undergoing to ventilated anaesthesia (VA) versus intravenous (IA) strategy during controlled ventilation.

High significant K^2_{HF} values (100% of the subjects) were found in both groups VA and IA while lower values of K^2_{LF} were found in both VA and IA (significant K^2_{LF} values are found in 33% and 53% respectively).

When excluding for Resp (SAP→RR$|_{\Omega-\{Resp\}}$) almost all subjects exhibited significant causal relation in both VA and IA (94% and 95% respectively). When accounting for respiration (SAP→RR$|_{\Omega}$) lower percentages of significant causal relation from SAP to RR were found both for VA (39%) and IA (63%).

TABLE 6.3

PERCENTAGES OF SIGNIFICANT K^2_{LF}, K^2_{HF} AND CAUSALITY FROM SAP TO RR (SAP→RR) DETECTED WHEN CONSIDERING $\Omega-\{Resp\}$ AND Ω IN HUMANS DURING VOLATILE (VA) AND INTRAVENOUS (IA) ANAESTHESIA

	VA	**IA**
$\mathbf{K^2_{LF}>0.5}$	33%	53%
$\mathbf{K^2_{HF}>0.5}$	100%	100%
$\mathbf{SAP\rightarrow RR|_{\Omega-\{Resp\}}}$	94%	95%
$\mathbf{SAP\rightarrow RR|_{\Omega}}$	39%	63%

As reported in Table 6.4, when pooling together VA and IA groups, a statistical significant difference was found between the percentage of subjects with $SAP \rightarrow RR|_{\Omega-\{Resp\}}$ and the one with $SAP \rightarrow RR|_{\Omega}$ thus suggesting the importance of accounting for respiration when assessing causality in the direction of baroreflex during deep anaesthesia in controlled ventilation.

TABLE 6.4

DIFFERENCE BETWEEN THE PERCETAGE OF SUBJECTS WITH $SAP \rightarrow RR|_{\Omega}$ AND THAT WITH $SAP \rightarrow RR|_{\Omega-\{Resp\}}$ DERIVED WHEN CONSIDERING DATA POOLING TOGETHER VOLATILE AND INTRAVENOUS ANAESTHESIA (VA U IA)

	VA U IA
$SAP \rightarrow RR|_{\Omega-\{Resp\}}$ vs $SAP \rightarrow RR|_{\Omega}$	$p<0.001$

6.3.2 Baroreflex sensitivity in humans

Results relevant to baroreflex sensitivity estimates, α_{LF} and α_{HF}, are presented in Figs. 6.2-a and 6.2-b respectively. During each experimental step the exclusion of subjects without significant $SAP \rightarrow RR|_{\Omega-\{Resp\}}$ and $SAP \rightarrow RR|_{\Omega}$ led to values of α_{LF} and α_{HF} similar to those computed when considering all subjects with a significant K^2_{LF} and K^2_{HF} respectively.

When baroreflex sensitivity indexes were pooled together independently of the strategy utilized to assess them, IA strategy significantly decreased α_{HF} with respect to VA as shown in Fig. 6.2-b, thus suggesting that VA preserves baroreflex control better than IA.

No significant difference was found between IA and VA when assessing α_{LF} even it was found lower in IA than in VA as shown in Fig. 6.2-a.

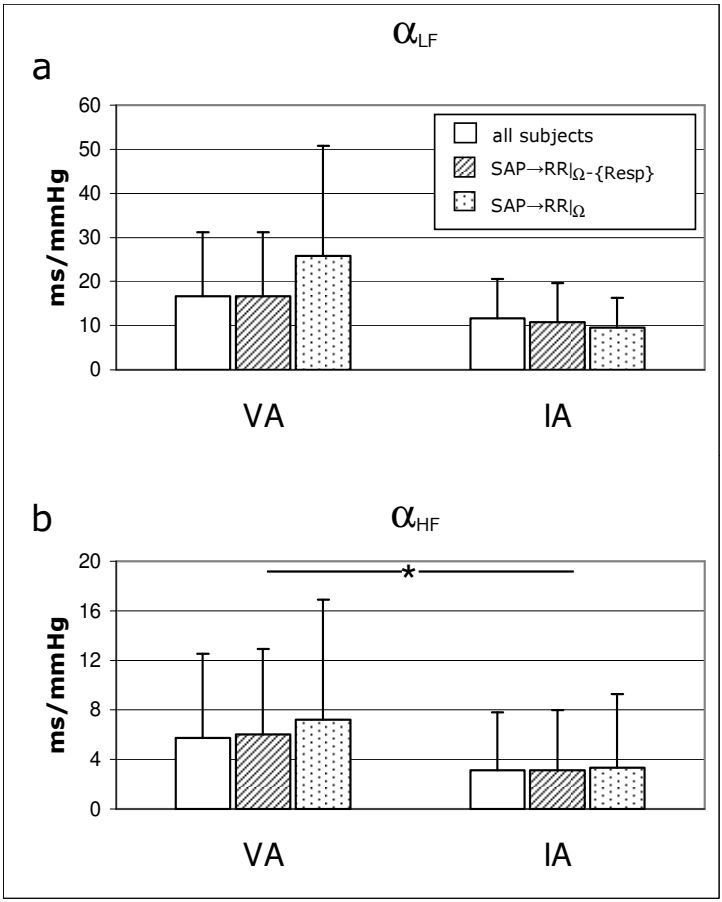

Fig. 6.2: Mean α_{LF} + SD (a) and mean α_{HF} + SD (b) expressed in ms/mmHg calculated when considering all subjects with K^2_{LF}>0.5 (a) and K^2_{HF}>0.5 (b) (open bar), when excluding subjects without SAP→RR|$_{\Omega\text{-}\{Resp\}}$ (slash-pattern bar) and when excluding subjects without SAP→RR|$_{\Omega}$ (dotted-pattern bar) in humans during volatile (VA) and intravenous (IA) anaesthesia. *, indicates p=0.01 statistical significance.

6.4 Paced breathing and head-up tilt manoeuvre in heart failure subjects

6.4.1 Causality along baroreflex in heart failure subjects

Table 6.5 shows the results of assessing coherence function and causal relation along baroreflex in heart failure patients undergoing paced breathing (C) and head-up tilt (T).

High significant K^2_{HF} values were found in more than 80% of the subjects during C, T and at rest (B). The percentage of subjects with significant K^2_{LF} was smaller (i.e. 55% during B and T and 41% during C).

When excluding for Resp ($SAP \rightarrow RR|_{\Omega-\{Resp\}}$) a significant causal relation from SAP to RR was found in more than 75% of the subjects in C, T and B. Accounting for respiration ($SAP \rightarrow RR|_{\Omega}$) diminished the percentage of detection of a significant causal relation from SAP to RR during C and T although differences did not reach a statistical significance.

TABLE 6.5

PERCENTAGES OF SIGNIFICANT K^2_{LF}, K^2_{HF} AND CAUSALITY FROM SAP TO RR (SAP→RR) DETECTED WHEN CONSIDERING $\Omega-\{Resp\}$ AND Ω IN HEART FAILURE PATIENTS AT REST (B), DURING PACED BREATHING (C) AND HEAD-UP TILT (T)

	B	**C**	**T**
$\boldsymbol{K^2_{LF}>0.5}$	55%	41%	55%
$\boldsymbol{K^2_{HF}>0.5}$	82%	91%	82%
$\boldsymbol{SAP \rightarrow RR|_{\Omega-\{Resp\}}}$	77%	91%	86%
$\boldsymbol{SAP \rightarrow RR|_{\Omega}}$	82%	68%	68%

6.4.2 Baroreflex sensitivity in heart failure subjects

Values of baroreflex sensitivity indexes, α_{LF} and α_{HF}, are reported in Figs. 6.3-a and 6.3-b respectively.

During each experimental step, the exclusion of subjects without a significant $SAP \rightarrow RR|_{\Omega - \{Resp\}}$ and $SAP \rightarrow RR|_{\Omega}$ led to values of α_{LF} and α_{HF} similar to those computed when considering all subjects with a significant K^2_{LF} and K^2_{HF} respectively.

When baroreflex sensitivity indexes were pooled together independently of the strategy utilized to assess them, α_{LF} was found significantly smaller during C and T with respect to B as shown in Fig. 6.5-a. The index α_{HF} decreased only during T compared to B as shown in Fig. 6.5-b.

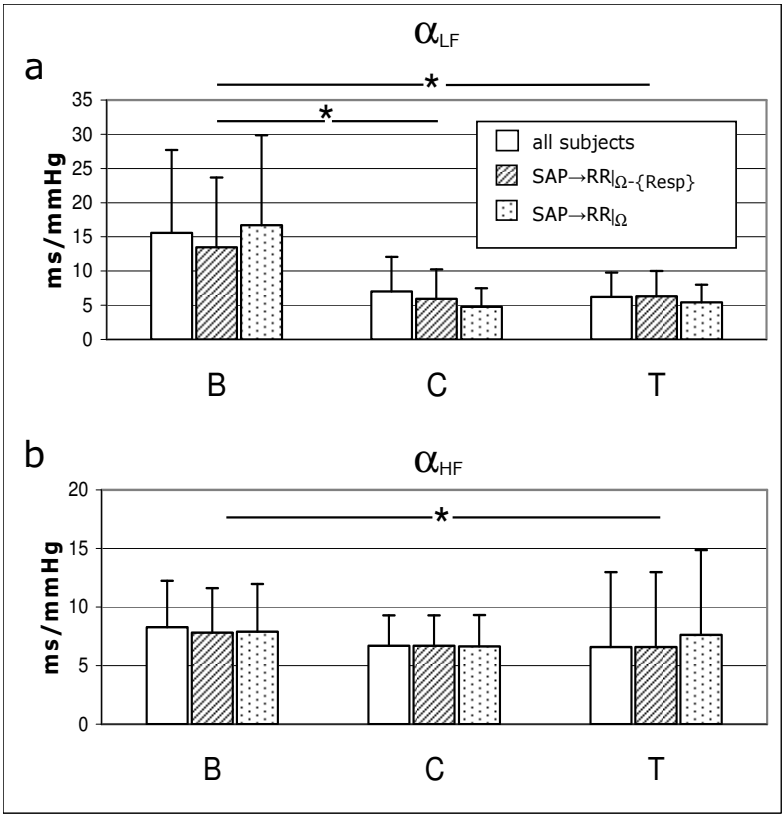

Fig. 6.3: Mean α_{LF} + SD (a) and mean α_{HF} + SD (b) expressed in ms/mmHg calculated when considering all subjects with K^2_{LF}>0.5 (a) and K^2_{HF}>0.5 (b) (open bar), when excluding subjects without SAP→RR|$_{\Omega\text{-}\{Resp\}}$ (slash-pattern bar) and when excluding subjects without SAP→RR|$_{\Omega}$ (dotted-pattern bar) in heart failure patients at rest (B), during paced breathing (C) and head-up tilt maneuver (T). *, indicates p<0.05 statistical significance.

6.5 Head-up tilt manoeuvres in healthy subjects

6.5.1 Causality along baroreflex in healthy subjects

Table 6.6 shows the results of assessing coherence function and causal relation along baroreflex in healthy subjects during rest (R), tilt manoeuvres at different angles (T45 and T90) and respective recovery sessions (R45 and R90).

The percentages of subjects with significant K^2_{LF} and K^2_{HF} values were high (larger than 60%) in all the experimental conditions. No differences were found between the percentages of subjects with $K^2_{LF}>0.5$ and those with $K^2_{HF}>0.5$.

When excluding for Resp ($SAP \rightarrow RR|_{\Omega-\{Resp\}}$) the percentages of subjects with a significant causal relation from SAP to RR was close to 100% in all the conditions. Accounting for respiration ($SAP \rightarrow RR|_{\Omega}$) slightly diminished the detection of causality with respect to $SAP \rightarrow RR|_{\Omega-\{Resp\}}$ although differences were not found statistically significant.

TABLE 6.6

PERCENTAGES OF SIGNIFICANT K^2_{LF}, K^2_{HF} AND CAUSALITY FROM SAP TO RR (SAP→RR) DETECTED WHEN CONSIDERING $\Omega-\{Resp\}$ AND Ω IN HEALTHY HUMANS AT REST (R), DURING HEAD-UP TILT MANEUVERS AT 45° AND 90° (T45 AND T90) AND RESPECTIVE RECOVERY SESSIONS (R45 AND R90)

	R	**T45**	**R45**	**T90**	**R90**
$\mathbf{K^2_{LF}>0.5}$	62%	93%	87%	100%	73%
$\mathbf{K^2_{HF}>0.5}$	77%	86%	67%	64%	80%
$\mathbf{SAP \rightarrow RR|_{\Omega-\{Resp\}}}$	85%	100%	100%	86%	87%
$\mathbf{SAP \rightarrow RR|_{\Omega}}$	76%	86%	79%	86%	73%

As reported in Table 6.7 the percentages of cases with $K^2_{LF}>0.5$ obtained during R were found significantly smaller with respect to that derived pooling together tilt sessions (T45 U T90).

No differences were found when assessing the percentage of subjects with $K^2_{HF}>0.5$, with $SAP \rightarrow RR|_{\Omega-\{Resp\}}$ and with $SAP \rightarrow RR|_{\Omega}$. The percentage of subjects with $K^2_{LF}>0.5$, with $K^2_{HF}>0.5$, with $SAP \rightarrow RR|_{\Omega-\{Resp\}}$ and with $SAP \rightarrow RR|_{\Omega}$ found during recovery sessions (R45 U R90) was similar to those detected at R.

TABLE 6.7

DIFFERENCE BETWEEN PERCENTAGES OF CASES WITH $K^2_{LF}>0.5$ OBTAINED DURING REST (R) VERSUS POOLED TILT SESSIONS (T45 U T90)

	R vs T45 U T90
$K^2_{LF}>0.5$	p=0.008

As reported in Table 6.8 the percentage of subjects with $SAP \rightarrow RR|_{\Omega-\{Resp\}}$ was found significantly larger than that with $SAP \rightarrow RR|_{\Omega}$ derived when considering data pooling together recovery sessions (R45 U R90), thus suggesting that during recovery respiration introduces a bias in the results of causality test.

TABLE 6.8

DIFFERENCE BETWEEN THE PERCETAGE OF SUBJECTS WITH SAP→RR|$_{\Omega}$ AND THAT WITH SAP→ RR|$_{\Omega-\{Resp\}}$ DERIVED WHEN CONSIDERING DATA POOLING TOGETHER RECOVERY SESSIONS (R45 U R90)

	R45 U R90
SAP→ RR|$_{\Omega-\{Resp\}}$ vs SAP→ RR|$_{\Omega}$	p=0.05

6.5.2 Baroreflex sensitivity in healthy subjects

Values of baroreflex sensitivity indexes, α_{LF} and α_{HF}, are reported in Figs. 6.4-a and 6.4-b respectively.

During each experimental step the exclusion of subjects without a significant SAP→RR|$_{\Omega-\{Resp\}}$ and SAP→RR|$_{\Omega}$ led to values of α_{LF} and α_{HF} similar to those computed when considering all subjects with a significant K^2.

As shown in Figs. 6.4-a and 6.4-b both α_{LF} and α_{HF} decreased during tilt (T45 and T90) and increased during recovery (R45 and R90) in comparison to R. Both α_{LF} and α_{HF} were found significantly different during T45 and T90 sessions compared to R.

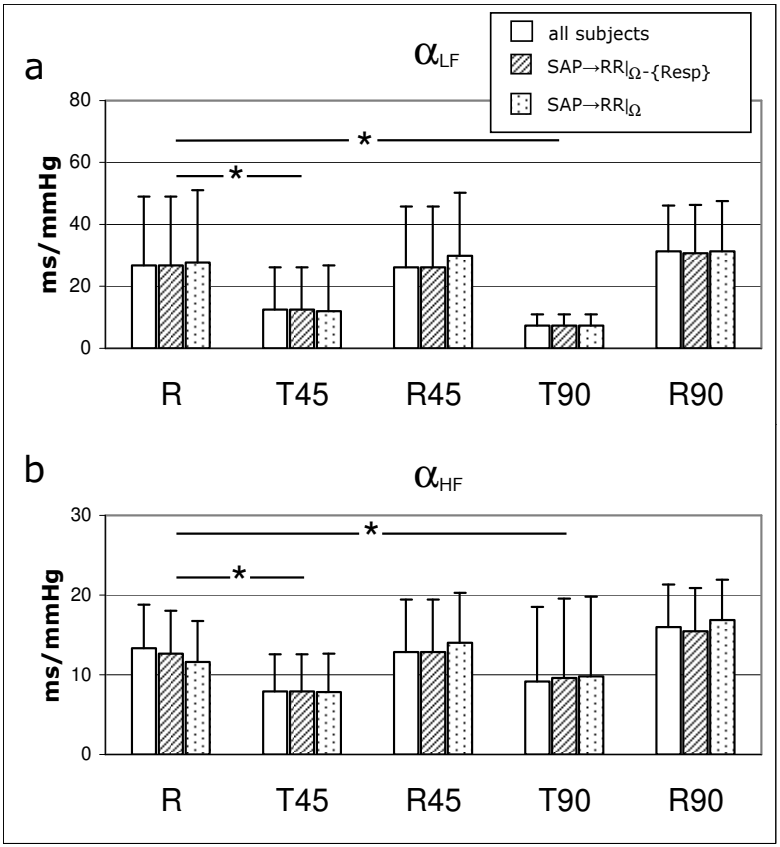

Fig. 6.4: Mean α_{LF} + SD (a) and mean α_{HF} + SD (b) expressed in ms/mmHg calculated when considering all subjects with K^2_{LF}>0.5 (a) and K^2_{HF}>0.5 (b) (open bar), when excluding subjects without SAP→RR|$_{\Omega\text{-}\{Resp\}}$ (slash-pattern bar) and when excluding subjects without SAP→RR|$_{\Omega}$ (dotted-pattern bar) in healthy humans at rest (R), during head-up tilt maneuvers at 45° and 90° (T45 and T90) and respective recovery sessions (R45 and R90). *, indicates p<0.05 statistical significance.

6.6 Conclusions

The present chapter reports the results obtained investigating four experimental protocols appropriate, on the one hand, to test causality in the direction of baroreflex in critical conditions in which this causal relation might be absent or weak, on the other hand to evaluate the role of respiration as exogenous source on the assessment of causality and on baroreflex sensitivity estimation calculated with non causal indexes.

The presence of a significant causal relation from SAP to RR was detected in a large percentage of humans or animals, thus suggesting that baroreflex control actively participated to the RR-SAP regulation in all the experimental situations.

When accounting for respiration, baroreflex control was found less involved in animals undergoing mechanical controlled ventilation in comparison to assisted ventilation, in humans undergoing deep anaesthesia during both volatile and intravenous administration strategies and in healthy subjects during recovery sessions.

As expected, baroreflex sensitivity was depressed during anaesthesia both in animals and humans, during paced breathing and head-up tilt in heart failure population and during tilt sessions in healthy subjects.

In all the considered situations baroreflex sensitivity derived after excluding the subjects without a significant causal relation along baroreflex was not significantly different from that derived when considering solely those subjects with a significant correlation between RR and SAP series as assessed using squared coherence.

Chapter 7

Discussion and Conclusions

7.1 Assessing causality along baroreflex in situations depressing baroreflex regulation

Arterial baroreflex function is an important short-term neural control system aiming at guaranteeing the homeostasis of the organism [Cohen and Taylor, 2002; La Rovere et al., 1998].

The characterization of baroreflex is based on the assessment of the baroreflex sensitivity derived as the variation of RR per unit change of SAP. Usually, in clinics, baroreflex sensitivity is evaluated by administering vasoactive agents to importantly modify SAP and by observing the evoked RR changes [Smyth et al., 1969].

Recently, several noninvasive techniques have been proposed for the estimation of the baroreflex sensitivity in more physiological conditions and without perturbing cardiovascular regulation. Unfortunately, spontaneous baroreflex indexes were found inconsistent with pharmacological baroreflex gains [Tanaka and Nishikawa, 2005; Lipman et al., 2003].

Techniques exploiting spontaneous RR and SAP variabilities are helpful in assessing baroreflex sensitivity only when causality is along baroreflex (i.e. SAP changes contribute to RR variations) [Porta et al., 2000]. Unfortunately, this prerequisite is not properly tested. Usually, assessing the significance of squared coherence function between RR

and SAP series is considered to be sufficient [De Boer et al., 1985], but unluckily coherence can be high even when RR variations contribute to SAP changes along the reverse causal direction [Porta et al., 2002] imposed by the mechanical feedforward pathway.

Without testing causality from SAP to RR any estimate of the baroreflex sensitivity derived from spontaneous variabilities could be conversely related to the gain of the feedforward mechanical pathway linking RR to SAP [Porta et al., 2002]. A lack of causality from SAP to RR could contribute to the disagreement between spontaneous and pharmacological baroreflex indexes [Tanaka and Nishikawa, 2005; Lipman et al., 2003].

Unfortunately, the estimate of causality between two signals might be biased by the presence of a third one affecting both. When considering RR and SAP, Resp acts on both, thus imposing to account for Resp when assessing causality between RR and SAP.

Indeed, mechanisms responsible for RR changes at the respiratory rate include the coupling between respiratory and autonomic centres modulating vagal and sympathetic efferent activities, cardiopulmonary reflexes mediated by the activation of atrial and pulmonary receptors, mechanical stimulation of the sinus node and baroreflex [Saul et al., 1991; Ecberg, 2003; Gilbey et al., 1984; Bainbridge, 1915; Desai et al., 1997; Bernardi et al., 1989]. SAP fluctuations synchronous with Resp are the result of respiratory-related fluctuations of stroke volume induced by changes of intrathoracic pressure and venous return [De Boer et al., 1987; Innes et al., 1993; Toska and Eriksen, 1993].

As a consequence disregarding Resp might determine an erroneous interpretation of RR-SAP causality and prompt for the inclusion of Resp into the minimal set of signals necessary to assess RR-SAP causality.

This Doctoral dissertation assesses causality from SAP to RR (i.e. along baroreflex). The presence of a significant causal relationship from SAP to RR was assessed using Granger causality approach [Granger, 1969] according to two traditional tests in the time domain

(i.e. F-test and Wald test). This evaluation was carried out by accounting for Resp as exogenous signal affecting both RR and SAP.

Causality from SAP to RR was explored with the final aim to improve baroreflex sensitivity estimate. Indeed, instead of checking the significance of squared coherence function as a prerequisite for the estimation of baroreflex sensitivity based on spontaneous RR and SAP values, this study proposes to test the significance of the causal link from SAP to RR along baroreflex. This idea was experimentally tested over four experimental protocols in which baroreflex should be insignificantly stimulated because SAP changes might be insufficient to explore baroreflex and the smallness of baroreflex sensitivity might produce insignificant RR changes.

The present chapter is organized as follows: Section 7.2 discusses the time domain approach to the assessment of Granger causality utilized in this study and the results of simulations performed to assess the reliability of Granger causality statistical tests. Sections 7.3 comments the results derived from experimental protocols (i.e. in animals and in humans under deep anaesthesia, in heart failure subjects during controlled respiration and head-up tilt and in healthy subjects during head-up tilt). Finally, Section 7.4 draws general conclusions and Section 7.5 suggests the limitations of this study and future developments.

7.2 Assessing Granger causality in time domain using F-test and Wald test

The assessment of causality relation among cardiovascular variables has been performed under the hypothesis of linear interaction occurring between RR, SAP and Resp time series.

Under this assumption two traditional statistical tests in the time domain (i.e. F-test and Wald test), the mathematical formulation of which is based on the linear regression modelling of stochastic processes proposed by Granger [1969], were adopted. The linear

approach was chosen due to its usefulness in gaining insight into cardiovascular control [Xiao et al., 2005; Batzel et al., 2009; Porta et al., 2009].

Indeed, the hypothesis of linearity can represent a valid approach when applied to beat-to-beat variability because the fluctuations in the measured signals (i.e. RR, SAP and Resp) are relatively small. Accordingly, linear models interpretation of control mechanisms is thought of as approximating small signal system behaviour around a given operating point [Xiao et al., 2005; Batzel et al., 2009; Porta et al., 2009]. In addition, the linear approach is particularly efficient when considered small amount of data and very fast when matrix factorization procedures are exploited (i.e. Cholesky decomposition).

Further, the choice of adopting methods assessing causality in time domain provides three advantages rendering them more appealing than those in frequency and information domain ones: i) they do not need to assume that the cardiovascular control mechanisms occur along specific temporal scales as in the case of techniques in the frequency domain; ii) the percentage of false causality detections can be rigorously kept under control by assigning the type I error probability accepted by the tests; iii) the distribution of the statistic assessing causality under the null hypothesis of absence of a causal relationship between the two series follows classical statistical distributions, thus allowing the analytical calculation of the critical value above which the null hypothesis is rejected (conversely techniques in frequency and information domain require time consuming Montecarlo techniques based on surrogate data generation) [Faes et al., 2010].

7.2.1 Reliability of F-test and Wald test in assessing Granger causality

The presence of a significant causal relationship between two discrete series, y_1 and y_2, has been assessed according to two traditional tests in the time domain (i.e. F-test and Wald test).

While the F-test checks whether the introduction of the supposed "cause" signal in the model of the "effect" one significantly improves the goodness of fit (i.e. predictability), the Wald test is carried out directly on the parameters that weight the contribution of the supposed "cause" signal towards the "effect" one.

Although the tests are based on different approaches, results on simulations suggest that both tests are equivalently reliable in assessing causality between discrete series when the number of observations is small (i.e. about 300 samples). Therefore, in the following only results of F-test will be discussed.

7.2.2 Assessing reliability of time-domain Granger causality tests over uncoupled signals

The simulations carried out in order to assess causality between uncoupled series pointed out the good performances in terms of low rate of detected false positives (<9%, see Table 5.1) thus confirming the ability of time-domain tests in detecting bidirectional absence of causality relation between uncoupled series (>90%) independently of theirs level of complexity and of the presence of dominant oscillations.

The false detection of causality relation, when detected, was found independent of frequency and sharpness of the dominant spectral peak characterizing series (see Figs. 5.1 and 5.2), thus confirming the robustness of the method.

7.2.3 Assessing reliability of time-domain Granger causality tests over coupled signals interacting in closed loop

When assessing causality relation between signals interacting in closed loop generated with bivariate AR process, results of causality tests depended on: i) the ratio between the variances of the residuals; ii) the ratio between the gains of the two pathways linking the two

variables; iii) the presence of the regression of one variable on its own past values (i.e. auto-loop).

With reference to i), as proved by Fig. 5.3, simulations demonstrated that causality depends on the ratio between the variances of the residuals (i.e. λ^2_1/λ^2_2). Unidirectional causality was found when λ^2_1/λ^2_2 was close to 0. The causal relation less contaminated by noise set the direction of causality: for example, if $\lambda^2_1<<\lambda^2_2$ then $y_2 \to y_1|_{\Omega_y}$. Indeed, if $\lambda^2_1<<\lambda^2_2$ the unpredictable part of y_1 (i.e. w_1) was very small with respect to the predictable one (i.e. $f_{12}(y_2)$, representing the predicted linear regression of y_2 over y_1), then $y_2 \to y_1|_{\Omega_y}$ was detected.

Unidirectional causality was found when λ^2_1/λ^2_2 was high. In this case the predictable part of y_2 (i.e. $f_{21}(y_1)$) became high and preeminent over the unpredictable one (i.e. w_2), thus leading to a detection of $y_1 \to y_2|_{\Omega_y}$. When the variances of the residuals were comparable (i.e. λ^2_1/λ^2_2 was close to 1), both directions of causality were found, thus identifying closed loop interactions. Bidirectional causality was detectable since the unpredictable parts of y_1 and y_2 (i.e. w_1 and w_2) were both negligible with respect to the predicable parts (i.e. $f_{12}(y_2)$ and $f_{21}(y_1)$).

With reference to ii), as proved by Fig. 5.4, simulations demonstrated that causality in bivariate AR closed loop processes is a function of ratio of the gains of the two pathways forming the closed loop (i.e. $|a_{12}/a_{21}|$). Unidirectional causality was found when $|a_{12}/a_{21}|$ was very high or close to 0. The causal relation with higher gain set the direction of causality. For example, if $a_{12}>>|a_{21}|$ then $y_2 \to y_1|_{\Omega_y}$. Indeed, if $a_{12}>>|a_{21}|$ the predictable part of y_1 (i.e. $f_{12}(y_2)$) was more important than that of y_2 (i.e. $f_{21}(y_1)$) on the reverse causal direction.

If the gains were comparable, bidirectional causality (i.e. closed loop relation) was found. A detection of full uncoupling would be expected if the gains decreased below a certain threshold that

depends on the variance of the residuals.

With reference to iii), as proved by Fig. 5.5, simulations demonstrated that the regression of one variable over its own past values, capable of producing a resonance loop with a gain larger than 1, did not alter dramatically the dependence of causality on the ratio between noise variances, λ^2_1/λ^2_2. However, when the effect of the auto-loop was to produce an amplification of one variable, a specific direction of causality tended to prevail.

Since in our simulation an auto-loop with a peak gain larger than 1 was created over y_2, amplification of y_2 strengthened the driving action of y_2 on y_1. Indeed, in Fig. 5.5 $y_1 \leftrightarrow y_2|_{\Omega_y}$ was more likely found at the highest values of λ^2_1/λ^2_2 (i.e. 100 and 1000) than in Fig. 5.3.

7.2.4 Assessing reliability of time-domain Granger causality tests over coupled signals interacting in closed loop under the action of an exogenous input

The importance of accounting for exogenous influences was proven by introducing an exogenous signal y_3 over the bivariate AR closed loop model.

Results obtained when the exogenous signal was included in the set of signals utilized to infer causality were compared with those derived when the exogenous signal was excluded from it. When the exogenous signal was accounted for (see Figs. 5.6-b and 5.7-b) results matched with those derived from the bivariate AR model according to the values of the parameters chosen (i.e. a_{21}=-0.7, a_{12}=0.7, $a_{22}(1)=a_{22}(2)=0$, λ^2_1=0.001, λ^2_2=1).

When the exogenous signals was not taken into consideration the expected unidirectional causality from y_2 to y_1 was not exclusively recognized and more complex causality patterns were detected (see Figs. 5.6-a and 5.7-a).

When y_3 was disregarded in type-III.a bivariate simulation (Fig. 5.6a), a large percentage of $y_2 \to y_1|_{\Omega_y - \{y_3\}}$ was initially recognized at a_{13}=0.001 (with a_{23}=1). This results can be explained by considering that the unpredictable part of y_1 was very small compared to the predictable one (i.e. $f_{12}(y_2)$) and the unpredictable part of y_2 was preeminent over the predictable one (i.e. $f_{21}(y_1)$). The progressive increase of a^2_{13} led to the erroneous detection of bidirectional interactions (Fig. 5.6-a). Indeed, the increase of a^2_{13} gradually enlarged the importance of unpredictable part of y_1, reducing the dominance of the causal relation from y_2 to y_1, and augmented the magnitude of the predictable part of y_2 (i.e. $f_{21}(y_1)$) thus leading to an increased relevance of causality from y_1 to y_2.

When y_3 was disregarded in type-III.b bivariate simulation (Fig. 5.7-a), the sole effect of y_3 on y_1 (a^2_{23}=0) provoked the invalid recognition of bidirectional interactions and of unidirectional causality from y_1 to y_2 at the highest a^2_{13} values. Indeed, both the unpredictable part of y_1 and the predictable part of y_2 (i.e. $f_{21}(y_1)$) progressively increased with a^2_{13}, thus leading to a gradual decrease of the importance of the causal relation from y_2 to y_1 and to an increased relevance of that from y_1 to y_2.

According to these findings it seems to be strongly recommended to account for any recognized exogenous signal when causality between two closed loop interacting processes is evaluated. In addition, these results prove that the bias occurring when the exogenous signal is disregarded depends on the gains of the pathways linking the exogenous signal to the two series.

7.3 Assessing causality along baroreflex in experimental protocols

Results of the four experimental protocols, selected among others because it is well-known that they depress baroreflex function, are

discussed in the following four sub-sections.

7.3.1 Assessing causality along baroreflex under deep anaesthesia in animals

The results reported in Sections 6.2.1 point out the different effects of mechanical ventilation techniques on baroreflex in pigs undergoing deep intravenous anaesthesia.

When assessing causality between SAP and RR accounting for Resp ($SAP \rightarrow RR|_{\Omega}$, Table 6.1), the percentage of causality along baroreflex was significant in both the ventilation strategies, thus suggesting that baroreflex was preserved during deep anaesthesia. However, lower percentages of causality from SAP to RR were detected during controlled ventilation with respect to supported technique, thus suggesting that supported ventilation was better suited to maintain baroreflex control.

This result seems to indicate that the predictable part of RR given SAP was lower during controlled respiration than during supported one. Interestingly when excluding respiration ($SAP \rightarrow RR|_{\Omega-\{Resp\}}$, Table 6.1) the percentage of causality from SAP to RR was found close to 100% for both controlled and supported ventilation, thus stressing the importance of accounting for respiration when assessing baroreflex activation during mechanical ventilation in deep anaesthesia.

Without accounting for Resp variations of RR driven by Resp via the stimulation of the sinus node and cardiopulmonary areas, can be erroneously interpreted as due to SAP and, thus, to baroreflex.

Pigs underwent mechanical ventilation exhibited a significant correlation between RR and SAP at HF (i.e. K^2_{HF}) both during controlled and supported ventilation (Table 6.1). This result could be ascribed to the relevant driving role of mechanical ventilator over SAP and RR during mechanical ventilation. Conversely, correlation at LF (i.e. K^2_{LF}) was lower especially during controlled ventilation. This result points out the better ability of supported ventilation to maintain

a link between SAP and RR even at a frequency slower than that of the ventilator (see Tables 6.1 and 6.2).

As suggested by De Boer et al [1985], values of squared coherence larger than 0.5 was taken as a prerequisite for the calculation of baroreflex sensitivity. As shown in Section 6.2.2, baroreflex sensitivity both at LF (α_{LF}, Fig. 6.1-a) and HF (α_{HF}, Fig. 6.1-b) were found depressed and significantly smaller during controlled ventilation than during supported ventilation, thus indicating that supported ventilation is more able to preserve baroreflex sensitivity.

The depressed baroreflex values exhibited during controlled ventilation agree with findings proposed by Wiklund et al. [2002] and Kolh et al. [2004] obtained when exploring deep anaesthesia on pigs in controlled ventilation.

The evaluation of the baroreflex sensitivity based on spectral methods was carried out also by considering only those animals with a significant link from SAP to RR according to causality analysis. Unfortunately, the exclusion of subjects without significant causality along baroreflex did not produce baroreflex sensitivity estimates different from those derived when excluding animals with squared coherence function smaller than 0.5. This result suggests that accounting for causality in this experimental protocol did not lead to produce any practical advantage compared to the more traditional approach based on coherence function.

7.3.2 Assessing causality along baroreflex under deep anaesthesia in humans

The importance of accounting for respiration when assessing causality from SAP to RR was confirmed during deep anaesthesia in humans.

Indeed, as shown in Table 6.4, when assessing causality from SAP to RR accounting for Resp ($SAP \rightarrow RR|_{\Omega}$, Table 6.3), the percentage of causality from SAP to RR was significantly lower than that detected

when excluding Resp ($SAP \rightarrow RR|_{\Omega-\{Resp\}}$, Table 6.3). These results strongly remark the necessity of accounting for respiration when assessing causality along baroreflex during deep anaesthesia under controlled mechanical ventilation. Indeed, a significant portion of the RR variability was not driven by SAP along baroreflex but directly by Resp. This portion is the result of the action of the mechanical ventilator able to cause RR changes due to the stimulation of the sinus node and to the activation of cardiopulmonary reflexes mediated by from lung and atrial receptors.

The percentage of subjects with a significant causal link from SAP to RR ($SAP \rightarrow RR|_{\Omega}$, Table 6.3) was quite low when using a volatile administration strategy (i.e. 39%) while it was larger (i.e. 63%) when using an intravenous one. This result suggests that intravenous administration better preserves an active baroreflex control (even though with a smaller baroreflex sensitivity compared to volatile administration, as shown in Figs. 6.2-a and 6.2-b) and prompts for the use of causality analysis for assessing aneasthesiological strategies.

Results of coherence functions in humans undergoing deep anaesthesia (see Section 6.3.1) were similar to those on animals during controlled ventilation (see Table 6.3). It is worth to point out that even if treated with different anaesthetic administration strategies (volatile, VA, versus intravenous, IA) both groups were mechanically controlled ventilated. In detail, coherence function was lower in the LF band and higher in HF band (Table 6.3). As shown in Section 6.3.2 baroreflex sensitivity at HF (α_{LF}, Fig. 6.2-b) was lower during IA than during VA.

These results seem to indicate that volatile anaesthetic administration is more able to preserve baroreflex sensitivity.

Baroreflex sensitivity values (mainly α_{HF}) agree with previous studies exploring deep anaesthesia in humans [Tanaka and Nishikawa, 1999; Sato et al., 2005]. Unfortunately, like in the protocol under deep anaesthesia in animals (see previous sub-section), results on

baroreflex sensitivity estimates assessed by taking into account causality from SAP to RR were not significantly different from those derived by accounting for RR-SAP correlation according to squared coherence function.

7.3.3 Assessing causality along baroreflex in heart failure subjects

When assessing causality from SAP to RR accounting for Resp ($SAP \rightarrow RR|_{\Omega}$, Table 6.5), slightly lower percentages of causality along baroreflex were detected during paced breathing and head-up tilt manoeuvre with respect to those obtained excluding Resp ($SAP \rightarrow RR|_{\Omega-\{Resp\}}$, Table 6.5). These results, although not statistically significant, suggest that Resp in heart failure population is a weak exogenous source perturbing cardiovascular system. Indeed, in heart failure population the amplitude of RR changes at HF (i.e. the respiratory sinus arrhythmia) is almost absent [Guzzetti et al., 2005] and tidal volume is reduced, thus decreasing venous return and intra-thoracic pressure changes responsible for SAP variations at HF [Mortara et al., 1997].

The percentage of significant coherence values at LF (i.e. $K^2_{LF}>0.5$) between RR and SAP was lower than that at HF ($K^2_{HF}>0.5$) in all the experimental conditions (Table 6.5). This result is in agreement with the loss of LF modulations in sympathetic activity observed in heart failure population [Van De Borne et al., 1997] in presence of higher levels of tonic activity [Guzzetti et al., 1995]

During paced breathing session the driving action of Resp on RR and SAP increased the percentage of significant K^2_{HF} values compared to rest and head-up tilt conditions.

As shown in Section 6.4.2 the baroreflex unloading caused by head-up tilt caused a significant decrease of baroreflex sensitivity in the LF band. These results agree with previous studies proposed by La

Rovere et al. [1998] and Pinna et al. [2005]. Controlled respiration left unchanged baroreflex in the HF band [Pinna et al. 2005].

No differences were detectable among baroreflex sensitivity estimates assessed according to the different strategies of accounting for RR-SAP correlation: even in this protocol introducing the concept of causality did not improve the estimate of baroreflex sensitivity compared to squared coherence.

7.3.4 Assessing causality along baroreflex in healthy subjects

When assessing causality from SAP to RR accounting for Resp ($SAP \rightarrow RR|_{\Omega}$, Table 6.6) significant lower percentages of causality were detected during recovery sessions (Table 6.8) with respect to those found when excluding for Resp ($SAP \rightarrow RR|_{\Omega - \{Resp\}}$, Table 6.6).

These results suggest that the contribution of Resp to the RR variability is significant during recovery and that a relevant stimulation of cardiopulmonary areas occurs during this condition. Therefore, causality analysis succeeded to distinguish baseline condition from recovery, even though the two experimental conditions are indistinguishable in terms of mean and variance of RR and SAP.

During head-up tilt angles in healthy subjects, higher correlation values at LF were found compared to rest (Table 6.7) in agreement with an increase modulation of sympathetic activity in LF band observed during head-up tilt in healthy subjects [Furlan et al., 2000].

As shown in Section 6.5.2, baroreflex sensitivity at LF (α_{LF}, Fig. 6.4-a) was found depressed during head-up tilt and significantly smaller with respect to rest. Significant lower baroreflex sensitivity values were also observed during head-up tilt with respect to rest at HF (α_{HF}, Fig. 6.4-b).

These findings agree with results presented in previous studies pointing out the diminished baroreflex sensitivity occurring both at LF and HF during head-up tilt [Baselli et al., 1994; Nollo et al., 2005].

Nevertheless, baroreflex sensitivity estimated values did not vary with the strategy adopted to evaluate correlation between RR and SAP series.

7.4 Conclusions

The Doctoral dissertation demonstrates over simulated and real data the importance of accounting for an exogenous source contaminating closed loop interactions in causality studies.

This result has been published in [Porta et al., 2011a]. The procedure to assess the consequence of disregarding an exogenous source on causality is general with possible applications in different fields of time series analysis ranging from physiology to economy, from neuroscience to finance, from social sciences to climatology.

In cardiovascular variability analysis, performed during deep anaesthesia in controlled mechanical ventilation and in healthy subjects during a recovery from a sympathetic activation maneouvre such as head-up tilt, disregarding Resp leads to erroneously attribute to baroreflex the direct influences of Resp on RR.

Even though baroreflex sensitivity was depressed during experimental protocols, analysis of causality from SAP to RR suggested that a relevant percentage of subjects preserved a significant causal relation along baroreflex.

This result has been published in [Bassani et al., 2011]. This conclusion holds even when respiration was accounted for, thus suggesting that baroreflex control is still present and working both during deep anaesthesia and in heart failure population. Notable exception is under deep anaesthesia in humans using a volatile administration strategy: the percentage of subjects exhibiting a significant link from SAP to RR is quite low (i.e. 39%).

Differences observed between aneasthesiological treatments and mechanical ventilation strategies in terms of percentages of causality along baroreflex suggest that causality analysis might be an helpful

tool to assess the abilities of different procedures during deep anaesthesia in preserving an active cardiovascular control.

In all the considered experimental protocols the estimate of baroreflex sensitivity computed after the exclusion of the subjects without a significant causal relation from SAP to RR along baroreflex was similar to that derived from the group of subjects with a significant RR-SAP correlation. This result suggests that assessing causality did not improve the estimate of baroreflex sensitivity with respect to the assessment of the correlation between RR and SAP series based on squared coherence.

This result was disappointing and largely unexpected since causality from SAP to RR is a prerequisite for a reliable assessment of baroreflex sensitivity. This finding indicates that the estimate of the baroreflex sensitivity from spontaneous RR and SAP variability, even when causality from SAP to RR is verified, might be still affected by important biases and unaccounted influences.

It can be hypothesized that using methods for the estimation of spontaneous baroreflex sensitivity more sophisticated than that here adopted (i.e. spectral method) and, thus, less affected by biases might make clearer the advantage of introducing causality analysis in the procedure for the estimate of baroreflex sensitivity.

7.5 Limitations and future developments

The study hypothesizes that Resp is an exogenous source acting on both SAP and RR. This hypothesis holds over temporal scales typical of short-term cardiovascular variability analysis (i.e. few minutes) but it might not be verified when slower regulations are involved (e.g. chemoreflex control). In this case neglecting influences of RR and SAP over Resp might introduce additional biases that deserve further simulation studies.

Future studies should compare the present approach in time domain with Granger causality techniques in frequency domain

[Baccalà and Sameshima, 2001; Kaminski et al., 2001; Porta et al., 2001] to clarify whether a directionality analysis carried out over temporal scales, known to be involved in short-term cardiovascular control (i.e. in LF and HF bands), could provide additional insights.

Directionality analyses based on nonlinear prediction approaches [Chen et al., 2004] or information domain methods [Faes et al., 2011] should be tested as well to overcome the hypothesis of linear interactions underlying the proposed approach.

Future applications should apply reinterpolation techniques in the time domain to achieve regularly sampled RR and SAP variability series and a synchronous Resp signal to verify whether a time domain representation of the signals might provide a more insightful description of the causal relations. Future applications in clinical settings might clarify the power of this analysis in distinguishing pathological populations, tailoring individual treatments, improving medical diagnosis and therapy, managing patients at risk and testing drugs.

Appendix A

Experimental Protocols: Temporal and Spectral Indexes

In the following are reported the calculated indexes of RR and SAP beat-to-beat series (defined in Section 4.7): I) mean (μ) and variance (σ^2); II) spectral indexes VLFa, LFa, HFa (defined in Section 4.8) and LFnu assessing RR normalized units spectral power in LF, ranging from 0 to 1, estimated as LFnu=LFa/(σ^2-VLFa); III) squared coherence functions K^2_{LF} and K^2_{HF}, ranging from 0 to 1 (defined in Section 4.8).

All indexes values are reported in Tables and expressed as mean±SD. Significance level $p<0.05$ was chosen in order to compare indexes mean values among experimental steps. Statistically significant differences among experimental steps (defined in Section 4.9) are reported, when present, at the bottom of Tables.

A.1 Indexes in animals undergoing anaesthesia

Table A.1.I, A.1.II and A.1.III show the results of indexes calculated for RR, SAP and coherence functions respectively. Data belong to experimental protocol described in Section 4.2 regarding pigs undergoing to controlled (PCV) versus supported mechanical ventilation (PSV) techniques and the random variable implementation

of the two strategies (nPCV and nPSV) during deep intravenous anaesthesia.

TABLE A.1.I

RR INDEXES IN PIGS DURING CONTROLLED AND SUPPORTED VENTILATION (PCV AND PSV) AND THE RANDOM VARIABLE IMPLEMENTATION OF THE TWO STRATEGIES (nPCV AND nPSV)

RR	**PCV**	**nPCV**	**PSV**	**nPSV**
μ [msec]	652.26 ± 44.56	650.55 ± 44.88	651.30 ± 76.20	689.84 ± 95.17
σ^2 [msec^2]	48.09 ± 47.90	207.19 ± 358.84	662.53 ± 936.40	1017.07 ± 1048.89
VLFa [msec^2]	4.19 ± 4.47	48.59 ± 43.65	46.81 ± 100.28	488.03 ± 846.83
LFnu [n.u.]	9.70 ± 15.84	4.43 ± 8.23	47.59 ± 37.47	40.82 ± 43.65
HFa [msec^2]	33.23 ± 28.27	115.09 ± 260.62	137.89 ± 228.87	359.70 ± 712.17

Statistical significance was found in σ^2, LFnu and HFa when comparing (PCV U nPCV) vs (PSV U nPSV).

TABLE A.1.II

SAP INDEXES IN PIGS DURING CONTROLLED AND SUPPORTED VENTILATION (PCV AND PSV) AND THE RANDOM VARIABLE IMPLEMENTATION OF THE TWO STRATEGIES (nPCVAND nPSV)

SAP	**PCV**	**nPCV**	**PSV**	**nPSV**
μ [mmHg]	121.92 ± 15.75	116.93 ± 11.51	120.21 ± 15.66	120.45 ± 12.64
σ^2 [mmHg ^{2}]	3.69 ± 2.71	5.05 ± 3.40	5.76 ± 2.79	8.47 ± 3.48
VLFa[mmHg ^{2}]	0.23 ± 0.39	1.75 ± 1.29	0.90 ± 1.58	2.85 ± 4.58
LFa [mmHg ^{2}]	0.35 ± 0.93	0.06 ± 0.08	2.06 ± 2.93	2.53 ± 2.90
HFa [mmHg ^{2}]	2.94 ± 2.36	3.11 ± 2.37	1.48 ± 1.10	1.84 ± 1.23

Statistical significance was found in σ^2, LFa and HFa when comparing (PCV U nPCV) vs (PSV U nPSV).

TABLE A.1.III

K^2_{LF} AND K^2_{HF} INDEXES IN PIGS DURING CONTROLLED AND SUPPORTED VENTILATION (PCV AND PSV) AND THE RANDOM VARIABLE IMPLEMENTATION OF THE TWO STRATEGIES (nPCV AND nPSV)

K^2(SAP-RR)	**PCV**	**nPCV**	**PSV**	**nPSV**
K^2_{LF}	0.59 ± 0.25	0.59 ± 0.16	0.72 ± 0.11	0.76 ± 0.13
K^2_{HF}	0.99 ± 0.03	0.99 ± 0.01	0.83 ± 0.15	0.69 ± 0.18

Statistical significance was found in K^2_{LF} and K^2_{LF} when comparing (PCV U nPCV) vs (PSV U nPSV).

A.2 Indexes in humans undergoing anaesthesia

Table A.2.I, A.2.II and A.2.III show the results of indexes calculated for RR, SAP and coherence functions respectively. Data belong to experimental protocol described in Section 4.3 regarding humans undergoing to ventilated anaesthesia (VA) versus intravenous (IA) strategy during controlled ventilation.

TABLE A.2.I

RR INDEXES IN HUMANS DURING VOLATILE (VA) AND INTRAVENOUS (IA) ANAESTHESIA

RR	**VA**	**IA**
μ [msec]	958.19 ± 161.13	925.00 ± 147.40
σ^2 [msec^2]	582.59 ± 981.32	352.47 ± 744.93
VLFa[msec^2]	271.47 ± 583.69	160.46 ± 336.00
LFnu [n.u.]	24.82 ± 19.53	59.47 ± 26.26
HFa [msec^2]	205.21 ± 339.37	117.48 ± 336.16

Statistical significance was found in LFnu when comparing VA vs IA.

TABLE A.2.II

SAP INDEXES IN HUMANS DURING VOLATILE (VA) AND INTRAVENOUS (IA) ANAESTHESIA

SAP	**VA**	**IA**
μ [mmHg]	107.13 ± 9.24	117.22 ± 16.22
σ^2 [mmHg^2]	11.40 ± 15.47	15.58 ± 14.81
VLFa[mmHg^2]	5.90 ± 15.48	6.25 ± 13.57
LFa [mmHg^2]	0.56 ± 0.73	0.94 ± 1.21
HFa [mmHg^2]	4.91 ± 2.70	8.38 ± 6.44

Statistical significance was found in μ and σ^2 when comparing VA vs IA.

TABLE A.2.III

K^2_{LF} AND K^2_{HF} INDEXES IN HUMANS DURING VOLATILE (VA) AND INTRAVENOUS (IA) ANAESTHESIA

K^2(SAP-RR)	**VA**	**IA**
K^2_{LF}	0.44 ± 0.25	0.47 ± 0.24
K^2_{HF}	0.94 ± 0.11	0.94 ± 0.11

A.3 Indexes in heart failure subjects

Table A.3.I, A.3.II and A.3.III show the results of indexes calculated for RR, SAP and coherence functions respectively. Data belong to experimental protocol described in Section 4.4 regarding heart failure patients at rest (B) and undergoing paced breathing (C) and head-up tilt manoeuvre (T).

TABLE A.3.I

RR INDEXES IN HEART FAILURE SUBJECTS AT REST (B), DURING PACED BREATHING (C) AND HEAD-UP TILT (T)

RR	B	C	T
μ [msec]	917.43 ± 138.77	935.95 ± 121.73	870.64 ± 123.64
σ^2 [msec^2]	966.31 ± 1312.36	658.23 ± 555.37	721.46 ± 675.50
VLFa[msec^2]	647.07 ± 1237.17	360.45 ± 388.32	479.71 ± 478.24
LFnu [n.u.]	49.72 ± 26.60	39.25 ± 21.80	40.32 ± 25.40
HFa [msec^2]	116.64 ± 117.16	168.49 ± 211.56	125.45 ± 255.67

TABLE A.3.II

SAP INDEXES IN HEART FAILURE SUBJECTS AT REST (B), DURING PACED BREATHING (C) AND HEAD-UP TILT (T)

SAP	**B**	**C**	**T**
μ [mmHg]	93,54 ± 14,94	93,16 ± 16,78	103,15 ± 19,45
σ^2 [mmHg^2]	16,91 ± 17,53	15,17 ± 17,59	24,49 ± 29,13
VLFa[mmHg^2]	11,21 ± 12,11	8,77 ± 14,33	18,28 ± 25,39
LFa [mmHg^2]	2,46 ± 3,17	1,99 ± 1,91	2,47 ± 2,31
HFa [mmHg^2]	1,97 ± 1,71	4,18 ± 3,46	3,18 ± 2,81

Statistical significance was found in HFa when comparing C vs B.

TABLE A.3.III

K^2_{LF} AND K^2_{HF} INDEXES IN HEART FAILURE SUBJECTS AT REST (B), DURING PACED BREATHING (C) AND HEAD-UP TILT (T)

K^2(SAP-RR)	**B**	**C**	**T**
K^2_{LF}	0.54 ± 0.21	0.48 ± 0.20	0.49 ± 0.19
K^2_{HF}	0.67 ± 0.21	0.86 ± 0.19	0.68 ± 0.20

Statistical significance was found in K^2_{HF} when comparing C vs B.

A.4 Indexes in healthy subjects

Table A.4.I. A.4.II and A.4.III show the results of indexes calculated for RR. SAP and coherence functions respectively. Data belong to experimental protocol described in Section 4.5 regarding healthy subjects during rest (R). head-up manoeuvres at different tilt angles (T45 and T90) and respective recovery sessions (R45 and R90).

TABLE A.4.I

RR INDEXES IN HEALTHY HUMANS AT REST (R). DURING HEAD-UP TILT MANEUVERS AT 45° AND 90° (T45 AND T90) AND RESPECTIVE RECOVERY SESSIONS (R45 AND R90)

RR	**R**	**T45**	**R45**	**T90**	**R90**
μ [msec]	924,95 ± 94,80	793,64 ± 87,29	990,98 ± 109,40	707,48 ± 94,06	997,90 ± 112,77
σ^2 [msec^2]	5439,84 ± 2944,02	3661,80 ± 1595,14	6484,96 ± 3528,18	2970,19 ± 1831,54	6907,77 ± 3442,13
VLFa[msec^2]	2325,38 ± 1600,27	1712,56 ± 1189,61	2542,27 ± 2220,43	1309,58 ± 924,85	2648,82 ± 1316,84
LFnu [n.u.]	48,13 ± 19,09	74,08 ± 16,97	46,85 ± 20,71	81,54 ± 7,87	48,68 ± 14,64
HFa [msec^2]	1819,88 ± 1515,09	456,54 ± 466,34	1893,89 ± 1816,64	246,93 ± 161,40	2273,44 ± 1770,03

Statistical significance was found in μ, LFnu and HFa when comparing (T45 U T90) vs R.

TABLE A.4.II

SAP INDEXES IN HEALTHY HUMANS AT REST (R). DURING HEAD-UP TILT MANEUVERS AT 45° AND 90° (T45 AND T90) AND RESPECTIVE RECOVERY SESSIONS (R45 AND R90)

SAP	R	T45	R45	T90	R90
μ [mmHg]	116.87 ± 16.97	132.45 ± 30.57	129.06 ± 25.22	130.88 ± 18.76	117.76 ± 21.51
σ^2 [mmHg^2]	104.97 ± 116.59	105.08 ± 102.77	108.55 ± 132.11	89.51 ± 62.93	60.24 ± 76.06
VLFa[mmHg^2]	78.04 ± 95.90	56.10 ± 74.62	77.04 ± 116.84	45.87 ± 31.95	41.47 ± 44.47
LFa [mmHg^2]	17.84 ± 19.34	42.87 ± 43.99	20.82 ± 19.94	33.60 ± 31.65	14.25 ± 23.97
HFa [mmHg^2]	8.10 ± 11.73	7.81 ± 8.36	5.41 ± 4.30	8.44 ± 9.71	4.44 ± 9.15

TABLE A.4.III

K^2_{LF} AND K^2_{HF} INDEXES IN HEALTHY HUMANS AT REST (R). DURING HEAD-UP TILT MANEUVERS AT 45° AND 90° (T45 AND T90) AND RESPECTIVE RECOVERY SESSIONS (R45 AND R90)

K^2(SAP-RR)	R	T45	R45	T90	R90
K^2_{LF}	0.54 ± 0.18	0.74 ± 0.10	0.61 ± 0.16	0.76 ± 0.14	0.58 ± 0.13
K^2_{HF}	0.60 ± 0.22	0.65 ± 0.15	0.60 ± 0.24	0.52 ± 0.18	0.69 ± 0.21

Statistical significance was found in K^2_{LF} when comparing (T45 U T90) vs R and (R45 U R90) vs R.

BIBLIOGRAPHY

Akaike H., *A new look at the statistical novel identification*, IEEE Transactions on Automatic Control, 19, 716-723, 1974.

Akselrod S., Gordon D., Ubel F.A., Shannon D.C., Berger R.D., Cohen R.J., *Power spectrum analysis of heart rate fluctuations: a quantitative probe of beat-to-beat cardiovascular control*, Science, 213, 220-223, 1981.

Astolfi L., Cincotti F., Mattia D., Marciani M.G., Baccala L.A., Fallani F.D., Salinari S., Ursino M., Zavaglia M., Babiloni F., *Assessing cortical functional connectivity by partial directed coherence: simulations and application to real data*, IEEE Transaction of Biomedical Engineering, 53(9), 1802–1812, 2006.

Baccalà L., Sameshima K., *Partial directed coherence: a new concept in neural structure determination*, Biological Cybernetics, 84, 463-474, 2001.

Bainbridge F.A., *The influence of venous filling upon the rate of the heart*, Journal of Physiology, 50, 65-84, 1915.

Baselli G., Cerutti S., Civardi S., Liberati D., Lombardi F., Malliani A. and Pagani M. *Spectral and cross-spectral analysis of heart rate and arterial blood pressure variability signals*, Computers and Biomedical Research, 19, 520-534, 1986.

Baselli G., Cerutti S., Civardi S., Malliani A., Pagani M., *Cardiovascular variability signals: towards the identification of a closed-loop model of the neural control mechanisms*, IEEE Transaction on Biomedical Engineering. 35, 1033–1046, 1988.

Baselli G., Cerutti S., Badilini F., Biancardi L., Porta A., Pagani M., Lombardi F., Rimoldi O., Furlan R. and Malliani A., *Model for the assessment of heart period and arterial pressure variability interactions and respiratory influences*, Medical and Biological Engineering and Computing, 32, 143-152, 1994.

Baselli G., Porta A., Rimordi O., Pagani M., Cerutti S., *Spectral decomposition in multi-channel recordings based on multi-variate Z Parametric identification*, IEEE Transaction on Biomedical Engineering, 44(11), 1092–1101, 1997.

Baselli G., Caiani E., Porta A., Montano N., Signorini M.G., Cerutti S., *Biomedical Signal Processing and Modeling in Cardiovascular Systems*, Critical Review in Biomedical Engineering, 30(1-3), 55-84, 2002.

Bassani T., Magagnin V., Guzzetti S., Baselli G., Citerio G., and Porta A., *Testing the involvement of baroreflex during general anesthesia through Granger causality approach*, Computers in Biology and Medicine, in press, 2011.

Batzel J., Baselli G., Mukkamala R., Chon K.. *Modelling and disentangling physiological mechanisms: linear and nonlinear identification techniques for analysis of cardiovascular regulation*, Philosophical Transactions of the Royal Society A, 367(1892), 1377-1391, 2009.

Beda A., Spieth P.M., Handzsuj T., Pelosi P., Carvalho N.C., Koch E., Koch T., de Abreu M.G., *A novel adaptive control system for noisy*

pressure-controlled ventilation: a numerical simulation and bench test study, Intensive Care Medicine, 36(1), 164-168, 2010.

Bell D., Kay J., Malley J., *A nonparametric approach to nonlinear causality testing*, Economics Letters, 51, 7–18, 1996.

Bernardi L., Keller F., Sanders M., Reddy P.S., Griffhth B., Meno F., and Pinsky R., *Respiratory sinus arrhythmia in the denervated human heart*, Journal of Applied Physiology, 67, 1447-1455, 1989.

Bernasconi C. and König P., *On the directionality of cortical interactions studied by structural analysis of electrophysiological recordings*, Biological Cybernetics, 81, 199-210, 1999.

Brown T.E., Beightol L.A., Kob J. and Eckberg D.L., *Important influence of respiration on human RR interval power spectra is largely ignored*, Journal of Applied Physiology, 75, 2310-2317, 1993.

Chàvez M., Martinerie J., Le Van Quyen M., *Statistical assessment of nonlinear causality: application to epileptic EEG signals*, Journal of Neuroscience Methods, 124(2), 113-128, 2003.

Chen Y., Rangarajan G., Feng J. and Ding M., *Analyzing multiple nonlinear time series with extended Granger Causality*, Physics Letters A, 324, 26-35, 2004.

Citerio G., Franzosi M.G., Latini R., Masson S., Barlera S., Guzzetti S., Pesenti A., *Anaesthesiological strategies in elective craniotomy: randomized, equivalence, open trial - The NeuroMorpfeo trial*, Trials, 10 19, 2009.

Cohen M.A., Taylor J.A., *Short-term cardiovascular oscillations in man: measuring and modelling the physiologies*, Journal of Physiology 542, 669-683, 2002.

Constant I., Laude D., Hentzgen E., Murat I., *Does halothane really preserve cardiac baroreflex better than sevoflurane? A non invasive study of spontaneous baroreflex in children anesthetized with sevoflurane versus halothane*, Anesthesia & Analgesia, 99, 360-369, 2004.

De Boer R.W., Karemaker J.M., Strackee J., *Relationships between short-term blood pressure fluctuations and heart rate variability in resting subjects I: a spectral analysis approach*, Medical & Biological Engineering & Computing 23, 352-358, 1985.

De Boer R. W., Karemaker J. M. and Strackee J., *Hemodynamic fluctuations and baroreflex sensitivity in humans: a beat-to-beat model*, American Journal of Physiology, 253, H680-H689, 1987.

Desai T.H., Collins J.C., Snell M. and Moscheda-Garcia R., *Modeling of arterial and cardiopulmonary baroreflex control of heart rate*, American Journal of Physiology, 272, H2343-H2352, 1997.

Dhamala M., Rangarajan G., Ding M.. *Analyzing information flow in brain networks with non parametric Granger causality*, NeuroImage, 41(2), 354–362, 2008.

Ebert T.J., Harkin C.P., Muzi M., *Cardiovascular responses to sevoflurane: a review,* Anesthesia & Analgesia, 81, 511-522, 1995.

Ebert T.J., Muzi M., Berens R., Goff D., Kampine J.P., *Sympathetic responses to induction of anesthesia in humans with propofol or etomidate*, Anesthesiology, 76, 725-733, 1992.

Eckberg D. L., *The human respiratory gate*, Journal of Physiology, 548, 339-352, 2003.

Faes L., Nollo G., Chon K., *Assessment of Granger causality by nonlinear model identification: application to short-term*

cardiovascular variability, Annals of Biomedical Engineering 36(3), 381-95, 2008.

Faes L., Nollo G. and Porta A., *Information-based detection of non linear Granger causality in multivariate processes via a non uniform embedding technique*, Physical Review E, 83, 051112, 2011.

Faes L., Porta A. and Nollo G., *Mutual non linear prediction as a tool to evaluate coupling strength and directionality in bivariate time series: comparison among different strategies based on k nearest neighbors*, Physical Review E, vol. 78, p. 026201, 2008.

Faes L., Porta A., Nollo G., *Testing frequency-domain causality in multivariate series*, IEEE Transactions on Biomedical Engineering, 57, 1897-1906, 2010.

Freiwald W.A., Valdes P., Bosch J., Biscay R., Jimenez J.C., Luis Rodriguez M., Rodriguez V., Kreiter K., Singer W., *Testing non-linearity and directedness of interactions between neural groups in the macaque inferotemporal cortex,* Journal of Neuroscience Methods, 94, 105–119, 1999.

Furlan R., Porta A., Costa F., Tank J., Baker L., Schiavi R., Robertson D., Malliani A., Mosqueda-Garcia R., *Oscillatory patterns in sympathetic neural discharge and cardiovascular variables during orthostatic stimulus*, Circulation, 101, 886-892, 2000.

Gama de Abreu M., Spieth P.M., Pelosi P., Carvalho A.R., Walter C., Schreiber-Ferstl A., Aikele P., Neykova B., Hubler M., Koch T., *Noisy pressure support ventilation: a pilot study on a new assisted ventilation mode in experimental lung injury.* Critical Care Medicine, 36(3), 818-827, 2008.

Geweke J., Meese R. and Dent W., *Comparing alternative tests of causality in temporal systems: analytic results and experimental evidence*, Journal of Econometric, 21, 161-194, 1983.

Gilbey M.P., Jordan D., Richter D.W. and Spyer K.M., *Synaptic mechanisms involved in the inspiratory modulation of vagal cardio-inhibitory neurones in the cat*, Journal of Physiology, 356, 65-78, 1984.

Granger C.W.J., *Investigating causal relations by econometric models and cross-spectral methods*, Econometrica, 37, 424-438, 1969.

Granger C.W.J., *Testing for causality: A personal viewpoint*, Journal of Economic Dynamics and Control, 2(1), 329-352, 1980.

Guzzetti S., Cogliati C., Turiel M., Crema C., Lombardi F., Malliani A., *Sympathetic predominance followed by functional denervation in the progression of chronic heart failure*, European Heart Journal, 16, 1100-1107, 1995.

Guzzetti S., La Rovere M.T., Pinna G.D., Maestri R., Borroni E., Porta A., Mortara A., Malliani A., *Different spectral components of 24h heart rate variability are related to different modes of death in chronic heart failure*, European Heart Journal, 26, 357-362, 2005.

Hesse W,. Moller E., Arnold M., Schack B., *The use of time-variant EEG Granger causality for inspecting directed interdependencies of neural assemblies*, Journal of Neuroscience Methods, 124(1), 27-44, 2003.

Hlavackova-Schindler K., Palus M., Vejmelka M. and Bhattacharya J., *Causality detection based on information-theoretic approaches in time series analysis*, Physics Reports, 441, 1-46, 2007.

Hyndman B.W., Kitney I.R., Sayers McA., *Spontaneous Rhytms in Physiological Control Systems,* Nature, 233, 5318, 339-341, 1971.

Innes J., De Cort S., Kox W. and Guz A., *Within-breath modulation of left ventricular function during normal breathing and positive-pressure ventilation in man*, Journal of Physiology, 460, 487-502, 1993.

Kaminski M., Ding M., Truccolo W.A., Bressler S., *Evaluating causal relations in neural systems: Granger causality, directed transfer function and statistical assessment of significance*, Biological Cybernetics, 85, 145-157, 2001.

Kay S.M., Marple S.L., *Spectrum analysis: a modern perspective*, Proceedings of the IEEE, 69, 1380-1418, 1981.

Kashihara K., Kawada T., Sugimachi M., and Sunagawa K., *Wavelet-based system identification of short-term dynamic characteristics of arterial baroreflex*, Annals of Biomedical Engineering, 37, 112-128, 2008.

Kitney R., Linkens D., Selman A. and McDonald A., *The interaction between heart rate and respiration: part II – nonlinear analysis based on computer modeling,* Automedica, 4, 141-153, 1982.

Koepchen H.P., Klussendorf D., Sommer D., *Neurophysiological background of central neural cardiovascular-respiratory coordination: basic remarks and experimental approach,* Journal of the Autonomic Nervous System, 3, 335–368, 1981.

Koepchen H.P., Miyakawa K., Polosa C., *History of studies and concepts of blood pressure waves*, Mechanisms of Blood PressureWaves, Springer-Verlag, 3–23, 1984.

Kolh P., Lambermont B., Ghuysen A., Tchana-Sato V., Dogné J.M., D'Orio V., Gerard P., Larbuisson R. and Limet R., *Comparison of the effects of propofol and pentobarbital on left ventricular adaptation to an increased afterload*, Journal of Cardiovascular Pharmacology, 44(3), 294-301, 2004.

La Rovere M.T., Bigger J.T Jr, Marcus F.I., Mortara A., Schwartz P.J. *Baroreflex sensitivity and heart-rate variability in prediction of total cardiac mortality after myocardial infarction*, The Lancet, 351(9101), 478-484, 1998.

Laude D., Elghozi J.L., Girard A., Bellard F., Bouhaddi M., Castiglioni P., Cerutti C., Cividjian A., di Rienzo M., Fortrat J.O., Janssen B., Karemaker J.M., Leftheriotis G., Parati G., Persson P.B., Porta A., Quintin L., Regnard J., Rudiger H., Stauss H.M., *Comparison of various techniques used to estimate spontaneous baroreflex sensitivity (the EuroBaVar study)*, American Journal of Physiology, 286, R226-R231, 2004.

Lipman R.D., Salisbury J.K. and Taylor J.A., *Spontaneous indices are inconsistent with arterial baroreflex gain*, Hypertension, 42(4), 481-487, 2003.

Londei A., D'Ausilio A., Basso D. and Olivetti Belardinelli M.. *A new method for detecting causality in fMRI data of cognitive processing*, Cognitive processing, 7(1), 42-52, 2006.

Lutkepohl H., *New introduction to multiple time series analysis*, Berlin Heidelberg: Springer-Verlag, 2005.

Malliani A., Pagani M., Lombardi F., Cerutti S.,. *Cardiovascular neural regulation explored in the frequency domain*, Circulation, 84, 482–492, 1991.

Marinazzo D., Pellicoro M., Stramaglia S., *Nonlinear parametric model for Granger causality of time series*, Physical Review E, 73(6), 2006.

Mortara A., Sleight P., Pinna G.D., Maestri R., Prpa A., La Rovere M.T., Cobelli F., Tavazzi L., *Abnormal awake respiratory patterns are common in chronic heart failure and may prevent evaluation of*

autonomic tone by measures of heart rate variability, Circulation, 96, 246-252, 1997.

Nollo G., Faes L., Porta A., Antolini R., and Ravelli F., *Exploring directionality in spontaneous heart period and systolic arterial pressure variability interactions in humans: implications in the evaluation of baroreflex gain,* American Journal of Physiology, 288, H1777-H1785, 2005.

Nollo G., Faes L., Antolini R., Porta A., *Assessing causality in normal and impaired short-term cardiovascular regulation via nonlinear prediction methods*, Philosophical Transactions of the Royal Society A, 367(1892), 1423-1440, 2009.

Pagani M., Lombardi F., Guzzetti S., Rimoldi O., Furlan R., Pizzinelli P., et al. *Power spectral analysis of heart rate and arterial pressure variabilities as a marker of sympatho-vagal interaction in man and conscious dog*. Circulation Research, 59, 178–193, 1986.

Pagani M., Somers V.K., Furlan R., Dell'Orto S., Conway J., Baselli G., Cerutti S., Sleight P., Malliani A., *Changes in autonomic regulation induced by physical training in mild hypertension*, Hypertension, 12, 600-610, 1988.

Palus M., Komarek V., Hrncir Z. and Sterbova K., *Synchronization as adjustment of information rates: Detection from bivariate time series*, Physical Review E, 63, 046211, 2001.

Palus M. and Stefanovska A., *Direction of coupling from phases of interacting oscillators: an information-theoretic approach*, Physical Review E, 67, p. 055201, 2003.

Papoulis A., *Probability, Random Variables and Stochastic Processes*, McGraw-Hill, New York, 1984.

Pedotti A., *Tecnologie in Medicina – Prinicipi e Applicazioni*, Città Studi Edizioni, 1989.

Pinna G.D., Maestri R., Capomolla S., Febo O., Robbi E., Cobelli F. and La Rovere M.T., *Applicability and clinical relevance of the transfer function method in the assessment of baroreflex sensitivity in heart failure patients,* Journal of the American College of Cardiology, 46(7), 1314-1321, 2005.

Porta A., Bassani T., Bari V., Pinna G.D., Maestri R., and Guzzetti S., *Accounting for Respiration is Necessary to Reliably Infer Granger Causality from Cardiovascular Variability Series*, IEEE Transaction on Biomedical Engineering, in press, 2011a.

Porta A., Catai A. M., Takahashi A. C. M., Magagnin V., Bassani T., Tobaldini E., Van de Borne P. and Montano N., *Causal relationships between heart period and systolic arterial pressure during graded head-up tilt*, American Journal of Physiology, 300, R378-R386, 2011b.

Porta A., Aletti F., Vallais F., Baselli G., *Multimodal signal processing for the analysis of cardiovascular variability*, Philosophical Transactions of the Royal Society A, 367, 391-409, 2009.

Porta A., Baselli G., Rimoldi O., Malliani A., Pagani M., *Assessing baroreflex gain from spontaneous variability in conscious dogs: role of causality and respiration*, American Journal of Physiology, 279, H2558-H2567, 2000.

Porta A., Baselli G. and Cerutti C., *Implicit and explicit model-based signal processing for the analysis of short-term cardiovascular interactions*, Proceedings IEEE 1994, 805-818, 2006.

Porta A., Furlan R., Rimoldi O., Pagani M., Malliani A., Van de Borne P., *Quantifying the strength of the linear causal coupling in closed*

loop interacting cardiovascular variability signals, Biological Cybernetics, 86, 241-251, 2002.

Porta A., Baselli G., Lombardi F., Montano N., Malliani A. and Cerutti S., *Conditional entropy approach for the evaluation of the coupling strength*, Biological Cybernetics, 81, 119, 1999.

Riedl M., Suhrbier A., Stepan H., Kurths J. and Wessel N., *Short-term couplings of the cardiovascualr system in pregnant women suffering from pre-eclampsia*, Philosophical Transactions of the Royal Society A, 368, 2237-2250, 2010.

Roebroeck A., Formisano E., Goebel R., *Mapping directed influence over the brain using Granger causality and fMRI*, Neuroimage, 25(1), 230-242, 2005.

Rosenblum M.G., Cimponeriu L., Bezeriamos A., Patzak A. and Mrowka R., *Identification of coupling direction: application to cardiorespiratory interactions*, Physical Review E, 65, 041909, 2002.

Sameshima K., Baccala L.A., *Using partial directed coherence to describe neuronal ensemble interactions*. Journal of Neuroscience Methods, 94, 93-103, 1999.

Sato M., Tanaka M., Umehara S., Nishikawa T., *Baroreflex control of heart rate during and after propofol infusion in humans*, British Journal of Anaesthesia, 94, 577-581, 2005.

Saul J.P., Berger R.D., Albrecht P., Stein S P., Chen M.H., and Cohen R.J., *Transfer function analysis of the circulation: unique insights into cardiovascular regulation*, American Journal of Physiology, 261, H1231-H1245, 1991.

Schreiber T., Schmitz A., *Surrogate time series*, Physica D, 142, 346-382, 2000.

Schelter B., Timmer J., Eichler M., *Assessing the strength of directed influences among neural signals using renormalized partial directed coherence*, Journal of Neuroscience Methods, 179(1), 121-130, 2009.

Sitnikova E., Dikanev T., Smirnov D., Bezruchko B., van Luijtelaar G. *Granger causality: Cortico-thalamic interdependencies during absence seizures in WAG/Rij rats*, Journal of Neuroscience Methods, 170, 245–254, 2008.

Smyth H.S., Sleight P., Pickering G.W., *Reflex regulation of the arterial pressure during sleep in man. A quantitative method of assessing baroreflex sensitivity*, Circulation Research, 24, 109-121, 1969.

Soderstrom T. and P. Stoica, *System identification*, Englewood Cliffs, NJ: Prentice Hall, 1988.

Spieth P.M., Carvalho A.R., Pelosi P., Hoehn C., Meissner C., Kasper M., Hubler M., von Neindorff M., Dassow C., Barrenschee M., Uhlig S., Koch T., de Abreu M.G.. *Variable Tidal Volumes Improve Lung Protective Ventilation Strategies in Experimental Lung Injury*. American Journal of Respiratory and Critical Care Medicine, 179(8), 684-693, 2009.

Tanaka M., Nishikawa T., *Arterial baroreflex function in humans anaesthetized with sevoflurane*, British Journal of Anaesthesia, 82, 350-354, 1999.

Tanaka M., Nishikawa T., *The concentration-dependent effects of general anesthesia on spontanoeus baroreflex indexes and their correlations with pharmacological gains*, Anesthesia & Analgesia, 100, 1325-1332, 2005.

Taylor J.A. and. Eckberg D.L., *Fundamental relations between short-term RR interval and arterial pressure oscillations in humans*, Circulation, 93, 1527-1532, 1996.

Task Force of the European Society of Cardiology and the North American Society of Pacing and Electrophysiology, *Standard of measurement, physiological interpretation and clinical use*, Circulation, 93, 1043-1065, 1996.

Tobin M.J., *Advances in Mechanical Ventilation*, New England Journal of Medicine , 28-6, 344(26), 1986-1996, 2001.

Toska K. and Eriksen M., *Respiration-synchronous fluctuations in stroke volume, heart rate and arterial pressure in humans*, Journal of Physiology, 472, 501-512, 1993.

Van De Borne P., Montano N., Pagani M., Oren R., Somers V.K., *Absence of low-frequency variability of sympathetic nerve activity in severe heart failure*, Circulation, 95, 1449-1454, 1997.

Verdes P. F., *Assessing causality from multivariate time series*, Phys. Rev. E, 72, 026222, 2005.

Wald A., *Tests of statistical hypothesis concerning several parameters when the number of observations is large*, Transaction of American Mathematical Society, 54, 426–482, 1943.

Wang X., Chen Y., Bressler S., Ding M., *Granger causality between multiple interdependent neurobiological time series: Blockwise versus pairwise methods*, International Journal of Neural Systems, 17(2), 71, 2007.

Wiklund U., Akay M., Morrison S. and Niklasson U., *Wavelet decomposition of cardiovascular signals for baroreceptor function tests in pigs,* IEEE Transactions on Biomedical Engineering, 49(7), 651-661, 2002.

Xiao X., Mullen T.J. and Mukkamala R., *System identification: a multi-signal approach for probing neural cardiovascular regulation,* Physiological Measurement, 26, R41–R71, 2005.

Zetterberg L.H., *Estimation of parameters for a linear difference equation with application to EEG analysis*, Mathematical Biosciences, 5, 227-275, 1969.